Development and Test
of Interaction Potentials
for Complex Metallic Alloys

Entwicklung und Test von Wechselwirkungspotenzialen für komplexe intermetallische Verbindungen

Von der Fakultät für Mathematik und Physik der Universität Stuttgart zur Erlangung der Würde eines Doktors der Naturwissenschaften (Dr. rer. nat.) genehmigte Abhandlung

Vorgelegt von

Peter Brommer

aus Tübingen

Hauptberichter:	Prof. Dr. H.-R. Trebin
Mitberichter	Prof. Dr. U. Weiß
Tag der mündlichen Prüfung:	20. Dezember 2007

Institut für Theoretische und Angewandte Physik
der Universität Stuttgart

2008

FAUST:
So that no more with bitter sweat
I need to talk of what I don't know yet,
So that I may perceive whatever holds
The world together in its inmost folds,
See all its seeds, its working power,
And cease word-threshing from this hour.

J.W. VON GOETHE, Faust: The First Part of the Tragedy.

Meiner Großmutter Elisabeth Brommer.

Contents

List of Symbols

MPI   Message Passing Interface, page 87

NC-PP Norm-Conserving Pseudopotentials, page 49

PAW   Projector Augmented-Wave, page 50

QC   Quasicrystal, quasicrystalline, page 38

r_c Cutoff Radius, page 62

RMM-DIIS Residual Minimisation Method by Direct Inversion in the Iterative Subspace, page 52

rms   root-mean-square, page 76

SC   Self-Consistency cycle, page 52

τ $= \frac{1}{2}\left(\sqrt{5}+1\right)$, golden mean, page 105

TM   Transition Metal, page 104

T_m Melting point, page 100

US-PP Ultrasoft Pseudopotentials, page 50

VASP   Vienna Ab-initio Simulation Package, page 151

$Z_{\boldsymbol{\xi}}$ Target function of minimisation, page 63

List of Figures

List of Tables

Abstract

Complex metallic alloys and quasicrystals show extraordinary physical properties relevant for technological applications, for example hardness at low density. In the study of these systems, atomistic simulation with classical interaction potentials is a very promising tool, as it offers atomic resolution for millions of atoms. Both static and dynamic properties can be studied in a large temperature range. Such simulations require classical effective potentials describing the cohesive energy as a function of the atomic coordinates. The quality of the simulation depends crucially on the accuracy with which this potential describes the real interactions. One way to generate physically relevant potentials is the force matching method, where the parameters of a potential are adjusted to optimally reproduce the forces on individual atoms determined from quantum-mechanical calculation. The programme package *potfit* developed as part of this thesis implements the force matching method efficiently. Potentials are generated for a number of complex metallic alloy systems. A potential for the decagonal basic Ni-rich Al–Co–Ni quasicrystal is used to simulate diffusion processes and melting. In the $CaCd_6$ system built from multishelled clusters, the shape and orientation of the innermost cluster shell is studied. Finally, phonon dispersion in the Mg–Zn system is determined and compared to experiment. The programme *potfit* is shown to be an effective tool for generating physically justified effective potentials. Potentials created with *potfit* can greatly improve the understanding of complex metallic alloys through atomistic simulations.

Entwicklung und Test von Wechselwirkungspotenzialen für komplexe intermetallische Verbindungen

Zusammenfassung in deutscher Sprache

Einleitung

Komplexe intermetallische Verbindungen (CMA, nach engl. *Complex Metallic Alloys*) sind seit langem bekannt. 1923 stellte Pauling fest, dass das Röntgenbeugungsmuster von $NaCd_2$ zu kompliziert ist, als dass es zum damaligen Zeitpunkt hätte erklärt werden können. Erst dreißig Jahre später erkannte man, dass die kubische Einheitszelle mehr als 1100 Atome enthält. Ähnlich verhält es sich mit β-Mg_2Al_3, das – wie 1965 gezeigt werden konnte – 1832 Plätze in der Einheitszelle hat, von denen aber nur 1168 besetzt sind.

Vor fünfundzwanzig Jahren wurden die Quasikristalle entdeckt. Sie unterscheiden sich von anderen Kristallen durch eine quasiperiodische Translationssymmetrie und eine mit periodischer Translation unvereinbare Rotationssymmetrie. Quasikristalle können als Extrem der CMAs betrachtet werden: Sie haben eine unendlich große Einheitszelle. Sowohl die komplexen intermetallischen Verbindungen als auch die Quasikristalle zeigen besondere physikalische Eigenschaften, wie z.B. Härte bei niedriger Dichte oder hohe elektrische Leitfähigkeit bei niederer thermischer, die sie technologisch interessant machen könnten.

Hunderte intermetallischer Verbindungen sind bislang bekannt, und in beinahe jedem ternären Phasendiagramm findet man weitere Materialien mit riesigen Einheitszellen. Mit Sicherheit gibt es unter den noch zu entdeckenden CMAs einige mit hochinteressanten Eigenschaften.

Die numerische Simulation solcher komplexer Systeme ist ein wichtiges Werkzeug, das die experimentelle und theoretische Forschung ergänzt. Fortschritte in der Leistungsfähigkeit von Computern in den vergangenen Jahrzehnten erlauben immer kompliziertere Simulationen auf verschiedenen Ebenen. Die Simulation von Atomen mit klassischen Wechselwirkungspotenzialen ist nach wie vor sehr nützlich, da sie numerische Experimente mit vielen Millionen von Teilchen ermöglicht und dabei gleichzeitig noch die Position jedes einzelnen Atoms auflöst. Diese so genannte klassische Molekulardynamik (MD) wird verwendet, um statische und dynamische Eigenschaften über einen großen Temperaturbereich zu bestimmen.

Voraussetzung für MD-Simulationen ist auf der einen Seite natürlich eine Ausgangsstruktur. Dies können beispielsweise die Gleichgewichtspositionen der Atome sein, die in Kristallen durch Beugungsexperimente bestimmt werden. Viel wichtiger ist es allerdings, die Wechselwirkungen schnell aus den Atompositionen bestimmen zu können. Dafür verwendet man klassische effektive Potenziale, die die Kohäsionsenergie als Funktion der Atompositionen liefern.

Frühere Simulationen von komplexen Systemen wurden mit Modellpotenzialen in Modellsystemen durchgeführt – realistischere Simulationen erfordern allerdings wirklichkeitsnähere Potenziale. Solche Potenziale werden in der Regel an einige experimentell oder aus Ab-initio-Rechnungen bestimmte Größen angepasst. Bei komplexen intermetallischen Verbindungen jedoch versagt diese Vorgehensweise: Es gibt zu viele Parameter und zu wenige verlässliche Daten, um sie zu bestimmen. Dies ist einer der Gründe, warum es so wenige physikalisch gerechtfertigte Potenziale für diese Systeme existieren.

Realistische Simulationen sind aber nur mit physikalisch fundierten und qualitativ hochwertigen effektiven Potenzialen möglich. Insbesondere wenn man das Verhalten bereits bekannnter Materialien verstehen oder mögliche Kandidaten für eine detailliertere Untersuchung auswählen möchte, sind solche Simulationen unverzichtbar.

Die Force-Matching-Methode[1] setzt zur Potenzialerzeugung für komplexe Intermetalle bei der Zahl der verwendbaren Referenzinformationen an und verwendet die Kräfte auf jedes einzelne Atom in einer gewissen Anzahl von Referenzstrukturen als Größen, an die ein Potenzial angepasst wird. Die Kräfte werden ergänzt durch einige andere Daten wie

---

[1]Engl., etwa *Methode der Potenzialanpassung an Kräfte*

Kohäsionsenergie und Spannungen auf der Einheitszelle. Alle diese Werte bestimmt man mit quantenmechanischen Ab-initio-Rechnungen. Der Force-Matching-Methode liegt die Idee zugrunde, dass ein Potenzial, das die richtigen Kräfte in den Referenzstrukturen liefert, auch die Dynamik in dem System richtig beschreiben kann. Mit der großen Anzahl an Referenzwerten, die leicht in die Tausende gehen kann, lassen sich auch die vielen Parameter eines Potenzials für binäre oder ternäre Systeme ermitteln.

In dieser Arbeit beschreibe ich eine effiziente Umsetzung der Kraftanpassungsmethode. Das *potfit* genannte Programm passt die Parameter eines Potenzials so an, dass ein Satz von Referenzdaten optimal reproduziert wird. Die Vorgehensweise bei der Erzeugung eines Potenzials für Molekulardynamik-Simulationen wird detailliert beschrieben. Für einige komplexe intermetallische Verbindungen sind bereits solche Potenziale für bestimmte Einsatzzwecke ermittelt und in Untersuchungen – vom Grundzustand über Ordnungs-Unordnungsübergänge bei tiefen Temperaturen oder den phononischen Eigenschaften bei Zimmertemperatur bis hin zu Diffusion und Schmelzvorgängen – eingesetzt worden.

Die Arbeit ist in Englisch abgefasst. Das erste Kapitel liefert eine Einführung in die Dissertation. Im folgenden Kapitel finden sich die theoretischen Grundlagen der Force-Matching-Methode. In Kapitel 3 wird die Umsetzung der Methode im Programm *potfit* ausführlich geschildert. Daran schließt sich in Kapitel 4 eine Beschreibung an, wie ein Potenzial erzeugt wird. Dort berichte ich auch über die Ergebnisse, die bei der Simulation mit den angepassten Potenzialen ermittelt wurden. Im abschließenden Kapitel 5 wird die Arbeit zusammengefasst.

Grundlagen

Komplexe intermetallische Verbindungen

Auch wenn die komplexen intermetallischen Verbindungen (*Complex metallic alloys, CMA*) schon einige Zeit bekannt sind, gelang es erst in den vergangenen Jahren, sie in hinreichender Menge zu züchten, so dass die physikalischen Eigenschaften untersucht werden können. Ähnliches gilt für die numerischen Untersuchungen und theoretischen Modelle.

Komplexe metallische Verbindungen lassen sich über folgende Eigenschaften definieren: Sie haben eine große Einheitszelle (mit Hunderten oder

Tausenden von Atomen), die Einheitszelle hat eine clusterbasierte Unterstruktur, und sie enthalten von sich aus einen gewissen Grad an Unordnung. Diese Charakteristika beeinflussen natürlich auch das Verhalten der Legierungen. So sind die konkurrierenden Längenskalen von Einheitszelle und Clustern Ursache neuer Defekttypen wie beispielsweise Metaversetzungen. Die den CMAs innewohnende Unordnung kann temperaturabhängig sein und so zu Ordnungs-Unordnungs-Phasenübergängen führen.

Quasikristalle, die 1984 entdeckt wurden, sind Strukturen mit einer quasiperiodischen Translationsordnung und einer Rotationssymmetrie, die mit räumlicher Periodizität unvereinbar ist. Sie können als CMAs mit unendlich großer Zelle aufgefasst werden. Außer den dreidimensionalen ikosaedrischen oder i-Quasikristallen, deren Symmetrie die der Ikosaedergruppe ist, gibt es noch oktagonale, dekagonale und dodekagonale Quasikristalle. Diese bestehen aus einer periodischen Abfolge von Ebenen, die selbst wieder acht-, zehn- bzw. zwölfzählige Symmetrie besitzen. Beispiel für einen dekagonalen oder d-Quasikristall ist der Al–Co–Ni-Quasikristall.

Viele CMA-Strukturen können als rationale Approximanten eines Quasikristalls betrachtet werden. Sie haben dieselbe Nahordnung wie Quasikristalle, besitzen aber eine periodische Superstruktur. Computersimulationen mit periodischen Randbedingungen verwenden in der Regel große, aber periodische Approximanten.

Atomistische Computersimulationen

In den vergangenen Jahrzehnten wurden Computersimulationen zu einem unverzichtbaren Werkzeug in Naturwissenschaft und Technik. Mit Sicherheit wird die Bedeutung solcher Simulationen aufgrund der exponentiell ansteigenden Leistungsfähigkeit moderner Computer weiter zunehmen. Auch wenn Simulationen auf allen Größen- und Zeitskalen durchgeführt werden, beschäftigt sich diese Arbeit ausschließlich mit dem Verhalten von Materie auf der atomaren Ebene.

Quantenmechanische Simulationen: Ab-initio-Methoden

Die Quantentheorie der Elektronen und Atomkerne beschreibt Materie über einen weiten Temperatur- und Druckbereich mit einer beeindruckenden Genauigkeit. Daher hofft man, dass quantenmechanische Verfahren

auch bei komplexen intermetallischen Verbindungen neue Erkenntnisse bringen.

Zentrale Aufgabe ist die Lösung der zeitunabhängigen Schrödingergleichung $\hat{H}|\psi\rangle = E|\psi\rangle$, die die Energieeigenwerte E eines Hamiltonoperators $\hat{H}$ liefert. Die meisten physikalischen Eigenschaften können mit Energien oder Energiedifferenzen verknüpft werden. Da in die Schrödingergleichung nichts außer den Positionen der beteiligten Atome eingeht, spricht man auch von *Ab-initio-Methoden*[2].

Leider kann die Schrödingergleichung nur für wenige ausgesuchte Fälle exakt gelöst werden. Speziell für die Probleme, die sich in dieser Arbeit stellen, sind ausgeklügelte Näherungsverfahren essenziell. Die erste Näherung ist die von Born und Oppenheimer, die die Atomkern- und Elektronendynamik separiert. Aufgrund des großen Massenunterschieds befinden sich die Elektronen immer im momentanen Grundzustand des von den Atomkernen gebildeten externen Potenzials; sie folgen den Kernen adiabatisch. In der Regel werden Quanteneffekte bei der Bewegung der Atomkerne vernachlässigt. Dies führt zur so genannten Ab-initio-Moleulardynamik, bei der die Kräfte auf die Atomkerne aus dem elektronischen Grundzustand berechnet werden. Die Kerne werden entsprechend bewegt. Für die neue Konfiguration wird dann wieder der elektronische Grundzustand berechnet.

Nach der Dichtefunktionaltheorie (DFT) ist Gesamtenergie eines Elektronengases ein eindeutiges Funktional der Elektronendichte. Der Minimalwert des Funktionals entspricht der Grundzustandsenergie. Das Viel-Elektronen-Problem lässt sich dann in ein äquivalentes System von selbstkonsistenten Ein-Elektron-Gleichungen überführen. Die Lösung eines Systems von wechselwirkenden Elektronen wird so auf die eines Systems von nicht-wechselwirkenden Elektronen zurückgeführt, die sich in einem von den anderen Elektronen erzeugten Potenzial bewegen. Austausch- und Korrelationseffekte verstecken sich im so genannten Austausch-Korrelations-Funktional, für das es verschiedene Näherungen gibt. Die einfachste ist die Local Density Approximation[3] (LDA), nach der diese Effekte gleich denen in einem homogenen Elektronengas der gleichen Dichte sind.

Für periodische Systeme sind ebene Wellen der Form $c_{i,\boldsymbol{k}} \exp[i(\boldsymbol{k}) \cdot \boldsymbol{r}]$ eine geeignete Basis für die Darstellung der Wellenfunktionen. Diese sind dann

---

[2]Ab initio: lat. *vom Anfang an*
[3]engl. *Lokale-Dichte-Näherung*

durch die Angabe der Koeffizienten $c_{i,\boldsymbol{k}}$ vollständig definiert. Aufgrund der Periodizität werden nur die Koeffizienten aus der ersten Brillouin-Zone benötigt. Zur Berechnung wird der reziproke Raum diskretisiert, d.h. man benötigt nur eine begrenzte Zahl von Koeffizienten. Die Basis ist zwar prinzipiell unendlich groß, tatsächlich benötigt man aber nur Wellen bis zu einer endlichen kinetischen Energie E_{cut}. Mit dem Ansatz ebener Wellen erhält man eine Säkulargleichung für die Koeffizienten $c_{i,\boldsymbol{k}}$, die selbstkonsistent gelöst werden muss.

Mit der Wahl von ebenen Wellen als Basisfunktionen beschränkt man sich auf die Beschreibung periodischer Systeme. Defekte wie freie Oberflächen, Punktdefekte oder Korngrenzen müssen daher in eine geeignete Superzelle eingebettet werden.

Bei der Darstellung der Wellenfunktionen durch ebene Wellen stören die inneren Orbitale. Zum einen sind sie fest gebunden, zum anderen zwingen sie die äußeren Wellenfunktionen zu starken Oszillationen, um die Orthonormalität aufrecht zu erhalten. Beides bedingt eine hohe Cutoffenergie E_{cut}, was die maximale Systemgröße beschränkt. Die Verwendung von Pseudopotenzialen erlaubt eine Absenkung der Cutoff-Energie. Dazu wird innerhalb einer Kugel um jedes Atom das harte Coulombpotenzial durch ein weicheres Pseudopotenzial ersetzt, das aber die gleichen Streueigenschaften hat. Gleichzeitig werden die Wellenfunktionen durch knotenfreie Pseudo-Wellenfunktionen ausgetauscht. Alternativ dazu kann auch die Projector Augmented-Wave[4] Methode (PAW) verwendet werden, bei der in einer so genannten Erweiterungsregion um die Kerne die Wellenfunktion durch eine Partialwellenexpansion dargestellt werden. Mit geeigneten Korrekturen lassen sich so auch die Kernwellenfunktionen effizient darstellen.

Trotz aller dieser Verfahren benötigt man immer noch rund 100 ebene Wellen pro Atom. Da der Aufwand zur Lösung der Säkulargleichung mit der dritten Potenz wächst, braucht man effiziente Berechnungsverfahren. Eine Möglichkeit dazu sind verbesserte Selbstkonsistenzmethoden. Diese haben alle gemeinsam, dass von einer Test-Wellenfunktion ausgehend die Potenziale berechnet werden, denen die Elektronen unterliegen. Damit werden die Wellenfunktionen verbessert. Für den folgenden Schritt verwendet man dann eine Mischung aus alten und neuen Wellenfunktionen, bis eine selbstkonsistente Lösung erreicht ist. Auf diese Weise lassen sich auch Systeme mit Hunderten Atomen pro Einheitszelle berechnen.

---

[4]engl. *Projektoren-erweiterte Welle*

Effektive Potenziale

Für die Bewegung der Atome ist eine genaue Kenntnis der elektronischen Zustände eigentlich nicht notwendig. Man kann die potenzielle Energie der Atomrümpfe auch alleine in Abhängigkeit von den Atompositionen darstellen, muss aber dann das interatomare Potenzial so verändern, dass es auch die von den Elektronen herrührenden Effekte wiedergibt, d.h. man geht zu einem effektiven Potenzial über und die potenzielle Energie wird $E_{\mathrm{pot}} = V_{\mathrm{eff}}(\{r\})$, wobei $\{r\}$ die Atompositionen sind.

Während die obige Darstellung, nach der das effektive Potenzial von allen Atompositionen gleichzeitig abhängt, noch exakt ist, wird das Problem in der Regel dadurch genähert, dass nur einige wenige Abhängigkeiten betrachtet werden. Ein typisches Modell sind Paarpotenziale, die nur noch Funktionen der Paarabstände sind. Paarpotenziale sind zwar die einfachsten der üblichen Potenziale, sie zeigen aber leider einige Defizite in der Beschreibung metallischer Festkörper. Offensichtlich gibt es in diesen Systemen Mehrkörperwechselwirkungen, die durch Paarpotenziale nicht korrekt dargestellt werden können.

Verbesserung bringen hier die so genannten Potenziale nach der Embedded Atom Method[5] (EAM). Diese haben zusätzlich zum Paarterm noch einen Einbettungsterm, der von einer lokalen Dichte n abhängt, welche wiederum von den Nachbaratomen erzeugt wird. Diese Dichte kann als Elektronendichte betrachtet werden. Allerdings lassen sich aufgrund von Eichfreiheitsgraden Beiträge zwischen Paar- und Einbettungsterm hin- und herschieben, so dass diese Interpretation nur eingeschränkt sinnvoll ist. Man nennt EAM-Potenziale auch Glue- oder Klebstoffpotenziale, insbesondere wenn man ein allgemeines, empirisches Potenzial mit Paarwechselwirkung und einer isotropen Mehrkörperwechselwirkung meint.

Klassische Molekulardynamik

Molekulardynamik (MD) ist eine Simulationsmethode, bei der die Hamiltonschen Bewegungsgleichungen für alle Atome gleichzeitig numerisch integriert werden. Die Kräfte in diesen Gleichungen können entweder aus Ab-initio-Rechnungen – man spricht dann von Ab-initio-Molekulardynamik – oder aus effektiven Potenzialen stammen. Letzteres wird klassische Molekulardynamik oder einfach nur MD genannt. Zur Integration werden die

---

[5] engl. *Atomeinbettungsmethode*

Hamilton-Gleichungen in der Zeit diskretisiert.

Die Simulationen können in verschiedenen thermodynamischen Ensembles stattfinden. Neben dem mikrokanonischen Ensemble sind auch Simulationen bei konstanter Temperatur (kanonisch) und konstantem Druck möglich. Dazu wird die Simulation an ein Temperatur- bzw. Druckreservoir gekoppelt. Alternativ kann man durch kontinuierliche Energieentnahme auch den Grundzustand eines Systems ermitteln.

MD-Simulationen sind dann besonders effizient, wenn die verwendeten Potenziale eine begrenzte Reichweite haben. In diesem Fall wird jedes Atom nur von einer beschränkten, von der Systemgröße unabhängigen Zahl an Nachbarn beeinflusst. Der Rechenzeitaufwand wächst so nur linear mit der Zahl der Atome. Ebenfalls kann die Berechnung leicht parallelisiert werden.

Potenzialanpassung durch Force Matching

Beim Force Matching werden die Parameter eines Potenzials so angepasst, dass es Kräfte, Energien und Spannungen aus Ab-initio-Rechnungen bestmöglich reproduziert. Dazu wird die Summe der quadratischen Abweichungen von den Sollgrößen minimiert. Dies ist ein bekanntes Optimierungsproblem, nämlich die Methode der kleinsten Fehlerquadrate, wofür es viele Implementierungen gibt.

Aufgrund der Nichtlinearität der Quadratsumme, deren Berechnung dazu noch sehr aufwändig ist, müssen geeignete Optimierungsalgorithmen verwendet werden. Der eine ist ein von Powell beschriebenes iteratives Verfahren zur Minimierung einer Quadratsumme ohne die Verwendung von Ableitungen, das effizient Ergebnisse aus früheren Berechnungen wiederverwendet. Bei Powells Algorithmus wird zunächst die Gradientenmatrix, von der angenommen wird, dass sie sich nur langsam im Parameterraum ändert, am Ausgangspunkt berechnet. Von dort aus wird die Suchrichtung zum Minimum mit der Methode der Konjugierten Gradienten bestimmt. Entlang dieser Richtung wird die Quadratsumme minimiert. Am Minimum ersetzt dann der Suchrichtungsvektor einen der Vektoren, die den Parameterraum aufspannen. Nur für diese neue Richtung wird die Gradientenmatrix aktualisiert, wofür aber Ergebnisse aus der eindimensionalen Minimierung verwendet werden. Nur gelegentlich muss die volle Gradientenmatrix neu berechnet werden.

Während Powells Algorithmus sehr effizient das nächstbeste lokale Mini-

mum aufspürt, kann mit Simulated Annealing[6] ein größerer Bereich des Parameterraums abgesucht werden. Dafür sind allerdings dann auch viel mehr Auswertungen der Quadratsumme notwendig. Beim Simulated Annealing wird eine zufällige Änderung der Parameter auch bei einer Verschlechterung des Ergebnisses mit einer gewissen Wahrscheinlichkeit $P(\Delta Z) = e^{-\frac{\Delta Z}{T}}$ akzeptiert, die vom Ausmaß der Verschlechterung ΔZ abhängt. Im Laufe der Optimierung wird die „Temperatur" T langsam verringert. Beim Algorithmus nach Corana werden die Größen der zufälligen Änderungen von einem Schrittweitenregler überprüft, der sicherstellt, dass etwa die Hälfte der Änderungen angenommen wird.

Die Qualität eines mit Force Matching bestimmten Potenzials hängt kritisch von der Auswahl der Referenzdaten ab. Damit erzeugte Potenziale beherrschen nur solche Situationen gut, die sie auch aus den Referenzinformationen kennen. Deshalb sollten alle lokalen Umgebungen, die in der Simulation auftauchen könnten, auch in den Referenzstrukturen enthalten sein. Durch geeignete Auswahl kann man entweder Potenziale erzeugen, die über einen weiten Zusammensetzungs-, Temperatur- und/oder Druckbereich verwendbar sind – solche Potenziale nennt man transferierbar – oder auch hochspezialisierte, aber gleichzeitig sehr genaue Potenziale für eine eng gefasste Anwendung. Die Referenzkonfigurationen können entweder aus Ab-initio-MD oder aus Simulationen mit einem Ad-hoc-Potenzial erzeugt werden.

potfit – ein Potenzialanpassungs-Programm

Im Rahmen dieser Arbeit wurde das Programm *potfit* als effiziente Implementierung der Force-Matching-Methode entwickelt. *potfit* kann sowohl ein Potenzial an Referenzdaten anpassen als auch die Güte eines Potenzials überprüfen. Intern besteht *potfit* aus zwei Teilen: Der eine berechnet für ein gegebenes Potenzial die Abweichung von den Solldaten, der andere optimiert die Parameter im Hinblick auf diese Abweichungen. Diese Teile sind weitgehend unabhängig, so dass neue Potenzialmodelle oder Optimierungsverfahren relativ problemlos eingebaut werden können.

Zur Optimierung des Potenzials sind zwei Algorithmen eingebaut. Der eine ist ein Simulated-Annealing-Algorithmus. Hierbei wird zu einem Potenzialparameter ein zufälliger, normalverteilter Wert addiert. Das resultieren-

---

[6]engl. *Simuliertes Anlassen*

de Potenzial wird dann gemäß den Simulated-Annealing-Regeln behalten oder verworfen. Ist der veränderte Parameter eine Stützstelle eines interpolierten Potenzials, werden auch benachbarte Stützstellen so verändert, dass insgesamt eine Gausskurve zur Potenzialfunktion addiert wird. Der Algorithmus wird beendet, wenn sich die Fehlerquadratsumme nicht weiter signifikant verringert.

Der andere Algorithmus ist der oben beschriebene Conjugate-Gradient-Algorithmus nach Powell. Dabei wird zunächst die lokale Gradientenmatrix berechnet. Das zugehörige Lineare Gleichungssystem wird gelöst und so die Suchrichtung im Parameterraum festgelegt. Die Quadratsumme wird entlang dieser Richtung minimiert und der Richtungsvektor für einen der alten Basisvektoren des Parameterraums eingesetzt. Dies wird solange wiederholt, bis entweder die Gradientenmatrix singulär oder der Fehler in der Lösung des Gleichungssystem zu groß wird oder wenn ein Optimierungsschritt so weit war, dass von einer sich räumlich schwach ändernden Gradientenmatrix nicht mehr ausgegangen werden kann. Der Algorithmus wird immer wieder neu gestartet, bis sich keine Verbesserungen mehr ergeben.

potfit beherrscht momentan die Anpassung von Paar- und EAM-Potenzialen, die durch Werte an Stützstellen parametrisiert sind. Zwischen den Stützstellen wird mit Spline-Polynomen interpoliert. Die Steigung an den Rändern ist ebenfalls ein freier Parameter. Die Beiträge von Kräften, Energien und Spannungen können unterschiedlich gewichtet werden. Bei den Kräften hat es sich als nützlich herausgestellt, die relative statt der absoluten Abweichung zu verwenden.

Der größte Teil der Rechenzeit von *potfit* wird für die Berechnung der Kräfte, Spannungen und Energien des Testpotenzials verwendet. Daher kann eine Geschwindigkeitssteigerung nur erfolgen, indem entweder die benötigte Zahl der Kraftberechnungen reduziert oder die Zeit für eine einzelne Berechnung verkürzt wird. Powells Algorithmus ist schon sehr effizient, und der Simulated-Annealing-Algorithmus lebt geradezu davon, den bei der jeweiligen Temperatur zugänglichen Parameterraum gründlich abzutasten, so dass dort kein großer Spielraum für Verbesserungen ist.

Da die Konfigurationen statisch sind, kann die Kraftberechnung durch Nachbartabellen und Vorausberechnung von Teilen der Spline-Interpolation beschleunigt werden. Ebenso sind die einzelnen Referenzkonfigurationen voneinander unabhängig, weshalb die Berechnung der Kräfte auf verschiedene Prozesse verteilt werden kann. Dies wurde mit Hilfe des Message Passing Interfaces (MPI) umgesetzt.

Das Programm *potfit* wird in zwei Richtungen weiterentwickelt. Zum einen soll die Potenzialparametrisierung flexibilisiert werden, so dass auch beispielsweise durch einen analytischen Ausdruck gegebene Potenziale optimiert werden können. Zusätzlich sollen auch andere Potenzialmodelle in *potfit* angepasst werden können.

Berechnungen

Erzeugung effektiver Potenziale

Die Erzeugung eines neuen Potenzials mit der Force-Matching-Methode wird in folgende Schritte zerlegt:

1. Auswahl eines geeigneten Potenzialmodells und Ausgangspotenzials.

2. Auswahl eines Satzes Modellstrukturen.

3. Erzeugung von MD-Schnappschüssen unter unterschiedlichen Bedingungen, ggf. mit Ad-hoc-Potenzial.

4. Berechnung der Referenzdaten mit Ab-initio-Methoden.

5. Potenzialanpassung mit *potfit*.

6. Verbesserung der Referenzstrukturen mit dem neu erzeugten Potenzial. Bei Bedarf wiederholen.

7. Gründliches Überprüfen des Potenzials in MD-Simulationen.

Im Folgenden werde ich auf diese Punkte kurz eingehen.

Bei der Wahl des Potenzialmodells stellen für Metalle in der Regel EAM-Potenziale die erste Wahl dar. Der Benutzer sollte sich aber bewusst sein, dass eine unbefriedigende Anpassung an die Solldaten auch an Defiziten des Potenzialmodells liegen kann. Als Ausgangspotenziale haben sich Ergebnisse früherer Optimierungen bewährt; es kann aber auch jedes andere Potenzial und auch ein Potenzial ohne jede Voreingenommenheit verwendet werden.

Der Einsatzzweck des Potenzials bestimmt die Auswahl der Strukturmodelle, die den Referenzstrukturen zugrunde liegen. Hier entscheidet sich, ob ein breit gefächert einsetzbares Potenzial oder ein hochspezialisiertes

erzeugt wird. Von diesen Strukturmodellen ausgehend werden dann mit Molekulardynamik die eigentlichen Referenzstrukturen ermittelt, da die Modelle in der Regel zu wenig Informationen enthalten. Die Referenzdaten werden dann mit einem geeigneten Ab-initio-Programm berechnet.

Nach diesen Vorarbeiten können mit *potfit* neue Potenziale erzeugt werden. Normalerweise führt ein solcher Versuch nicht auf Anhieb zum Erfolg. Das dabei generierte Potenzial kann entweder verworfen oder als Ausgangspunkt eines neuen Versuchs unter geänderten Bedingungen verwendet werden. Sobald ein brauchbares Potenzial erstellt ist, kann man damit Referenzstrukturen erzeugen, die näher an der Realität liegen, um die Referenzdaten zu ergänzen oder ganz zu ersetzen. Insbesondere wenn die MD-Schnappschüsse mit einem improvisierten Potenzial berechnet wurden, bringt die iterative Potenzialverbesserung deutliche Fortschritte.

Anschließend muss das Potenzial getestet werden. Dazu bestimmt man Größen und Eigenschaften, meistens aus MD-Simulationen, die nicht oder nicht direkt bei der Optimierung verwendet wurden. Ein wichtiger Test ist, ob das Potenzial die gewünschten Strukturen stabilisiert und den richtigen Grundzustand liefert. Andere mögliche Größen sind die Schmelztemperatur, elastische Konstanten, dynamische Eigenschaften wie der dynamische Strukturfaktor oder die phononische Zustandsdichte und Defektenergien. Falls ein Potenzial geeignete Messgrößen nicht hinreichend gut wiedergeben kann, dann ist es entweder nicht vollständig ausoptimiert oder es wurden ungeeignete oder zu wenige Referenzdaten verwendet.

Beim Einsatz eines mit Force Matching bestimmten Potenzials muss unbedingt darauf geachtet werden, dass es nur unter zulässigen Bedingungen eingesetzt wird, nämlich unter denen, die auch durch die Auswahl von Referenzkonfigurationen abgedeckt ist. Die Zeit, die für die Erzeugung eines Potenzials benötigt wird, darf auf keinen Fall unterschätzt werden: Auch wenn eine einzelne Optimierung mit *potfit* nur Minuten dauert, so benötigt man doch viele Versuche, Geduld und Erfahrung, um ein qualitativ hochwertiges Potenzial zu erzeugen.

Diffusion im Al–Co–Ni-Quasikristall

Aluminium, Kobalt und Nickel bilden über einen ausgedehnten Zusammensetzungsbereich Quasikristalle. Von besonderem Interesse ist der einfache nickelreiche (b-Ni) Al–Co–Ni-Quasikristall, der zwischen 1100 K und 1300 K beinahe perfekte dekagonale Ordnung aufweist. Das System kann in

der quasiperiodischen Ebene als eine aus drei Fliesen (Hexagon, Boot und Stern) zusammengesetze Parkettierung verstanden werden. Mit bekannten Paarpotenzialen aus der verallgemeinerten Pseudopotenzialtheorie wurde zuvor schon die Aluminium-Mobilität untersucht. Allerdings können diese Potenziale das elastische Verhalten nur unzureichend beschreiben, so dass hier mit EAM-Potenzialen Fortschritte erwartet werden.

Referenzstrukturen waren MD-Momentaufnahmen bei verschiedenen, teilweise sehr hohen Temperaturen. Aus diesen wurden zwei verschiedene Potenziale erzeugt. Beim einen wurden die Referenzdaten in der Lokalen-Dichte-Näherung (LDA) ermittelt, beim anderen in der Verallgemeinerten-Gradienten-Näherung (GGA). Beide Potenziale stabilisieren den Quasikristall, doch während das LDA-Potenzial die elastischen Konstanten deutlich besser reproduziert, ist die mit dem GGA-Potenzial bestimmte Schmelztemperatur signifikant näher am experimentellen Wert. Dies zeigt, dass möglicherweise nicht alle Ziele für ein Potenzial gleichzeitig optimal erreicht werden können.

Die Diffusion wurde mit dem GGA-Potenzial, das ja bei hohen Temperaturen realistischere Ergebnisse liefert, qualitativ und quantitativ untersucht. Zum einen wurden Atom-Aufenthaltswahrscheinlichkeiten bei hohen Temperaturen betrachtet. Dabei zeigt sich, dass die mit EAM-Potenzialen bestimmten Zeitmittel die Ergebnisse aus der Ab-initio-MD wesentlich besser wiedergeben als die mit Paarpotenzialen berechneten. Besonders die Übergangsmetalle werden von Paarpotenzialen zu stark in ihrem Bewegungsraum eingeschränkt. Dafür ergaben sich allerdings auch im Laufe einer Simulation Positionswechsel von Übergangsmetallen, die so mit Ab-initio-MD nicht auftraten. Des weiteren wurden die Barrierenhöhen von verschiedenen Diffusionsprozessen ermittelt. Die Ergebnisse sind mit denen aus Dichtefunktionalrechnungen vergleichbar. Aus der mittleren quadratischen Verschiebung wurde mit einem Arrhenius-Gesetz die Aktivierungsenthalpie bestimmt. Diese ist zwar deutlich kleiner als die für Leerstellendiffusion in flächenzentriertem Aluminium, was aber daran liegt, dass mit der verwendeten Methode nur der Migrationsanteil der Enthalpie ermittelt werden kann; die Leerstellenbildungsenthalpie wird vernachlässigt.

Die Struktur von CaCd$_6$

CaCd$_6$ ist der kubische 1/1-Approximant des thermodynamisch stabilen ikosaedrischen Ca–Cd-Quasikristalls. Sowohl Quasikristall als auch Appro-

ximant können als Packungen identischer Cluster aufgefasst werden. Beim kubischen $CaCd_6$ sind diese Cluster kubisch-raumzentriert (krz) angeordnet. Die Cluster bestehen aus vier Schalen. Während die äußeren Schalen Ikosaedersymmetrie zeigen, bricht die innerste Cd_4-Schale diese Symmetrie. Bei etwa 100 K wurde experimentell ein Ordnungs-Unordnungs-Phasenübergang in $CaCd_6$ gefunden, der auf Umordnungen in der innersten Schale zurückgeführt wird. Aus Röntgenbeugungsexperimenten ist bekannt, dass die Atompositionen in dieser Schale ein stark verzerrtes Tetraeder bilden, für dessen vier Atome 24 Positionen zur Verfügung stehen.

Als Ausgangsstrukturen für die Potenzialerzeugung wurden Canonical-Cell-Approximanten[7] verwendet, die ich durch eine hexagonale Struktur ergänzte, um einige Lücken in der Ca–Cd-Paarverteilungsfunktion zu stopfen. Die MD-Schnappschüsse wurden mit einem Ad-hoc-Potenzial bei relativ niedrigen Temperaturen erzeugt; diese wurden später durch iterativ verbesserte Konfiguration ersetzt. Das erzeugte Potenzial kann die Ab-initio-Energieunterschiede zwischen verschiedenen Konfigurationen mit einer mittleren quadratischen Abweichung von weniger als $(1.3 \text{ meV})^2$ reproduzieren, womit es fast die Genauigkeit der Dichtefunktionalrechnungen erreicht. Es stabilisiert verschieden große Approximanten des Ca–Cd-Quasikristalls.

Ein vorläufiges, breiter einsetzbares Potenzial wurde erfolgreich zur Strukturoptimierung von verschiedenen Strukturen aus dem Ca–Cd-System eingesetzt. Mit dem endgültigen Potenzial wurde die Atomanordnung in der Cd_4-Schale untersucht. Bei Relaxationsrechnungen im aus zwei Clustern bestehenden 1/1-Approximanten stellte sich unabhängig von der Ausgangskonfiguration immer das gleiche verzerrte Tetraeder ein. Die Energieunterschiede zwischen verschieden Ausgangsstrukturen resultierten alleine aus der unterschiedlichen relativen Orientierung. Allerdings relaxierten die Atome im Vergleich zu den aus Röntgenstrukturanalyse gewonnenen Positionen um bis zu 0,29 Å.

MD-Simulationen von 250 Clustern bei endlicher Temperatur zeigen, dass ausgehend von einem geordneten Tieftemperaturzustand die Ordnung der Tetraeder bei etwa 100 K verloren geht. Allerdings war es nicht möglich, ein direktes Zeichen des Phasenübergangs zu finden, da dafür die Statistik der Simulationen nicht ausreicht. Deshalb habe ich die für den Übergang maßgeblichen Freiheitsgrade isoliert und bin zu einer effektiven Cluster-

---

[7]Canonical Cell, engl: *Kanonische Zelle*

Bindungs-Hamiltonfunktion übergegangen. Dazu betrachtet man nur noch die relative Orientierung zweier benachbarter Cluster und ordnet jeder Bindung eine Energie E_α zu. Es zeigt sich, dass es 26 unterschiedliche Bindungen in zweizähliger Richtung und 16 in dreizähliger Richtung gibt. Aus Symmetriegründen gibt es allerdings nur 36 unabhängige E_α. Zur Bestimmung der Koeffizienten wurden über 9000 $CaCd_6$-Superzellen relaxiert und die Fehlerquadrate minimiert.

Mit dieser Hamiltonfunktion wurden Monte-Carlo-Simulationen durchgeführt. In diesen zeigt sich ein eindeutiger Sprung in der inneren Energie bei etwa 91 K. Aus der Sprunghöhe wurde ein Entropieunterschied von 1 k_B pro Cluster ermittelt, was dem doppelten experimentellen Wert entspricht.

Der Grundzustand kleinerer Superzellen kann relativ schnell durch Vollerhebung aller möglichen Konfigurationen ermittelt werden. Hier wurde für die $\sqrt{2} \times \sqrt{2} \times 1$-Superzelle ein energieoptimaler Zustand gefunden, der auch durch Simulated Annealing in größeren Systemen nicht übertroffen wurde. Dies deckt sich mit experimentellen Erkenntnissen, die zu einer vergleichbaren optimalen Einheitszelle des geordneten Tieftemperaturzustands gelangen.

Dynamische Eigenschaften von MgZn$_2$

$MgZn_2$ ist eine C14 Friauf-Laves-Phase mit zwölf Atomen in der Einheitszelle, die (wie auch der ikosaedrische Mg-(Al,Zn)-Quasikristall) als Dekoration der dreidimensionalen Penrose-Parkettierung interpretiert werden kann. Ausgehend von Modellstrukturen aus dem Canonical-Cell-Formalismus und kleineren Approximanten wurde ein Potenzial entwickelt, bei dem besonderer Wert auf mittlere Temperaturen und verzerrte Strukturen bei den Referenzdaten gelegt wurde. Auch hier wurde das Potenzial iterativ verbessert. Dieses Potenzial wurde bei der Strukturoptimierung von einigen Mg-Zn-Legierungen eingesetzt.

Ein hochspezialisiertes $MgZn_2$-Potenzial konnte nicht erzeugt werden, da die verfügbaren Strukturmodelle nicht den Grundzustand enthielten, sondern verzerrt waren. Dieser systematische Fehler zog sich durch die Referenzstrukturen und verhinderte dadurch dramatische Verbesserungen gegenüber dem allgemeinen, nicht $MgZn_2$-spezifischen Mg–Zn-Potenzial.

Aus Molekulardynamik-Simulationen wurde die Phononenzustandsdichte ermittelt und mit experimentellen Daten aus Neutronenstreuexperimenten verglichen. Während das Potenzial zwei der drei Maxima wenigstens

qualitativ wiedergeben kann, fehlt der Peak mit der niedersten Energie. Dies kann mit der oben erwähnten elastischen Verzerrung der Referenzstrukturen zusammenhängen.

Der kohärente Anteil des dynamischen Strukturfaktors wurde ebenfalls aus MD-Simulationen ermittelt und mit dem Experiment verglichen. Hier zeigt sich eine gute Übereinstimmung bei der Form des akustischen Phononenzweigs bis zur Grenze der ersten Brillouin-Zone, und auch für einige optische Bänder. Dazu muss allerdings die Energie um 10–30% skaliert werden. Hier dürfte eine Verbesserung der Referenzstrukturen Fortschritte bringen.

Zusammenfassung

Das Programm *potfit* wurde als Implementierung der Force-Matching-Methode entwickelt und zur Erzeugung von EAM-Potenzialen für komplexe intermetallische Verbindungen verwendet. *potfit* beherrscht zur Zeit die Anpassung von Paar- und EAM-Potenzialen, die durch spline-interpolierte Werte an Stützstellen gegeben sind; aufgrund der Architektur können aber andere Potenzialmodelle und -darstellungen ohne großen Aufwand eingebaut werden.

Zur Minimierung werden nach Wahl des Benutzers zwei Algorithmen eingesetzt, ein Simulated-Annealing-Algorithmus und ein angepasster Conjugate-Gradient-Algorithmus. Das Programm wurde optimiert sowohl hinsichtlich der Zahl der notwendigen Auswertungen der zu minimierenden Quadratsumme als auch der Zeit, die für eine Auswertung benötigt wird. Es hat sich aber herausgestellt, dass das aufwändigste an der Potenzialerzeugung die Verifikation der Potenziale ist.

Im Rahmen dieser Arbeit wurden für drei Systeme Potenziale ermittelt. Die Einsatzzwecke dieser Potenziale sind komplett unterschiedlich, was sich in der Auswahl der Referenzstrukturen niederschlägt. Mit den Potenzialen konnte die Qualität der Molekulardynamiksimulationen verbessert werden.

Außer vom Autor wurde *potfit* auch von Kollegen am Institut für Theoretische und Angewandte Physik eingesetzt, und es wurde schon mehrfach aus dem Internet heruntergeladen. Die Arbeit am Programmpaket ist noch lange nicht abgeschlossen; es ist ein Kernstück des Projekts B1 des Sonderforschungsbereichs 716.

Abschließend bleibt festzuhalten, dass *potfit* ein effektives Werkzeug zur

Erzeugung von Potenzialen ist, die physikalisch gerechtfertigt werden kön-
nen. Auch mit *potfit* ist dieser Vorgang noch aufwändig, doch realistische
Potenziale sind unverzichtbar für Molekulardynamiksimulationen. So kann
das Programm neue Einblicke in Statik und Dynamik von komplexen me-
tallischen Verbindungen und Quasikristallen liefern.

Chapter 1

Introduction

Complex Metallic Alloys (CMAs) are known for a long time. In 1923 Pauling noted that the X-ray diffraction pattern of $NaCd_2$ was too complicated to be explained at that time. More than 30 years later it was found that the cubic unit cell contains more than 1100 atoms. Another example is β-Mg_2Al_3, whose structure was explained in 1965 by Samson. It has 1832 sites in the cubic unit cell, of which only 1168 are occupied.

Twenty-five years ago, quasicrystals were discovered. They are characterised by a quasiperiodic translational order and a rotational order irreconcilable with translational periodicity. Quasicrystals take the principle of complexity in metallic alloys to the extreme: Their unit cell is infinite. Both CMAs and quasicrystals show physical properties that could make them interesting in technological applications, for example hardness at low specific weight.

Hundreds of complex intermetallic compounds are known today, and in almost each newly studied ternary phase diagram more materials with gigantic unit cells are found. It is a safe guess that their number runs into thousands. Among those, materials with exciting properties may well remain to be discovered.

Numerical simulation is an important tool in the study of those complex systems, complementing experimental and theoretical studies. The progress in computer technology in the past decades allows for more and more complex simulations at different levels. The atomistic simulation with classical interaction potentials called molecular dynamics is a very promising tool, as it allows simulations with many millions of atoms while still resolving the position of each individual atom. It can be used to determine both static and dynamic properties in a large temperature range.

Classical molecular dynamics simulations of course need a starting structure, for example the equilibrium positions which in crystalline materials may be determined from diffraction experiments. More importantly, there

must be a simple and fast way to calculate the interactions from the atomic positions. This is done with classical effective potentials, which approximately describe the cohesive energy as a function of the atomic coordinates.

Earlier simulations of complex systems were done in model systems with model potentials, but more realistic simulations require more realistic potentials. Such potentials are usually fitted to reproduce quantities determined from experiment or first-principles simulations, but for binary or ternary complex metallic alloys this method fails: There are too many free parameters and not enough reliable data to determine them from. This is one reason why there are hardly any physically justified potentials for those systems.

However, realistic simulations are possible only with physically relevant, high-quality effective potentials. These molecular dynamics calculations can help both in explaining the behaviour of materials already known and selecting promising new candidates for closer study.

The force matching method attacks the generation of potentials for complex systems by dramatically increasing the amount of reference data available: The forces on all individual atoms in a number of reference structures are used as quantities to be reproduced, complemented by other data like cohesive energy and stresses on the unit cell. All these values are determined by first-principles calculations. The idea is that if a potential can reproduce the forces in the reference structures, it can correctly describe the dynamics in that system. The enormous number of reference data, which can easily reach several thousand values, makes it possible to fit the large number of parameters needed for potentials in binary and ternary systems.

In this work, an implementation of the force matching method is described. The programme called *potfit* provides an efficient way to optimise a potential to reproduce reference data. The process of generating a potential for molecular dynamics simulations is explained, and applications of force-matched potentials in a number of complex metallic alloy systems are discussed. Depending on the nature of the potential, it can be used to study processes in a wide range of conditions: ground state configurations, low-temperature order-disorder transition, phononic properties at room temperature up to diffusion and melting.

This thesis is structured as follows: In chapter 2, the theoretical foundations of force matching are given. Chapter 3 provides a detailed description of the *potfit* programme that implements the force matching method. In

chapter 4, the potential generation with *potfit* in general is discussed and results obtained with force-matched potentials in a number of systems are reported. The thesis is summarised in chapter 5.

Part of this work has been previously published in other publications of the author, cf. *List of Publications*, p. 165.

Chapter 2

Theoretical Background

2.1 Complex Metallic Alloys

Complex metallic alloys (CMAs) are a relatively old class of metallic materials [104]. But only in recent years has it become possible to prepare those materials in sufficient quantities to study physical properties. The same holds for computational and theoretical methods. In the following section, key points on CMAs are given, also including a small excursion to the even more complex quasicrystals and their relation to CMAs.

2.1.1 Definition and Properties

Urban and Feuerbacher [104] give the following characteristics of a complex metallic alloy:

1. They have a large unit cell (hundreds or thousands of atoms),

2. the unit cell has cluster substructure,

3. and there is inherent disorder in various ways.

These three key features of course also influence the properties of CMAs.

Competing Length Scales Many CMAs, including quasicrystals and their rational approximants (see below), are built upon a cluster substructure [98], for example from the 55 atom Mackay icosahedron [63], or the 105 atom Bergman cluster [8]. The length scale defined by these clusters may deviate significantly from the one given by the lattice parameters, thus allowing for new and interesting behaviour. One example is the observation of metadislocations in the Ξ-phases of AlPdMn [27].

Disorder   There are various types of disorder in CMAs. If a particular subcluster can appear in varying orientations within its cage of atoms, then the structure may be *configurationally* disordered. Fractional occupancy of lattice sites are signs of *chemical* or *substitutional* disorder. Partial site occupation (occupancy smaller than one) and split occupation (one of two close sites is occupied) may also be found in CMAs. The degree of disorder may depend on temperature, thus leading to order-disorder phase transitions [99].

2.1.2 Quasicrystals

Quasicrystals were discovered in 1984 by SHECHTMAN *et al.* [94], who observed a perfect fivefold symmetry in an X-ray diffraction experiment on an Al-Mn alloy, indicating long-range order. The full point group symmetry was that of the icosahedral group, a symmetry group that cannot be reconciled with periodic order. In periodic crystals, only two-, three-, four- and sixfold axes are permitted.

Quickly, the relationship between that material and quasiperiodic tilings (like for example the two-dimensional PENROSE tiling [79], see Fig. 2.1) was recognised. Those also show long-range nonperiodic translational and orientational order with a rotational symmetry incompatible with periodic translational order.

In the same year, LEVINE and STEINHARDT [62] coined the term *quasicrystal* (QC) for those structures with quasiperiodic translational order. Aside from the icosahedral (or *i*-) quasicrystals, there are also octagonal, decagonal and dodecagonal quasicrystals. These are ordered periodically in one direction and quasiperiodically with eight-, ten- and twelvefold symmetry respectively in the plane normal to it. Al–Co–Ni alloys may show a tenfold symmetry in the quasiperiodic plane. These phases are then called decagonal (or *d*-) quasicrystals [87].

Both *d*- and *i*-phases can be understood as a decoration of a two- or three-dimensional quasiperiodic tiling. The icosahedral $CaYb_{5.7}$ [102] and the isostructural $CaCd_{5.7}$ [39] alloys for example can be interpreted as decorations of the Canonical Cell Tiling (CCT) [42, 66]. Similarly, there are decorations of the Penrose rhomb tiling describing *d*-AlCoNi [65].

Quasiperiodic structures can be generated in various ways, e.g. by a set of tiles and associated matching rules [79]. More elegant is the cut-and-projection formalism working in a higher dimensional embedding space.

(a) Penrose rhomb tiling   (b) hexagon-boat-star tiling
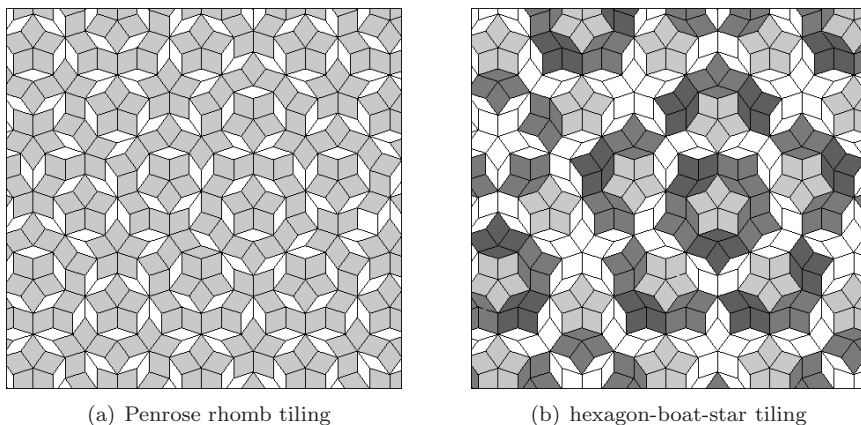
Figure 2.1: Two equivalent Penrose tilings: (a) is the Penrose rhomb tiling consisting of rhombs with an acute angle of $72°$ (light gray) or $36°$ (white). (b) is the same pattern as a hexagon-boat-star tiling with white hexagons, light gray stars and dark gray boats (the colour of the boats varies slightly for illustrative purposes). From [11].

The physical or parallel space $\mathbb{E}_{\parallel}$ is an irrational cut of the hyperspace. Orthogonal to $\mathbb{E}_{\parallel}$ is the perpendicular or perp space $\mathbb{E}_{\perp}$. Those two together span the embedding space. The Penrose tiling is a projection of a part of the five-dimensional embedding space onto a plane, while many icosahedral tilings are three-dimensional projections of a six-dimensional hypercubic lattice. An example for the cut-and-projection formalism to generate a one-dimensional quasiperiodic sequence from a square net is shown in Fig. 2.2.

Many CMA structures can also be understood within the framework of the cut-and-projection formalism [104]. There, the physical space is a suitable rational cut – in contrast to the irrational cut for quasicrystals. The resulting periodic structures have similar local neighbourhoods, but a different long range order. This is why complex metallic alloys are frequently referred to as rational quasicrystal approximants [50]. Computer simulations are often performed with periodic boundary conditions. This also dictates the use of large but periodic approximants.
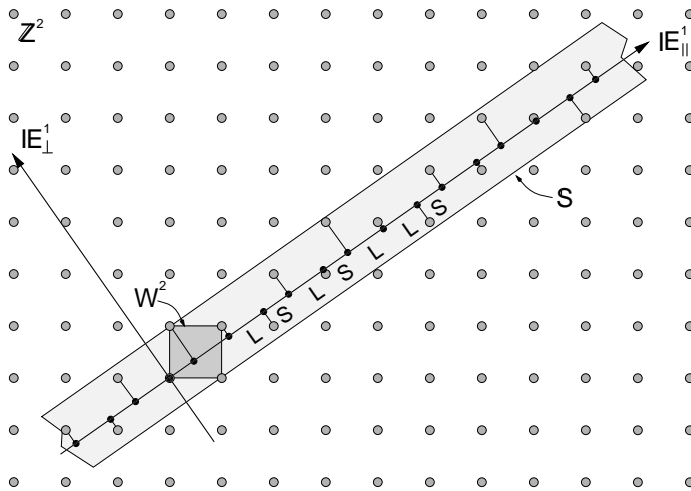
Figure 2.2: Generation of a one-dimensional quasiperiodic sequence by cutting and projecting from the two-dimensional hyperspace. The acceptance domain W^2 is moved along the parallel space axis $\mathbb{E}_\parallel$. The points of the square net $\mathbb{Z}^2$ that lie in the covered strip S are projected onto $\mathbb{E}_\parallel$. If the gradient of $\mathbb{E}_\parallel$ is irrational, these points form a quasiperiodic sequence of long (L) and short (S) intervals. From [24].

2.1.3 History

The first evidence for a CMA was given by PAULING [75] in 1923. An X-ray diffraction pattern of $NaCd_2$ was so complicated that it was at that time impossible to index many of the diffraction spots. It took more than thirty years [76] to solve the structure. The cubic unit cell of $NaCd_2$ has an edge length of 3 nm and contains 1152 atoms. This justifies the name 'giant unit cell crystals' for those intermetallic compounds. Another interesting structure studied as early as 1965 is β-Mg_2Al_3 [92] with a unit cell of 1832 atomic positions, of which only 1168 are occupied – the structure is inherently disordered.

Due to the characteristic structural features of CMAs, URBAN and FEUERBACHER [104] first called those materials 'structurally complex alloy phases' (SCAPs), a term that later was given up in favour of the now

standard name 'complex metallic alloys'.

Since 2005, the European Commission funds CMA research in Europe through the Network of Excellence Complex Metallic Alloys[1], which bundles the activities of 19 core groups. Its objective is to develop new CMAs from basic research to industrial application in an effort that could not be handled by any single institution.

2.2 Atomistic Computer Simulations

In the last decades, computer simulations have become indispensable in the sciences and engineering. It is a safe bet that the rapidly increasing computing power will make simulations an even more important tool in the future. Simulations are done on all length scales, from elementary particles to the universe as a whole. This work is concerned with the behaviour of matter on the atomic scale, and therefore simulation methods that treat each atom individually are described in this section.

2.2.1 Quantum Mechanical Calculations: Ab-initio Methods

The quantum theory of electrons and nuclei governs the behaviour of matter over wide ranges in temperature and pressure (as opposed to the conditions in the centre of the sun, e.g., where the quantum mechanics of nuclear reactions dominate). Quantum mechanics has an enormous predictive power, for example in the description of energy levels in atoms, and contradictions with reality have not yet been found. This gives reason to hope that it can also shed light into the statics and dynamics of complex metallic alloys.

Many quantum mechanical problems can be linked to the solution of the time-independent Schrödinger equation

$$\hat{H}|\psi\rangle = E|\psi\rangle, \tag{2.1}$$

which yields the energy eigenvalues E of the Hamiltonian $\hat{H}$. Most physical properties can be linked to energies or differences between energies.

The Schrödinger equation has no parameters beyond types and positions of the atoms involved. This is why methods based on the solution of

---

[1]see http://www.cma-ecnoe.org

the quantum mechanical problems are called *ab-initio*[2] or first-principles methods.

As simple as equation (2.1) may look, it cannot be solved in this form except for systems up to a few particles. Especially for problems of interest in the scope of this thesis, elaborate approximations and improvements to calculation methods are required. PAYNE *et al.* give an overview of the subject in [78].

Hamiltonian of a Many-Atom System, Born-Oppenheimer Approximation

The Hamilton operator of a non-relativistic system of N nuclei with coordinates $\boldsymbol{R}_I$, momenta $\boldsymbol{P}_I$, charges Z_I and masses M_I and N_e electrons with coordinates $\boldsymbol{r}_i$, momenta $\boldsymbol{p}_i$ and mass m reads as follows:

$$
\begin{aligned}
\hat{H} = &\sum_{I=1}^{N} \frac{\boldsymbol{P}_I^2}{2M_I} && + \sum_{i=1}^{N_e} \frac{\boldsymbol{p}_i^2}{2m} \\
&+ \sum_{I>J} \frac{Z_I Z_J e^2}{|\boldsymbol{R}_I - \boldsymbol{R}_J|} && + \sum_{i>j} \frac{e^2}{|\boldsymbol{r}_i - \boldsymbol{r}_j|} && + \sum_{i,I} \frac{Z_I e^2}{|\boldsymbol{r}_i - \boldsymbol{R}_I|} && (2.2) \\
= &\, T_N && + T_e \\
&+ V_{NN}(\boldsymbol{R}) && + V_{ee}(\boldsymbol{r}) && + V_{Ne}(\boldsymbol{r}, \boldsymbol{R}).
\end{aligned}
$$

It consists of the kinetic energy operators T and the Coulomb interaction V of the various particles.

With (2.2), the Schrödinger equation (2.1) becomes

$$
[T_N + T_e + V_{NN}(\boldsymbol{R}) + V_{ee}(\boldsymbol{r}) + V_{Ne}(\boldsymbol{r}, \boldsymbol{R})] \, \Phi(\boldsymbol{x}, \boldsymbol{R}) = E\Phi(\boldsymbol{x}, \boldsymbol{R}), \quad (2.3)
$$

where $\boldsymbol{x} \equiv (\boldsymbol{r}, s)$ combines all translational and spin degrees of freedom of the electrons and $\boldsymbol{R}$ signifies the nuclear coordinates.

The nuclear mass exceeds the electron mass by more than three orders of magnitude, and so the time scales also differ. Thus, the wave function $\Phi(\boldsymbol{x}, \boldsymbol{R})$ can be separated into an electronic part $\Psi(\boldsymbol{x}, \boldsymbol{R})$ and a nuclear wave function $\chi(\boldsymbol{R})$:

$$
\Phi(\boldsymbol{x}, \boldsymbol{R}) = \Psi(\boldsymbol{x}, \boldsymbol{R})\chi(\boldsymbol{R}). \quad (2.4)
$$

---

[2]ab initio: (Latin) from the beginning

The nuclear wave function is much more localised ($\nabla_I \chi(\boldsymbol{R}) \gg \nabla_I \Psi(\boldsymbol{x}, \boldsymbol{R})$), which is why the Schrödinger equation can be separated into two parts:

$$[T_e + V_{ee}(\boldsymbol{r}) + V_{Ne}(\boldsymbol{r}, \boldsymbol{R})]\Psi(\boldsymbol{x}, \boldsymbol{R}) = \epsilon_n(\boldsymbol{R})\Psi(\boldsymbol{x}, \boldsymbol{R}) \qquad (2.5)$$

$$[T_N + V_{NN}(\boldsymbol{R}) + \epsilon_n(\boldsymbol{R})]\chi(\boldsymbol{R}) \quad = E\chi(\boldsymbol{R}). \qquad (2.6)$$

The nuclear positions $\boldsymbol{R}$ enter the electronic equation (2.5) only as parameters and it is possible use the adiabatic or Born-Oppenheimer approximation. On the timescale of the nuclear motion, the electronic system is always in the instantaneous ground state; the electrons follow the ions adiabatically.

As a further approximation, the quantum effects on the motion of the nuclei are neglected and the time dependent Schrödinger equation is replaced by Newton's equations of motion:

$$\frac{\partial \boldsymbol{P}_I}{\partial t} = -\nabla_I E_0(\boldsymbol{R}) \qquad (2.7)$$

$$\text{with} \qquad E_0(\boldsymbol{R}) = \epsilon_0(\boldsymbol{R}) + V_{NN}(\boldsymbol{R}). \qquad (2.8)$$

This leads to the so called ab-initio molecular dynamics, where the (classical) forces that act on the nuclei are calculated from the electronic ground state. The ions are moved according to those forces and for this new configuration, the electronic ground state is re-calculated.

Density Functional Theory

Even after separating the nuclear motion from the Hamiltonian, solving equation (2.5) for the many-electron wave function $\Psi(\boldsymbol{x}, \boldsymbol{R})$ is impossible for most systems of interest due to the electron-electron interaction.

HOHENBERG and KOHN [47] showed that the total energy of an electron gas including exchange and correlation effects is a unique functional of the electron density. Hence the name: density functional theory (DFT). The minimal value of the functional yields the ground state energy, and the corresponding electron density is the ground state density. KOHN and SHAM [54] then showed how the many-electron problem can be replaced by an equivalent set of self-consistent single electron equations. The KOHN-SHAM energy functional for a basis of doubly occupied electronic states ψ_i

can be written as follows:

$$E[\{\psi_i\}] = 2 \sum_i \int \psi_i \left(\frac{\hbar^2}{2m} \right) \nabla^2 \psi_i \, d^3r + \int V_{Ne}(\boldsymbol{r}) n(\boldsymbol{r}) \, d^3r$$
$$+ \frac{e^2}{2} \int \frac{n(\boldsymbol{r}) n(\boldsymbol{r}')}{|\boldsymbol{r} - \boldsymbol{r}'|} \, d^3r \, d^3r' + E_{XC}[n(\boldsymbol{r})] + V_{NN}(\{\boldsymbol{R}_I\}). \tag{2.9}$$

Here, V_{NN} is the Coulomb energy between the nuclei at coordinates $\boldsymbol{R}_I$, V_{Ne} is the electron-ion potential, $n(\boldsymbol{r})$ is the electronic density given by[3]

$$n(\boldsymbol{r}) = 2 \sum_i |\psi_i(\boldsymbol{x})|^2, \tag{2.10}$$

and $E_{XC}[n(\boldsymbol{r})]$ is the so-called *exchange-correlation* functional, which is assumed to be system independent.

The wave functions ψ_i minimising the functional (2.9) are the self consistent solutions of the KOHN-SHAM equations [54]:

$$\left[\frac{-\hbar^2}{2m} \nabla^2 + V_{\text{ion}}(\boldsymbol{r}) + V_H(\boldsymbol{r}) + V_{XC}(\boldsymbol{r}) \right] \psi_i(\boldsymbol{x}) = \epsilon_i \psi_i(\boldsymbol{x}). \tag{2.11}$$

Here, V_H is the so-called Hartree potential given by

$$V_H(\boldsymbol{r}) = e^2 \int \frac{n(\boldsymbol{r}')}{|\boldsymbol{r} - \boldsymbol{r}'|} \, d^3r, \tag{2.12}$$

i.e. the Coulomb interaction between an electron at $\boldsymbol{r}$ and the electronic density around it. The exchange-correlation potential V_{XC} is formally defined as functional derivative of the exchange-correlation energy:

$$V_{XC}(\boldsymbol{r}) = \frac{\delta E_{XC}[n(\boldsymbol{r})]}{\delta n(\boldsymbol{r})} \tag{2.13}$$

Thus, the problem of interacting electrons is reduced to the solution of a system of non-interacting electrons moving in the effective potential created by the other electrons. The critical term is the exchange-correlation functional, which is not known exactly. The most basic approximation is the *Local Density Approximation* (LDA) developed by KOHN and SHAM

---

[3]The electronic density could also be specified spin dependent as $n(\boldsymbol{x})$.

[54]. In the LDA, the exchange-correlation energy per electron at coordinates $\boldsymbol{r}$, $\epsilon_{XC}(\boldsymbol{r})$, is assumed to be equal to the exchange-correlation energy in an homogeneous electron gas with the local density $n(\boldsymbol{r})$. Thus

$$E_{XC}[n(\boldsymbol{r})] = \int \epsilon_{XC}(\boldsymbol{r})n(\boldsymbol{r})\,d^3r \qquad (2.14)$$

and
$$\frac{\delta E_{XC}[n(\boldsymbol{r})]}{\delta n(\boldsymbol{r})} = \frac{\partial[n(\boldsymbol{r})\epsilon_{XC}(\boldsymbol{r})]}{\partial n(\boldsymbol{r})} \qquad (2.15)$$

with
$$\epsilon_{XC}(\boldsymbol{r}) = \epsilon_{XC}^{\text{hom}}[n(\boldsymbol{r})]. \qquad (2.16)$$

There are various parametrisations the exchange-correlation energy of a homogeneous electron gas, which all lead to similar results (e.g. PERDEW and ZUNGER, [82]).

In the *Generalised Gradient Approximation*, the exchange-correlation energy may also depend on the gradient of the spin components of the charge density:

$$E_{XC}^{GGA}[n_\uparrow, n_\downarrow] = \int d^3r \; f(n_\uparrow, n_\downarrow, \nabla n_\uparrow, \nabla n_\downarrow). \qquad (2.17)$$

This improves the description of systems with inhomogeneous charge density. The function $f(n_\uparrow, n_\downarrow, \nabla n_\uparrow, \nabla n_\downarrow)$ can be implemented in various ways, e.g. according to PERDEW and WANG (PW91) [80] or PERDEW, BURKE and ERNZERHOF (PBE) [81].

Periodic Boundary Conditions: Plane Wave Basis Set

According to Bloch's theorem, any electronic wave function in a periodic system can be separated into a plane wave and a function with the periodicity of the lattice (see e.g. [6]):

$$\psi_i(\boldsymbol{r}) = \exp(i\boldsymbol{k} \cdot \boldsymbol{r})f_i(\boldsymbol{r}) \qquad (2.18)$$

with
$$f_i(\boldsymbol{r} + \boldsymbol{l}) = f_i(\boldsymbol{r}), \qquad (2.19)$$

where $\boldsymbol{l}$ is an arbitrary lattice vector. The periodic part can then be expanded in a plane wave basis set taking reciprocal lattice vectors as wave vectors:

$$f_i(\boldsymbol{r}) = \sum_{\boldsymbol{G}} c_{i,\boldsymbol{G}} \exp(i\boldsymbol{G} \cdot \boldsymbol{r}), \qquad (2.20)$$

with
$$\boldsymbol{G} \cdot \boldsymbol{l} = 2\pi m, \; m \in \mathbb{Z}, \qquad (2.21)$$

for all lattice vectors l. The electronic wave functions in periodic systems can thus be written as a sum of plane waves:

$$\psi_i(\boldsymbol{r}) = \sum_{\boldsymbol{G}} c_{i,\boldsymbol{k}+\boldsymbol{G}} \exp[i(\boldsymbol{k} + \boldsymbol{G}) \cdot \boldsymbol{r}]. \tag{2.22}$$

Due to the periodicity one only needs to calculate the coefficients $c_{i,\boldsymbol{k}+\boldsymbol{G}}$ in the first Brillouin zone. The expansion can be discretised in reciprocal space, i.e. all calculations are performed on a discrete set of points in $\boldsymbol{k}$-space only. There are various algorithms to select these representative points, for example the one by MONKHORST and PACK [70]. The number of $\boldsymbol{k}$-points required depends on the desired precision and on the size of the system. When doubling the unit cell size, only half the number of $\boldsymbol{k}$-points is needed to cover reciprocal space with the same density. In any case calculations should be checked for $\boldsymbol{k}$-convergence by recalculating a system with a denser $\boldsymbol{k}$-point grid.

While in principle the plane wave basis set is infinite, only coefficients $c_{i,\boldsymbol{k}+\boldsymbol{G}}$ belonging to plane waves with limited kinetic energy $(\hbar^2/2m)|\boldsymbol{k} + \boldsymbol{G}|^2$ will contribute in the expansion. Because of this only plane waves with energies below the *cutoff energy* E_{cut} are used. E_{cut} has to be chosen to accommodate all oscillations occurring in the wave functions, and all calculations should be checked for cutoff energy convergence.

By inserting the plane wave basis set (2.22) into the KOHN-SHAM equations (2.11) and integrating over $\boldsymbol{r}$ one arrives at the secular equation

$$\sum_{\boldsymbol{G'}} \left[\frac{\hbar^2}{2m} |\boldsymbol{k} + \boldsymbol{G}|^2 \delta_{\boldsymbol{G}\boldsymbol{G'}} + V_{\text{ion}}(\boldsymbol{G} - \boldsymbol{G'}) + V_H(\boldsymbol{G} - \boldsymbol{G'}) + V_{XC}(\boldsymbol{G} - \boldsymbol{G'}) \right]$$
$$\cdot c_{i,\boldsymbol{k}+\boldsymbol{G'}} = \epsilon_i c_{i,\boldsymbol{k}+\boldsymbol{G}} \quad (2.23)$$

for the plane wave coefficients $c_{i,\boldsymbol{k}+\boldsymbol{G}}$. The potentials are now represented by their Fourier transforms.

Equation (2.23) is solved by diagonalising the Hamiltonian matrix, whose elements $H_{\boldsymbol{k}+\boldsymbol{G},\boldsymbol{k}+\boldsymbol{G'}}$ are given by the terms in brackets. The dimension of this matrix is finite but of course depends on the cutoff energy.

Wave function expansion by plane waves is limited to periodic systems. This has to be taken into account when studying systems that originally lack periodicity, like free surfaces, vacancies, molecules or clusters. In the plane wave formalism, those systems can only be calculated after embedding them into a periodic framework, a so called *supercell*, as shown in

(a) Vacancy   (b) Surface
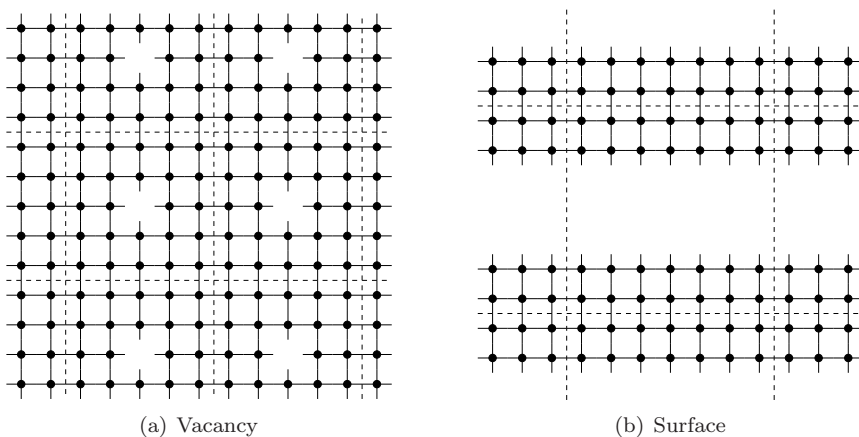
Figure 2.3: The supercells depicted here show schematically, how defects or surfaces can be embedded into a periodic superstructure, thereby transferring the problem to a periodic arrangement of free surfaces or defects. Those defects or surfaces have to be separated far enough, so that interaction with neighbouring cells can be neglected. From [11].

Fig. 2.3. The calculation of defect energy is then transferred to the calculation of a periodic arrangement of defects. The supercell has to be chosen large enough so that neighbouring surfaces or defects do not interact.

Pseudopotentials

Plane waves in general are not the optimal basis set to describe electronic wave functions. The hard[4] Coulomb potential near the nucleus tightly binds the core electrons, while the valence electrons oscillate strongly in order to keep up orthonormality to the core states. So if all electrons, including tightly bound core electrons, are to be described by plane waves, the cutoff energy E_{cut} has to be chosen so high that the size of the Hamilton matrix (2.23) involved becomes enormous, thus limiting the number of atoms that can be handled in the unit cell. The method of *pseudopotentials*

---

[4]A hard potential is characterised by a deep well with tightly bound states.
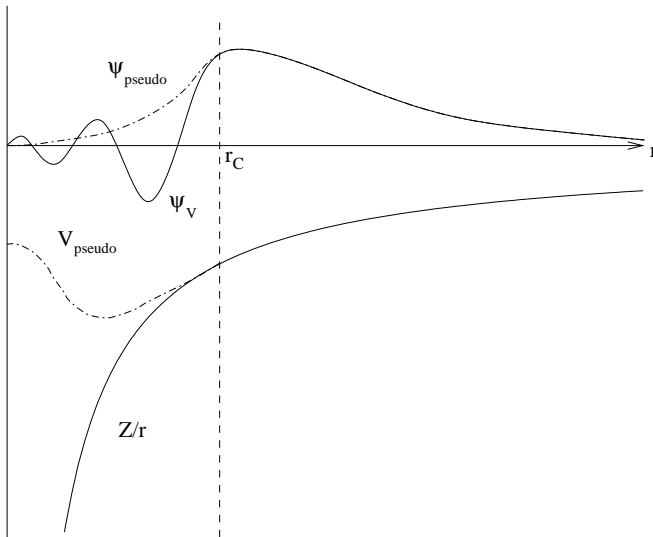
Figure 2.4: Schematic display of the pseudisation of potential and wave function. In the upper part, the oscillating real wave function of a valence electron ψ_V (solid) and the node free pseudo wave function ψ_{pseudo} (dashed) are shown. Below the hard Coulomb potential Z/r and the softer pseudopotential V_{pseudo} are shown. Outside a sphere of radius r_c pseudo and real functions agree. From [11].

first used by PHILLIPS [83] helps in treating both core states and valence states in the core region.

Material properties depend – at least at energies of interest in this publication – much more on the valence than on the core electrons. The pseudopotential method exploits this and replaces the hard potential close to the nucleus by a much softer pseudopotential. This pseudopotential now acts on the pseudo wave functions of the valence electrons instead of the ordinary wave functions of all electrons. Both pseudopotential and pseudo wave functions are displayed schematically in Fig. 2.4.

There are various conditions a pseudopotential has to fulfil: Outside a sphere with radius r_c, potential and pseudopotential have to be identical. Within the sphere, the node-free pseudo wave function shall scatter off the

pseudopotential in the same way as the real wave function scatters off the nucleus and the core electrons. The process of replacing wave functions and potentials by the respective pseudo functions is called pseudisation.

In general the phase shift valence electron wave functions get while scattering off the atomic core depends on the angular momentum l of the wave function. So the pseudopotential must also vary with l. The most general form of the pseudopotential is thus

$$V_{NL} = \sum_{lm} |lm\rangle V_l \langle lm|, \tag{2.24}$$

where the $|lm\rangle$ are the spherical harmonics and V_l the pseudopotential belonging to angular momentum l.

Pseudopotentials are generated by calculating the ground state and a few excited states of a single atom with all its electrons. The parameters of the pseudopotential (e.g. Bessel functions or spherical harmonics) are adjusted until the pseudo-calculations yields a pseudo wave function that agrees with the valence wave function outside of r_c. At the same time, pseudo and real eigenvalues have to coincide.

The advantages of pseudopotentials are obvious: Core states and hard potentials require a large cutoff energy. Once those are taken care of, E_{cut} can be reduced significantly, thereby shortening the plane wave basis set. This of course directly decreases computing time and memory requirements, making calculations with more than a few atoms possible in the first place.

In the following paragraphs a few kinds of pseudopotentials are discussed. Further information on this topic can be found in [18].

Norm-Conserving Pseudopotentials (NC-PP)   As the exchange-correlation energy of the electronic system depends on the electron density, pseudo and real wave functions must have the same charge distribution between core and outside region. In the outer region, both functions coincide. Hence the total charge density created in the core region ($r < r_c$) must be the same before and after pseudisation:

$$\int_0^{r_C} |\psi_V(r)|^2 4\pi r^2 \ dr = \int_0^{r_C} |\psi_{\text{pseudo}}(r)|^2 4\pi r^2 \ dr. \tag{2.25}$$

If additionally the logarithmic derivatives of the real and pseudo wave function and their first energy derivative agree in the outer region, it is guar-

anteed that the scattering properties of the real ion cores are reproduced as well as possible in different chemical environments [40]. This ensures optimal transferability. The downside of NC-PP is a relatively high cutoff radius and thus increased memory and CPU requirements.

Ultrasoft Pseudopotentials (US-PP) Norm conservation constrains the pseudopotentials severely, because it may require that there be a strongly peaked charge density in the core region. Thus, for many important cases, like the O $2p$ orbitals, it has been found impossible to construct a pseudopotential that allows a significant reduction of E_{cut}. VANDERBILT [105] suggested to relax the norm conservation in favour of smoother (i.e. softer) potentials. Missing charges in the interior region are compensated by additional charges at the atom locations, which in turn are pseudised again. US-PP are difficult to construct and require extensive testing [59].

Projector Augmented-Wave Method (PAW) While electronic wave functions oscillate wildly near the nuclei, they vary rather slowly in the bonding area between the atoms. This is one source of the problems related to expanding them into plane waves in the whole space. Augmented-wave methods attack this issue by separating the wave functions in two parts. The first is a partial wave expansion inside an atom-centred sphere called the augmentation region and a plane wave expansion outside. Both expansions are then matched continuously differentiable at the boundary. ANDERSEN gives an overview on these augmented-wave methods [4].

BLÖCHL [9] now postulates that there be a linear transformation from the all-electron to the pseudo wave functions. The transformation

$$|\Psi\rangle = |\tilde{\Psi}\rangle + \sum_i (|\phi_i\rangle - |\tilde{\phi}_i\rangle)\langle\tilde{p}_i|\tilde{\Psi}\rangle. \tag{2.26}$$

does just this. Here, ϕ_i are the partial waves within the augmentation regions, and $\langle\tilde{p}_i|$ is a projector with $\langle\tilde{p}_i|\tilde{\phi}_j\rangle = \delta_{ij}$. The tilde denotes quantities related to the pseudo representation.

The real (all-electron) valence wave functions (and other physical quantities) are obtained by subtracting from the the pseudo quantities the pseudo contributions and adding the all-electron part. The PAW method also yields information on the core electrons; the nodal structure of the valence wave function is maintained.

KRESSE and JOUBERT [59] establish a formal link between PAW and US-PP and describe, how the PAW method can be implemented into existing pseudopotential code. In general, it is less complicated to generate a transferable PAW dataset compared to a ultrasoft pseudopotential. Whichever pseudopotential method one prefers: Large scale first principles calculations are impossible without them.

Improved Calculation Methods

Finding a solution to the KOHN-SHAM equations (2.11) is for large systems unfortunately not as straightforward as it might seem. Even with pseudopotentials, around 100 plane waves per atom are required. As the computational effort for inversion of the Hamilton matrix in the secular equation (2.23) increases with the third power of the dimension and storage space with the second, it is absolutely necessary to improve the algorithms for more than a few tens of atoms in the unit cell. In the following, three methods are outlined. All of them do not require the explicit storage of the Hamilton matrix.

Car-Parinello Molecular Dynamics   CAR and PARINELLO [14] suggest to treat the wave functions as dynamic variables. After expanding the wave functions ψ_i into plane waves

$$\psi_i = \sum_n c_{in}\phi_n, \tag{2.27}$$

the KOHN-SHAM functional can be written depending on these parameters c_{in}, similar to the energy of a system of classical particles depending on their positions R_i. To minimise the functional, methods from classical molecular dynamics (cf. Sec. 2.2.3) to find the ground state configuration of a many-body systems can be applied. A fictitious mass μ is attached to each coefficient, and constraints are implemented through Lagrangian multipliers. Then, the equations of motion are integrated with damping, and the potentials are adjusted to the current charge density after each step, until the self-consistent solution of the KOHN-SHAM equations is obtained. This method is described in more detail in [78].

Direct Minimisation   The KOHN-SHAM energy functional can be minimised directly, using e.g. a conjugate gradient (CG) algorithm. Here, the

functional is minimised along a given search directly exactly, and the direction for the next step is chosen conjugate to previous search directions. The downside of this method is that it is rather difficult to maintain wave function orthonormality. Additionally, only one electronic band can be optimised at a time due to memory constraints. This slows down the method considerably.

Improved Self-Consistency Methods All self-consistency cycle (SC) methods share the basic self-consistency loop: Starting from a set of trial wave functions and the associated charge density, the Hartree and exchange-correlation potentials are calculated. The trial wave functions are then improved and finally new wave functions are created by mixing the starting and the improved wave functions, which are then used in the next loop as starting point.

Two methods for the iterative improvement of the trial wave functions are mentioned here: The residual minimisation method by direct inversion in the iterative subspace (RMM-DIIS) [86] and the blocked (i.e. several orbitals are improved at once) Davidson method (DAV2) [21]. Both algorithms avoid the inversion of the Hamilton matrix, and arrive at a self-consistent solution faster compared to conjugate gradient or CAR-PARINELLO methods. Additionally, RMM-DIIS keeps operations that grow with the third power of the system size very small, so that up to 1000 electrons per unit cell the computer effort scales as $O(N^2)$. More information about SC methods can be found in the article by KRESSE and FURTHMÜLLER [56].

Calculation of atomic forces

In general, the force $\boldsymbol{F}_I$ acting on atom I at coordinates $\boldsymbol{R}_I$ can be calculated as the derivative of the energy in respect to the atomic coordinates:

$$
\begin{aligned}
-\boldsymbol{F}_I = \nabla_I E_0(\boldsymbol{R}) &= \frac{\partial}{\partial \boldsymbol{R}_I} \langle \Psi_0(\boldsymbol{R})|H(\boldsymbol{R})|\Psi_0(\boldsymbol{R})\rangle \\
&= \langle \nabla_I \Psi_0|H|\Psi_0\rangle + \langle \Psi_0|\nabla_I H|\Psi_0\rangle + \langle \Psi_0|H|\nabla_I \Psi_0\rangle.
\end{aligned}
\tag{2.28}
$$

Using the HELLMANN-FEYNMAN theorem [30], this expression can be simplified dramatically: $|\Psi_0\rangle$ is an eigenstate of the Hamiltonian, so $H|\Psi_0\rangle = E|\Psi_0\rangle$. The sum of the first and the last term in the force equation (2.28) is

thus $E\nabla_I\langle\Psi_0|\Psi_0\rangle = 0$ due to the normalisation of $\langle\Psi_0|\Psi_0\rangle$. What remains is

$$- \boldsymbol{F}_I = \langle\Psi_0(\boldsymbol{R})|\nabla_I H(\boldsymbol{R})|\Psi_0(\boldsymbol{R})\rangle. \qquad (2.29)$$

The stress tensor can be treated in a similar way.

If stresses and forces are to be calculated with first-principles methods, the ground state needs to be known with relatively high precision. Deviations from the ground state of the wave functions enters the energy in second order only, while acting in first order on the forces calculated with the HELLMANN-FEYNMAN theorem.

2.2.2 Effective Potentials

Ab-initio or first principles calculations as described in the previous section can be performed with impressive success. Unfortunately, even with the most advanced computer systems, these methods are limited to a few thousand atoms at most. The memory demands and computational time scale very unfavourable with system size ($O(N^3)$) for larger systems.

Usually, information on the *electronic* structure is not necessary to follow processes and study mechanical properties at an *atomic* scale, especially as the electronic structure depends parametrically on the atomic positions according to the Born-Oppenheimer approximation. Removing the electrons from the calculation (and thus getting rid of most of the particles) would allow much larger simulations. To do just that one must write the energy of the system as a function of the atomic positions only. This is achieved by replacing the interatomic Coulomb potential by an *effective potential* that includes all interactions and energy contributions from the electrons. The energy in the nuclear equation of motion (2.8) then becomes

$$E_0 = V_{\text{eff}}(\{\boldsymbol{R}\}). \qquad (2.30)$$

As electronic coordinates are of no further importance, I will write atomic coordinates (in agreement with literature on effective potentials and molecular dynamics simulations) as a lower case letter $\boldsymbol{r}$ from now on.

In most cases, effective potentials do not depend on the full set $\{\boldsymbol{r}\}$ of atomic coordinates, but only on much simpler subsets, like for example pair distances. In the following sections I will describe some of the most common types of effective potentials.

Pair Potentials

In general, the potential energy of a system of n particles can be expanded into multibody contributions:

$$V_{\text{eff}}(\{\boldsymbol{r}\}) = \sum_i \phi_1(\boldsymbol{r}_i) + \frac{1}{2} \sum_{\substack{i,j \\ i \neq j}} \phi_2(\boldsymbol{r}_i, \boldsymbol{r}_j) + \frac{1}{6} \sum_{\substack{i,j,k \\ i \neq j \neq k \\ i \neq k}} \phi_3(\boldsymbol{r}_i, \boldsymbol{r}_j, \boldsymbol{r}_k) + \dots \quad (2.31)$$

The first term is an external potential depending on the coordinates of each atom only. The second term is the pair term, then comes the three body term and so on.

For pair potentials, the second term of this series is now isolated. In the scope of this work, pair potentials are assumed to be isotropic and homogeneous, i.e. the dependence on the atom coordinates is restricted to pair *distances* $r_{ij} = |\boldsymbol{r}_i - \boldsymbol{r}_j|$ only. Pair potentials are probably the potentials that are most easily handled. The interaction between two particles is a function of their distance r and may depend on the species of atoms involved. The potential energy of a system described by pair potentials is thus

$$V(\{\boldsymbol{r}\}) = \frac{1}{2} \sum_{\substack{i,j \\ i \neq j}} \phi_{ij}(r_{ij}), \qquad i,j = 1, \dots, n, \quad (2.32)$$

where the pair potential ϕ_{ij} only depends on the *species*[5] of atoms i and j. The sum runs over all pairs of atoms (i,j) with $i \neq j$ and the factor $\frac{1}{2}$ takes into account that each pair is summed over twice.

Without loss of generality, the pair potential function ϕ_{ij} is symmetric in its indices, i.e. $\phi_{ij}(r_{ij}) = \phi_{ji}(r_{ji})$. If ϕ_{ij} and ϕ_{ji} were to differ, they can be symmetrised without changing the physics:

$$\phi_{ij}^* = \phi_{ji}^* := \frac{1}{2}(\phi_{ji} + \phi_{ij}). \quad (2.33)$$

The force $\boldsymbol{F}$ acting on atom i is determined by the gradient ∇_i of the energy with respect to the position $\boldsymbol{r}_i$ of that atom. Applying the chain

---

[5]Most correctly, one should write $\phi_{s_i s_j}$ to represent the dependence on species s only. For reasons of simplicity, the s is omitted from all future interaction functions. Please remember that all functions depend on atom type only, not on individual atoms

rule to (2.32), one obtains the p component ($p \in \{x, y, z\}$) of the force on atom i, F_{i_p}, as

$$F_{i_p} = -\sum_{j \neq i} \frac{\partial}{\partial x_{i_p}} \phi_{k_i k_j}(r_{ij}) = -\sum_{j \neq i} \left(\frac{(\boldsymbol{x}_j - \boldsymbol{x}_i)_p}{r_{ij}} \cdot \phi'_{k_i k_j}(r_{ij}) \right). \quad (2.34)$$

Here, $(\boldsymbol{x}_j - \boldsymbol{x}_i)_p$ is the p component of the distance vector between atoms i and j. Primes mark differentiated functions.

To calculate the total energy, the forces on each atom and the stresses on the unit cell, one only needs to sum once over all pairs of atoms. This makes pair potentials the most simple of all interaction potentials, but still many systems can be described rather well with pair potentials, e.g. noble gas solids. Further information on pair potentials and their application in Molecular Dynamics simulation can be found in the book from ALLEN and TILDESLEY [2].

Deficiencies of Pair Potentials Pure pair potentials of the form (2.32) treat all bonds of an atom separately. If two crystal structures of an element differed only by the coordination number Z of an atom, then pair potentials would always favour the structure with the larger Z, because the cohesive energy is proportional to the coordination number. In reality, the energy should rather scale with $Z^{1/2}$ [41], as additional bonds will contribute less and less to the cohesion.

Less easy to see is that a pair potential solid will always satisfy the Cauchy relation $C_{12} = C_{44}$ [29], which is well satisfied for solid noble gases. However, in noble metals $\frac{C_{12}}{C_{44}}$ can reach values of up to 3.7. The vacancy formation energy shows similar discrepancies: While this energy is equal to the cohesive energy in pair potential solids, it is between 25 and 40 percent of that in metals, and even less in gold. Also, the ratio of melting temperature and cohesive energy is much too low in pair potential solids [23]. In a similar vein, free surfaces relax outward with pair potentials (instead of inward as in reality), which leads to an increased evaporation rate.

Summarising, simple pair potentials have deficiencies in the description of metals. The interaction in those materials apparently has multi-body contributions that two-body potentials cannot reproduce.

Embedded Atom Method (EAM) Potentials

With pair potentials (2.32), the energy of an atom depends linearly on its neighbourhood, i.e. with n neighbours in a distance r, the energy is equal to n times the energy of an atom with a single neighbour. In contrast, EAM potentials allow non-linear relationships. Here, the neighbourhood of atom i is characterised by a scalar n_i. Each surrounding atom j in a distance r_{ij} contributes to n_i an amount $\rho_{ij}(r_{ij})$. Often, this transfer is identified with the contribution of atom j to the electronic density at the site of atom i. All these contributions are summed up and an energy $U_i(n_i)$ is assigned to the atom; the atom is embedded into the local surroundings. Hence, this potential model was named *Embedded Atom Method* (EAM) by DAW and BASKES [22], who used it to describe embrittlement of metals through hydrogen.

The roots of EAM lie in the density functional theory. HOHENBERG and KOHN showed that the energy is a functional of the total electron density [47]. STOTT AND ZAREMBA later added, that the embedding energy of an impurity atom depends on the electron density without this atom [97]. In EAM, each atom is treated as an impurity atom which is embedded into the host crystal consisting of the other atoms, just with radially symmetric transfer functions.

In EAM, the embedding function U links the cohesive energy to the local density created by the transfer functions ρ:

$$V = \sum_i U_i(n_i), \qquad (2.35)$$

$$\text{where} \qquad n_i = \sum_{j \neq i} \rho(r_{ij}), \qquad i, j = 1, \dots, N. \qquad (2.36)$$

Here, the embedding function U_i depends on the species of the embedded atom and the transfer function ρ_j on the species of the donating atom.

To account for the nuclear repulsion, DAW and BASKES also introduced a pair potential, which is combined with the embedding term to form the full EAM potential:

$$V = \sum_{i,j<i} \phi_{ij}(r_{ij}) + \sum_i U_i(n_i), \qquad i, j = 1, \dots, N, \qquad (2.37)$$

where n_i is the "local density" given by (2.36). While the original authors of EAM identify this density n_i with the local electronic density, and the pair

term in (2.37) with the actual screened nuclear Coulomb interaction, there is the alternative view to take this model as an empirical description of an isotropic multi-body interaction that is easy to compute. Potentials in the latter context are often called glue potentials. In this work, all potentials that have the functional form (2.37) are called EAM potentials or glue potentials independent of any interpretation of the functions involved.

The potential model derived by FINNIS and SINCLAIR [31] also shares the functional form of the glue potentials. It is however not based on density functional theory like EAM, but on the tight binding method. In Finnis-Sinclair potentials the embedding function is taken to be proportional to $\sqrt{n}$ to mimic the results of tight binding theory.

Potentials of the form (2.37) show some remarkable invariance properties. In monatomic systems, the EAM potential is invariant under the transformation

$$
\begin{aligned}
\phi(r) &\rightarrow \phi(r) + 2\lambda\rho(r) \\
U(n_i) &\rightarrow U(n_i) - \lambda n_i, \qquad \text{with} \quad n_i = \sum_{j \neq i} \rho(r_{ij}),
\end{aligned} \tag{2.38}
$$

where λ is an arbitrary real number [29]. This implies that any linear embedding function U can be replaced entirely by pair potentials. More importantly, U and ϕ cannot be determined uniquely, as one can always shift an energy contribution linear in n from one function to the other. Thus one can also not assign any separate physical meaning (like electron density) to each of the functions separately, which justifies calling all potentials of this form by the same names. Additionally, only those quantities can be physically relevant, that are invariant under (2.38).

For more than one atom species, (2.38) turns into

$$
\begin{aligned}
\phi_{ij}(r) &\rightarrow \phi_{ij}(r) + \lambda_i \rho_j(r) + \lambda_j \rho_i(r) \\
U_i(n_i) &\rightarrow U_i(n_i) - \lambda_i n_i,
\end{aligned} \tag{2.39}
$$

with one λ_i for each atomic type [11].

The other, more obvious invariance is

$$
\begin{aligned}
\rho(r) &\rightarrow \kappa\rho(r) \\
U(n_i) &\rightarrow U(\tfrac{n_i}{\kappa}),
\end{aligned} \tag{2.40}
$$

which implies that the total density n_i can be scaled arbitrarily. In systems with more than one atom species, *all* transfer functions have to be scaled simultaneously, as the ratio between them has to stay fixed.

Therefore, in systems with k different atom types, there are $k + 1$ gauge degrees of freedom. When comparing potentials these invariances need to be fixed. Usually one requires the gradient of the embedding functions U_i to vanish at a certain n_0, most times at the average density $n_{i,\mathrm{avg}}$ for atom type i. Additionally, the transfer functions must be scaled so that the total density takes a fixed value in defined conditions, for example $n_{i,\mathrm{avg}} = 1$ for one atom species i.

Glue potentials require slightly more computational effort than pair potentials. The atomic forces resulting from the embedding term are again calculated from the gradient of the energy:

$$F_{i_p} = -\sum_{j \neq i} \left(U_i'(n_i) \rho_j'(r_{ij}) + U_j'(n_j) \rho_i'(r_{ij}) \right) \frac{(\boldsymbol{x}_j - \boldsymbol{x}_i)_p}{r_{ij}}. \qquad (2.41)$$

To establish forces, one needs to loop twice over all pairs of neighbours. In the first loop the transfer densities are calculated and the pair potential contributions to forces and energy are determined. In the second loop (2.41) is added. In total, EAM calculations are slower by a factor of about two [35].

The additional effort is justified: Many metallic systems that can not satisfactorily be described by pair potentials are accessible to molecular dynamics simulations with EAM potentials. More information on the Embedded Atom Method can be found in the review paper by DAW, FOILES and BASKES [23]. There, the authors also list more cases of successful application of EAM potentials, like phonons, grain boundaries, surfaces, alloys and mechanical properties.

Other Potential Models

Both EAM and pair potentials fail in the description of non-isotropic interactions. While EAM does account for many-body interactions, it is still perfectly spherical and thus cannot be used to simulate the effects of directed bonds. There are potential classes that do account for those, some of which were applied to metallic systems and are sketched below.

Modified Embedded Atom Method (MEAM) To describe shear elasticity in Silicon, BASKES [7] modifies the EAM method by adding an angular dependent term to the density n_i:

$$\tilde{n}_i = \sum_{j \neq i} \rho(r_{ij}) - a \sum_{\substack{j \neq i \\ k \neq i}} (1 - 3\cos^2 \theta_{jik}) \rho(r_{ij}) \rho(r_{ik}), \qquad (2.42)$$

where θ_{jik} is the angle enclosed by atoms j, i and k, and a is an empirical quantity to be determined from the shear moduli. This density $\tilde{n}_i$ is then used to calculate the energy (cf. (2.37))

$$V = \frac{1}{2} \sum_{i \neq j} \phi(r_{ij}) + \sum_i U(\tilde{n}_i). \qquad (2.43)$$

Due to the summation over triplets of atoms this method is computationally much more demanding and usually requires greater changes when implemented into an existing MD code.

Angular-Dependent Potentials (ADP) In [69], MISHIN *et al.* propose a different (M)EAM-inspired potential, where the total energy in an orthogonal Cartesian system is given by

$$V = \frac{1}{2} \sum_{i \neq j} \phi(r_{ij}) + \sum_i U(n_i) + \frac{1}{2} \sum_{i,\alpha} (\mu_i^\alpha)^2 + \frac{1}{2} \sum_{i,\alpha,\beta} (\lambda_i^{\alpha\beta})^2 - \frac{1}{6} \sum_i \nu_i^2. \ (2.44)$$

The first two terms are the standard glue potentials from (2.37). The following three terms introduce non-isotropic components through the vectors

$$\mu_i^\alpha = \sum_{j \neq i} u_{ij}(r_{ij}) r_{ij}^\alpha \qquad (2.45)$$

and tensors

$$\lambda_i^{\alpha\beta} = \sum_{j \neq i} w_{ij}(r_{ij}) r_{ij}^\alpha r_{ij}^\beta. \qquad (2.46)$$

The quantities ν_i are traces of the tensors $\lambda_i^{\alpha\beta}$:

$$\nu_i = \sum_\alpha \lambda_i^{\alpha\alpha}. \qquad (2.47)$$

In the equations above, α and β represent the Cartesian coordinates x, y or z. The quantities μ and λ are measures of the dipole and quadrupole distortion of the local environment of atom i. In MEAM, these and higher order multipoles are represented through the angular dependent density, while in ADP they contribute directly to the energy. The terms can be linked to MEAM by an expansion of the embedding energy in the multipole contribution to the density cut off after the quadrupole term.

ADP potentials can be implemented much easier into existing MD codes at a cost of factor two in computational effort compared to EAM. Expressions for the forces are given in [69].

Transferability

Effective potentials are inherently less general than DFT calculations. The ideal effective potential is completely transferable, i.e. it works correctly in all imaginable situations. In reality, effective potentials only have a limited application range (crystal structure, composition, pressure, temperature) and will not yield correct results beyond that range. For example, potentials that can describe elemental solids will fail when combined to simulate a compound of different elements. Usually, there is a trade-off between precision and transferability: Potentials that cover a wide domain are often less precise under certain conditions than a special potential for this situation. Using a potential beyond its transferability range might lead to incorrect results and simulation artefacts and should be avoided.

When generating potentials with force matching (cf. Sec. 2.3), transferability becomes a very important issue. There, the application range can be controlled directly through the selection of reference configurations, which allows the generation of highly specialised potentials with limited transferability on one hand and more general potentials on the other hand. More information can be found in Sec. 2.3.2.

2.2.3 Classical Molecular Dynamics

Molecular Dynamics (MD) is a simulation method, where the Hamiltonian equations of motion are integrated simultaneously for a set of atoms. The forces in these equations can either be derived from first-principles calculations (see Sec. 2.2.1), in which case one speaks of ab-initio MD, or from
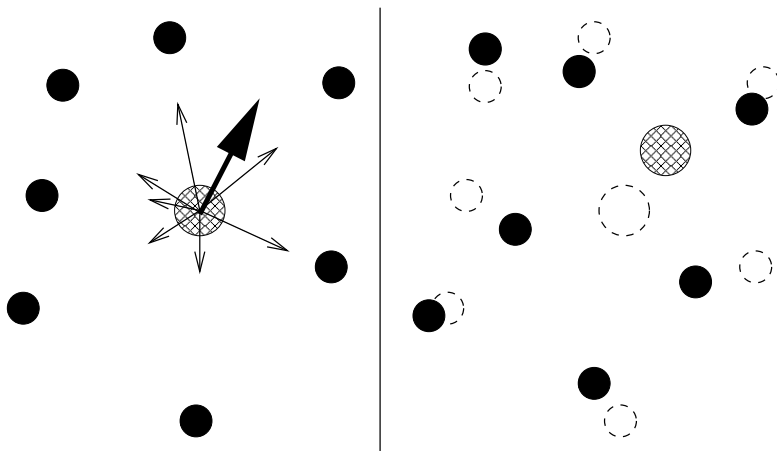
Figure 2.5: In MD simulations, the forces on the atoms are calculated at their instantaneous positions (shown here for the hatched atom). The left side shows the atoms at t_0. The thin arrows represent the forces created by the individual neighbours, the thick arrow shows the resulting force. On the right the situation is shown at $t_0 + \Delta t$: All atoms were advanced simultaneously. From [11].

effective potentials (see Sec. 2.2.2), which is called classical MD. Unless specified otherwise, MD in this publication refers to the latter method.

The N-particle Hamiltonian equations of motion form a $6N$-dimensional system of first order differential equations that in general cannot be solved exactly. Instead the equations are discretised in time: For a configuration (coordinates and momenta) at time t_0 and a potential, the forces on the atoms are calculated and the atom positions and momenta are adjusted accordingly for $t_0 + \Delta t$. This is shown schematically in Fig. 2.5. There are well-known algorithms for the numerical integration of a system of first-order differential equations, like the Gauss, Runge-Kutta or Verlet algorithms. These algorithms are well documented in any numerical mathematics textbook (e.g. [15]); for notes on the implementation see PRESS *et al.* [85].

Integrating the Hamilton equations in their standard form conserves number of particles, volume, and energy of the system (NVE); this is equiv-

alent to the microcanonical ensemble of statistical physics. By coupling the simulation to an external heat reservoir one can keep the temperature constant instead of the energy (NVT), which is equivalent to the canonical ensemble [72]. The system can similarly be coupled to a volume reservoir to arrive at the constant pressure constant temperature (NPT) ensemble.

Molecular Dynamics algorithms can also be used to find the ground state of a system. To arrive at this state as fast as possible, one can take kinetic energy out of the system by either setting the atom velocities of those atoms to zero that move uphill in the potential landscape (microconvergence), or by stopping all atoms, when the system as a whole moves against the potential gradient (i.e. the scalar product between all momenta and all forces is negative).

Boundary conditions can be chosen arbitrarily. Most common are periodic boundaries for the simulation of bulk material or open boundary conditions for single molecules or clusters. Free surfaces or fracture simulations are often treated in a combination of those, e.g. the system is periodic along the surface but non-periodic in the normal direction.

The computational effort of simultaneously integrating the equations of motion of thousands of particles is not to be neglected, and so it is not surprising that MD methods came into fashion with the availability of more and more powerful computer systems. MD simulations are most effective, when the range of the interactions is limited to a cutoff radius r_c, thus limiting the number of neighbours an atom is interacting with. Then the computational effort in pair or EAM potential simulations scales linearly with system size, compared to $O(N^2)$ for potentials with infinite range. Very large simulation cells (10^9 atoms or more) can be realised through parallelisation. The system is split in cells, so that an atom only interacts with atoms in the same or in neighbouring cells. These cells are then distributed to several communicating processes, thereby dividing the problem into handy chunks [96].

Limited range potentials are a good approximation for most metallic solids. Long-range interactions, like the Coulomb interaction in ionic solids, have to be treated separately, e.g. with the Ewald summation technique, before efficient simulation is possible.

The quality and validity of MD simulations crucially depends on the interaction potentials used. Many model systems were treated with toy potentials (like the well-known Lennard-Jones potential used far beyond its validity) for lack of realistic interaction potentials. The method of force

matching as described in the following section is an elegant way to provide MD simulations with such physically justified potentials.

More information on Molecular Dynamics can be found in the book of ALLEN and TILDESLEY [2].

2.3 Force Matching

As described above, classical MD calculations require effective potentials, which for many simple materials are matched to well-known experimental values. For structurally or chemically complex materials, there are generally more potential parameters to be determined, and the number of usable experimental measurements does not cover the increased need for data. In some cases, the exact structure and composition of the samples is not even known reliably, thus making it difficult to infer the potentials from the measurements.

Here, ab-initio calculations open the door to a modified approach. The experimental data a potential is matched against is supplemented or replaced by values from first-principles DFT calculations. By including information like cohesive energies and forces from a set of reference configurations, potentials for both simple and complex materials can be put on a solid physical base. The vastly increased number of reference information additionally allows more flexible potentials compared to the experimental approach, where only few parameters can be determined reliably.

The method of including forces from ab-initio calculations in the potential generation is called *Force Matching* and was first described by ERCO-LESSI and ADAMS [28], where it was used to determine a glue potential for Aluminium. In the following section, this method is described in detail.

To determine a potential with force matching one needs first a potential model, where the potential is given by a set of n parameters ξ_i. These parameters might be the values of the potential functions at sampling points or parameters of an analytic potential. This set $\boldsymbol{\xi}$ is then adjusted to optimally reproduce quantities calculated from DFT in a number of reference calculations. This optimisation is realised by minimising the sum of squares of the deviations between reference values and those calculated from the potential.

The function to be minimised is the so-called target function $Z(\boldsymbol{\xi})$ defined

as

$$Z(\boldsymbol{\xi}) = Z_F(\boldsymbol{\xi}) + Z_C(\boldsymbol{\xi}), \tag{2.48}$$

where

$$Z_F(\boldsymbol{\xi}) = \sum_{k=1}^{m} u_k (F_k(\boldsymbol{\xi}) - F_k^0)^2, \tag{2.49}$$

$$Z_C(\boldsymbol{\xi}) = \sum_{r=1}^{N_c} w_r (A_r(\boldsymbol{\xi}) - A_r^0)^2. \tag{2.50}$$

Here, the index k in Z_F, the sum of reference contributions to the target function, runs over all reference information, be it cohesive energies, force vector components or entries of the stress tensor. F_k^0 are the reference values and $F_k(\boldsymbol{\xi})$ the corresponding values calculated from the potential, and the u_k are the weights attached to each contribution to Z_F. Additional minimisation criteria are accounted for in Z_C, where $A_r(\boldsymbol{\xi})$ is the actual and A_r^0 the nominal value of a quantity, the importance of which is controlled by the weights w_r. These additional contributions can be used to implement constraints on the potential functions, like for example fixing the gauge degrees of freedom of glue potentials (see Sec. 2.2.2, Eq. (2.38)).

The target function $Z(\boldsymbol{\xi})$ is then optimised. As the evaluation of the target function is quite costly, the algorithms used must be efficient to reduce computing time. A selection of suitable algorithms is described in section 2.3.1.

Crucial for the quality of force matched potentials is the selection of reference configurations. Methods to generate and pick these configurations sensibly are covered in section 2.3.2. The third ingredient of successful force matching is a suitable potential model and representation; section 2.3.3 elaborates on this topic.

2.3.1 Optimisation

Few mathematical topics have such a widespread effect on many subjects in science and engineering like optimisation. Finding the optimal order of conductors on a chip, the optimal reaction conditions in a chemical plant or the optimal curve to represent a series of measurements: One always

searches for the best solution. This is of course also the case for finding the optimal potential that yields the correct forces, stresses and energies in molecular dynamics simulation.

For quantitative treatment of an optimisation problem one defines a target function Z, which is a function of the parameters ξ_i (reaction conditions, function parameters, ...) of the problem. Without loss of generality, the minimum of the target function solves the optimisation problem, thereby reducing it to minimising a function of several variables – a well-known task with many well-documented algorithms.

Method of Least Squares   Force Matching is closely related to determining the parameters ξ_i, $i = 1, \ldots, n$ of a parametrised function $f_{\{\xi_i\}}(x)$ from a series of m measurements, with $m \gg n$:

$$f_{\{\xi_i\}}(x_j) = y_j, \quad j = 1, \ldots, m. \tag{2.51}$$

Due to measurement errors, this system can generally not be solved exactly. The best solution minimises the deviations of the particular measurements from the function. The definition of those deviations is far from trivial, but if one assumes the measurement errors to be independent, then using the squares of the differences between measurement and function is the method of choice. This is called the method of least squares and goes back to C.F. Gauss. In a further refinement one may assign a weight w_j to measurement j. Then the target function becomes

$$Z(\{\xi_i\}) = \sum_{j=1}^{m} w_j \left(f_{\{\xi_i\}}(x_j) - y_j \right)^2, \quad i = 1, \ldots, n. \tag{2.52}$$

If the function $f_{\{\xi_i\}}(x)$ in Eq. (2.51) depends linearly on the parameters ξ_i, i.e.

$$f_{\{\xi_i\}}(x) = \sum_{i=1}^{n} c_i(x)\xi_i, \tag{2.53}$$

then the solution of the linear least square problem is reduced to the solution of a linear system of equations. The deviation of a measured value y_j from $f_{\{\xi_i\}}(x_j)$ is the so-called residue r_j. An overdetermined system of m equations in n variables ξ_i is defined as

$$\sum_{i=1}^{n} c_i(x_j)\xi_i - y_j = r_j, \tag{2.54}$$

or in matrix notation

$$\mathbf{C}\boldsymbol{\xi} - \boldsymbol{y} = \boldsymbol{r}, \quad \mathbf{C} \in \mathbb{R}^{m \times n},\ \boldsymbol{\xi} \in \mathbb{R}^n,\ \boldsymbol{y}, \boldsymbol{r} \in \mathbb{R}^m. \qquad (2.55)$$

These are the so-called error equations. The objective is now minimising the squares of the residues r_j, which is just the Euclidian norm $|\boldsymbol{r}|^2$ of the vector $\boldsymbol{r}$. This is equivalent to solving the linear system of equations

$$\mathbf{A}\boldsymbol{\xi} + \boldsymbol{b} = 0, \quad \text{where } \mathbf{A} := \mathbf{C}^T \mathbf{C} \in \mathbb{R}^{n \times n},\ \boldsymbol{b} := -\mathbf{C}^T \boldsymbol{y} \in \mathbb{R}^n. \qquad (2.56)$$

The above equations are the normal equations to the error equations (2.55).

There are various efficient numerical implementations of the linear least squares problem. Unfortunately, force matching is a highly nonlinear problem, and the minimum can only be obtained in an iterative fashion. Two methods that were implemented in this work and are described below.

Minimisation without Derivatives According to Powell Even if the minimum of a function of many variables cannot be obtained in a single calculation, it is usually possible to iteratively improve a starting point until one arrives at an extremal position. The most basic way to do this is following the gradient of the target function to the minimum. Starting at $\boldsymbol{\xi}_0$, the negative gradient vector $\boldsymbol{g}_0 = -\nabla Z(\boldsymbol{\xi})|_{\boldsymbol{\xi}=\boldsymbol{\xi}_0}$ of the target function is calculated at $\boldsymbol{\xi}_0$. The next point $\boldsymbol{\xi}_1$ is at the minimum of $Z(\boldsymbol{\xi})$ along the straight line through $\boldsymbol{\xi}_0$ with the direction vector $\boldsymbol{g}_0$. Algorithms for one-dimensional minimisation are described below. At $\boldsymbol{\xi}_1$, the gradient of $Z(\boldsymbol{\xi})$ is evaluated again and a new search direction is chosen. As each step always goes parallel to the negative gradient of the target function, this is called the method of steepest descent.

Though this method is simple to understand, it is quite inefficient in the number of iteration steps. Consecutive gradients $\boldsymbol{g}_i, \boldsymbol{g}_{i+1}$ are perpendicular $(\boldsymbol{g}_i \cdot \nabla Z(\boldsymbol{\xi})|_{\boldsymbol{\xi}=\boldsymbol{\xi}_0} = 0$, otherwise $\boldsymbol{\xi}_{i+1}$ would not be at the minimum of Z along $\boldsymbol{g}_i$), and the minimisation along $\boldsymbol{g}_{i+i}$ will generally break the optimisation in the direction of $\boldsymbol{g}_i$. In unfortunate target function landscapes this might lead to a large number of inefficient steps.

The method of conjugate gradients (CG) avoids this by choosing a new gradient direction $\boldsymbol{g}_i$ in a way that will not disturb earlier minimisation

steps. At the point $\boldsymbol{\xi}_i$, the Taylor expansion of Z is

$$Z(\boldsymbol{x}) = Z(\boldsymbol{\xi}_i) + \sum_l \frac{\partial Z}{\partial x_l} x_l + \frac{1}{2} \sum_{l,m} \frac{\partial^2 Z}{\partial x_l \partial x_m} x_l x_m + \dots \quad \text{with} \quad \boldsymbol{x} = \boldsymbol{\xi} - \boldsymbol{\xi}_i,$$
(2.57)

$$\approx c \quad - \boldsymbol{b} \cdot \boldsymbol{x} \quad + \frac{1}{2} \, \boldsymbol{x}^T \cdot \mathbf{A} \cdot \boldsymbol{x}, \tag{2.58}$$

where

$$c \equiv Z(\boldsymbol{\xi}_i), \qquad \boldsymbol{b} \equiv -\nabla Z|_{\boldsymbol{\xi}_i}, \qquad [\mathbf{A}]_{lm} \equiv \left.\frac{\partial^2 Z}{\partial x_l \partial x_m}\right|_{\boldsymbol{\xi}_i}. \tag{2.59}$$

The matrix $\mathbf{A}$ is the Hessian of Z in $\boldsymbol{\xi}_i$. In the approximation (2.58), the gradient is

$$\nabla Z = \mathbf{A} \cdot \boldsymbol{x} - \boldsymbol{b}. \tag{2.60}$$

When moving by $\delta \boldsymbol{x}$, the change in the gradient is

$$\delta(\nabla Z) = \mathbf{A} \cdot (\delta \boldsymbol{x}). \tag{2.61}$$

As $\boldsymbol{\xi}_i$ is at the minimum of the target function along $\boldsymbol{g}_{i-i}$, the condition that motion along the new direction $\boldsymbol{g}_i$ conserve this optimum is equivalent to demanding the gradient of Z remain perpendicular to $\boldsymbol{g}_{i-1}$ during that motion. This implies that the also change of the gradient be perpendicular to $\boldsymbol{g}_i$, or

$$0 = \boldsymbol{g}_{i-1} \cdot \delta(\nabla Z) = \boldsymbol{g}_{i-1} \cdot \mathbf{A} \cdot \boldsymbol{g}_i. \tag{2.62}$$

Directions that fulfil (2.62) are called *conjugated*. n pairwise conjugated vectors spanning the $\mathbb{R}^n$ form a conjugated basis. If the approximation (2.58) is exact (i.e. Z is a quadratic form), the minimum of Z will be acquired after n steps along the conjugated basis directions. Otherwise, this method ensures quadratic convergence towards the minimum. Many well-documented implementations of this minimisation algorithm (see e.g. [85]) do neither take into account the special form of Z in the case of Force Matching (being a sum of squares) nor the high cost involved in calculating the gradient of Z.

A target function of the functional form (2.52) can also be written as

$$Z(\boldsymbol{\xi}) = \sum_{k=1}^m [f^{(k)}(\boldsymbol{\xi})]^2, \tag{2.63}$$

where the $f^{(k)}$ represent the various functions, whose squares contribute to the sum. The vector $\boldsymbol{\xi}$ formed by the parameters ξ_i has dimension n. The first and second derivatives of the $f^{(k)}$ will be written as follows:

$$g_i^{(k)}(\boldsymbol{\xi}) \quad = \quad \frac{\partial}{\partial \xi_i} f^{(k)}(\boldsymbol{\xi}) \tag{2.64}$$

$$\text{and} \quad G_{ij}^{(k)}(\boldsymbol{\xi}) \quad = \quad \frac{\partial^2}{\partial \xi_i \partial \xi_j} f^{(k)}(\boldsymbol{\xi}). \tag{2.65}$$

Let $\boldsymbol{x}$ be an approximation to the minimum at $\boldsymbol{x} + \boldsymbol{\delta}$. The derivative of (2.63) vanishes at the minimum:

$$\sum_{k=1}^{m} g_i^{(k)}(\boldsymbol{x} + \boldsymbol{\delta}) \cdot f^{(k)}(\boldsymbol{x} + \boldsymbol{\delta}) = 0 \qquad i = 1, \ldots, n. \tag{2.66}$$

The first two terms of the Taylor expansion of (2.66) around $\boldsymbol{x}$ yield

$$\sum_{k=1}^{m} \left[g_i^{(k)}(\boldsymbol{x}) \cdot f^{(k)}(\boldsymbol{x}) + \sum_{j=1}^{n} \{ G_{ij}^{(k)}(\boldsymbol{x}) f^{(k)}(\boldsymbol{x}) + g_i^{(k)}(\boldsymbol{x}) \cdot g_j^{(k)}(\boldsymbol{x}) \} \delta_j \right] \approx 0. \tag{2.67}$$

In a further approximation, the term $G_{ij}^{(k)}(\boldsymbol{x}) f^{(k)}(\boldsymbol{x})$ is neglected. The correction $\boldsymbol{\delta}$ to $\boldsymbol{x}$ results from the solution of the linear system of equations

$$\sum_{j=1}^{n} \left\{ \sum_{k=1}^{m-1} g_i^{(k)}(\boldsymbol{x}) g_j^{(k)}(\boldsymbol{x}) \right\} \delta_j = - \sum_{k=1}^{m} g_i^{(k)}(\boldsymbol{x}) f^{(k)}(\boldsymbol{x}); \qquad i = 1, \ldots, n. \tag{2.68}$$

The new approximation is of course $\boldsymbol{x} + \lambda_m \boldsymbol{\delta}$, where λ_m minimises the function $Z(\boldsymbol{x} + \lambda \boldsymbol{\delta})$. In general, the matrix in (2.68) is positive definite and (unless $\boldsymbol{x}$ is a stationary point) there is a $\lambda_m > 0$ that improves $Z(\boldsymbol{x} + \lambda_m \boldsymbol{\delta})$, thus theoretically guaranteeing convergence. This is the so-called generalised least squares method.

The derivatives (2.64) are in the case of Force Matching not known explicitly, so they have to be determined numerically at each point $\boldsymbol{\xi}_i$ – a very costly operation. POWELL [84] removes the need for explicit gradient calculations beyond the initialisation. He also shows that if the functions $f^{(k)}(\boldsymbol{x})$ are of the same order as the correction $\boldsymbol{\delta}$, errors in the numerical approximate derivatives $g_j^{(k)}(\boldsymbol{x})$ are acceptable to ensure convergence

properties comparable to the generalised least squares method described above.

One starts with n linearly independent direction vectors $\boldsymbol{d}(1), \ldots, \boldsymbol{d}(n)$ spanning the parameter space, together with approximations of the gradients $\gamma_i^{(k)}$ along these directions, i.e.

$$\gamma_i^{(k)} \approx \sum_{j=1}^{n} g_j^{(k)}(\boldsymbol{\xi}) \cdot d_j(i) \qquad i = 1, \ldots, n; \quad k = 1, \ldots, m \qquad (2.69)$$

is the derivative of $f^{(k)}$ in the direction $\boldsymbol{d}_i$. These gradients are explicitly taken as independent of the location in configuration space $\boldsymbol{\xi}$. A change of $\boldsymbol{\xi}$ by $\boldsymbol{\delta}$ causes an error of order $\boldsymbol{\delta}$ times a second derivative in $\gamma_i^{(k)}$, which is – as stated above – acceptable. In the first iteration, the coordinate directions are chosen as $\boldsymbol{d}(i)$, and the $\gamma_i^{(k)}$ are initialised with the difference quotients with increments ϵ_i

$$\gamma^{(k)}(i) = \frac{f^{(k)}(x_1, x_2, \ldots, x_{i-1}, x_i + \epsilon_i, x_{i+1}, \ldots, x_n) - f^{(k)}(\boldsymbol{x})}{\epsilon_i}. \qquad (2.70)$$

The correction $\boldsymbol{\delta}$ to the starting point $\boldsymbol{x}$ is the solution of a system of linear equations given by putting the numerical estimates for the derivatives into (2.68):

$$\sum_{j=1}^{n} \left\{ \sum_{k=1}^{m} \gamma^{(k)}(i)\gamma^{(k)}(j) \right\} q(j) = p(i); \qquad i = 1, \ldots, n, \qquad (2.71)$$

$$\text{where} \quad \boldsymbol{\delta} = \sum_{i=}^{n} q(i) \cdot \boldsymbol{d}(i) \qquad (2.72)$$

$$\text{and} \quad p(i) = -\sum_{k=}^{m} \gamma^{(k)}(i) f^{(k)}(\boldsymbol{x}). \qquad (2.73)$$

For numerical reasons it is beneficial to scale the direction vectors $\boldsymbol{d}(i)$, so that

$$\sum_{k=1}^{m} [\gamma^{(k)}(i)]^2 = 1, \qquad i = 1, \ldots, n. \qquad (2.74)$$

Again, the next step is to determine the $\lambda_{\min}$ that minimises $Z(\boldsymbol{x} + \lambda\boldsymbol{\delta})$. Due to the errors in (2.69), this $\lambda_{\min}$ need not be positive. To find this

optimal $\lambda_{\min}$, one first brackets a minimum (i.e. find a $f(a) > f(m) < f(b)$ with $a < m < b$) by increasing the bracket size, and then locates the minimum with BRENT's algorithm [10]. This algorithm combines the fast-converging parabolic interpolation with the golden section search. Thus it provides a little insurance: Even in very unfavourable cases, it converges at least linearly.

The best and second best values for λ, λ_1 and λ_2, that were obtained during the minimisation along $\boldsymbol{\delta}$, and the associated function values $f^{(k)}(\boldsymbol{x} + \lambda_{1,2}\boldsymbol{\delta})$ are used to approximate the gradient in direction $\boldsymbol{\delta}$ by the difference quotient

$$\frac{\partial}{\partial \lambda} f^{(k)}(\boldsymbol{x} + \lambda\boldsymbol{\delta}) \approx \frac{f^{(k)}(\boldsymbol{x} + \lambda_1\boldsymbol{\delta}) - f^{(k)}(\boldsymbol{x} + \lambda_2\boldsymbol{\delta})}{\lambda_1 - \lambda_2} = u^{(k)}(\boldsymbol{\delta}). \qquad (2.75)$$

By exploiting the fact, that the gradient of $Z(\boldsymbol{\xi})$ in the direction $\boldsymbol{\delta}$ vanishes at $\boldsymbol{x} + \lambda_{\min}\boldsymbol{\delta}$, one can improve this approximation to $v^{(k)}(\boldsymbol{\delta})$, where

$$v^{(k)}(\boldsymbol{\delta}) = u^{(k)}(\boldsymbol{\delta}) - \mu f^{(k)}(\boldsymbol{x} + \lambda_{\min}\boldsymbol{\delta}) \qquad (2.76)$$

$$\text{with} \quad \mu = \frac{1}{Z(\boldsymbol{x} + \lambda_{\min}\boldsymbol{\delta})} \sum_{k=0}^{m-1} [u^{(k)}(\boldsymbol{\delta}) \cdot f^{(k)}(\boldsymbol{x} + \lambda_{\min}\boldsymbol{\delta})]. \quad (2.77)$$

and scaling both $v^{(k)}(\boldsymbol{\delta})$ and $\boldsymbol{\delta}$, so that (2.74) still holds when replacing one of the $\gamma^{(k)}(t)$ by $v^{(k)}(\boldsymbol{\delta})$ and one of the directions $\boldsymbol{d}(t)$ by δ. The integer t is selected to maximise the absolute value of the product $p(t) \cdot q(t)$, i.e.

$$|p(t) \cdot q(t)| = \max_{1 \leq i \leq n} |p(i) \cdot q(i)|. \qquad (2.78)$$

The next iteration step is then started from $\boldsymbol{x} + \lambda_{\min}\boldsymbol{\delta}$. The iteration is finished, if the components of both $\boldsymbol{\delta}$ and $\lambda_{\min}\boldsymbol{\delta}$ are sufficiently small.

The advantages of POWELL's method are discussed in detail in [84] and [11]. Among others, consecutive vectors $\boldsymbol{\delta}$ tend to be mutually conjugate through the matrix

$$\Gamma_{ij} = \sum_{k=0}^{m-1} g_i^{(k)}(\boldsymbol{x}) g_j^{(k)}(\boldsymbol{x}). \qquad (2.79)$$

This makes the algorithm an approximation to the conjugate gradient scheme. Most important for force matching purposes, though, is that beyond the initial n difference quotients no further numeric derivatives are

needed explicitly. The only function calls after the initialisation are in the one-dimensional minimisation according to BRENT; the results are then reused to calculate the new $\gamma^{(k)}(t)$. Still, the convergence is comparable to the generalised least squares algorithm described above.

Simulated Annealing If there is a disadvantage to POWELL's method as described above, it is that it readily jumps to the closest local minimum available, ignoring any other, perhaps even better local minima. As the sequence of $Z(\boldsymbol{\xi}_i)$ is strictly monotonous, it is impossible to escape the attraction regime of a minimum. If this minimum does not happen to be the global optimum of the target function, the algorithm will not end up with the optimal solution. The *Simulated Annealing* method can be used to sample configuration space in search of the global minimum. It was first described by KIRKPATRICK *et al.* [53] and is based on the work of METROPOLIS *et al.* [64].

The idea of METROPOLIS and coworkers is rather basic: When simulating an ensemble of atoms, a small random change is accepted, if the resulting change in energy ΔE is negative. Changes with $\Delta E > 0$ are accepted with a probability $P(\Delta E) = \exp(-\Delta E/k_B T)$ and rejected otherwise. Frequent application of this basic step is comparable to simulating the ensemble in a heat bath of temperature T. Due to the introduction of chance to the simulation, methods based on this idea are called *Monte Carlo* methods, as an allusion to the famous casino.

KIRKPATRICK and coworkers now link statistical mechanics to the minimisation of a target function and apply the Metropolis rule to the latter problem. Starting from a state $\boldsymbol{x}$ a change by $\delta\boldsymbol{x}$ is accepted, if the target function $Z(\boldsymbol{\xi})$ is improved by this step. Additionally, a change for the worse is accepted with a probability $P(\Delta Z) = \exp(-\Delta Z/T)$. T is no longer a physical temperature, but an effective temperature in the units of the target function.

Analogous to annealing in metals, a system is first "heated" at a high effective temperature. Then T is decreased slowly until the system "solidifies". The temperature sequence is decisive: While quenching, i.e. a rapid decrease in temperature, will lead to trapping the target function in a local minimum (equivalent to a metastable state in a physical system), it is possible to attain the global minimum with a certain probability when cooling slowly enough.

Simulated annealing was first applied to discrete systems (e.g. the travelling salesman problem), where the "basic step", which is either accepted or rejected, is clearly defined. In a system with continuous degrees of freedom like force matching, the basic step length has to be specified first. CORANA *et al.* [19] describe how this can be done adaptively. A step length vector $\boldsymbol{v} \in \mathbb{R}^n$ is defined, where the components are the typical step lengths in each coordinate direction of the configuration space. From a starting point $\boldsymbol{x}$ one generates a new point $\boldsymbol{x}'$ for one of the coordinate directions $h = 1, \ldots, n$ with

$$\boldsymbol{x}' = \boldsymbol{x} + r v_h \boldsymbol{e}_h, \tag{2.80}$$

where r is a (pseudo-)random number in $[-1, 1]$ and $\boldsymbol{e}_h$ the hth coordinate unit vector. The Metropolis criterion is then applied to the $\boldsymbol{x}'$: A pseudorandom number $p' \in [0, 1]$ is generated and the new $\boldsymbol{x}'$ is accepted if $p' < p = \exp(-\frac{Z(\boldsymbol{x}') - Z(\boldsymbol{x})}{T})$ and $\boldsymbol{x} := \boldsymbol{x}'$. Then a trial point $\boldsymbol{x}'$ for the next coordinate direction is generated.

This is repeated N_s times for each coordinate direction and the number of successful trials n_h is recorded. That information is then used to adapt the step length v_h. The algorithm is most efficient, if approximately half of the suggested changes is accepted. A lower rejection rate implies that the steps are too small and too many function evaluations are needed to sample the configuration space. If the rejection rate is higher, much work is done in vain, because the steps are too big for the accessible configuration space. CORANA and coworkers suggest changing $\boldsymbol{v}$ in the following way:

$$v_h := v_h \left(1 + 2 \, \frac{n_h/N_s - 0.6}{0.4} \right) \qquad \text{if } n_h > 0.6 \, N_s, \tag{2.81a}$$

$$v_h := \frac{v_h}{1 + 2 \, \frac{0.4 - n_h/N_s}{0.4}} \qquad \text{if } n_h < 0.4 \, N_s, \tag{2.81b}$$

$$v_h := v_h \qquad \text{else.} \tag{2.81c}$$

This will modify the basic step length by a factor between $\frac{1}{3}$ and 3. The step scaling function is plotted in Fig. 2.6.

After N_T step length adjustments, when the system is believed to have sampled the entire accessible configuration space, the effective temperature is reduced by a factor (e.g. $T' = 0.85 \, T$), and the whole procedure is repeated at the lower temperature. Thus, the system is "cooled" slowly. Two conditions must be fulfilled to stop the algorithm:
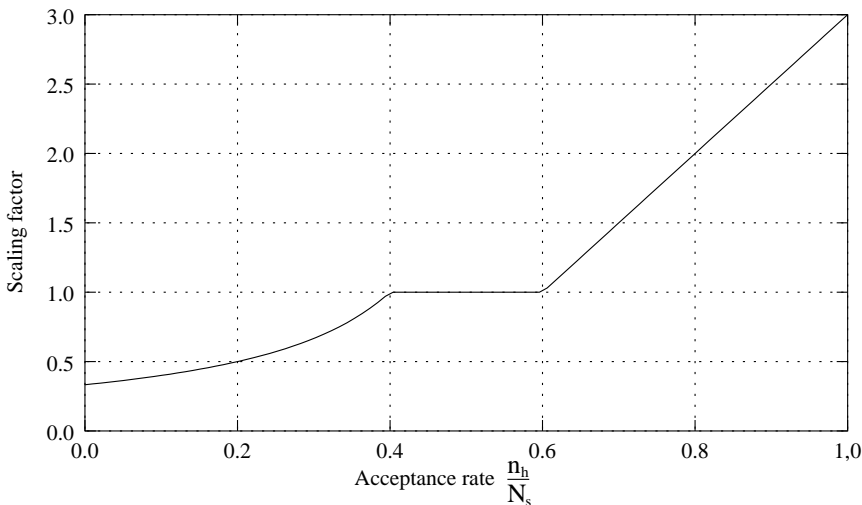
Figure 2.6: The scaling factor for the basic MC step length depends on the acceptance rate. Both extremely high and extremely low rates are inefficient. From [11].

1. Function values $Z(\boldsymbol{x})$ at the end of consecutive temperature loops are close together, i.e. the system is trapped in a minimum.

2. The current function value is close to the optimal value $Z(x_{\mathrm{opt}})$ reached so far.

If both criteria are met, $\boldsymbol{x}_{\mathrm{opt}}$ is returned as a result. If only the first condition is fulfilled, the algorithm is stuck in a local minimum after visiting a better location. In this case, $\boldsymbol{x}$ is set to $\boldsymbol{x}_{\mathrm{opt}}$ and the algorithm is continued from there.

Simulated Annealing is extremely expensive in function calls and thus in computation time, especially compared to Powell's method described above, but it has a chance of finding the global minimum, even if the starting point is not in the attraction regime. In [19], Corana *et al.* compare their algorithm to other optimisation procedures. They claim that although Simulated Annealing does need many function evaluations, it has the highest chance of obtaining the global minimum.

2.3.2 Reference Data

The quality of potentials generated by force matching crucially depends on the selection of reference structures. Force-matched potentials will only work well in situations they have been trained to. Therefore, all local environments that might occur in the simulation should also be present in the set of reference configurations. Otherwise the results may not be reliable. Using a very broad selection of reference configurations will make the potential more *transferable* (cf. Sec. 2.2.2 above), making it usable for many different situations, e.g. for different phases of a given alloy. On the other hand, giving up some transferability may lead to a higher precision in a given situation. By carefully constraining the variety of reference structures (and thus reducing the contradictions in the reference data) one may generate a potential that is much more precise in a specific situation than a general purpose potential, which was trained on a broader set of reference structures. The latter potential, on the other hand, will be more versatile, but less accurate on average. Finding sufficiently many suitable reference structures might not always be trivial. For certain complex structure like quasicrystals, there may be only very few (if any) approximating periodic structures with sufficiently small unit cell.

A further problem is that any potential function depending on the interatomic distance must be determined for the entire argument range between $r_{\min}$ and r_{cut}. If tabulated functions are used, for each tabulation interval there must be distances actually occurring in the reference structures, for otherwise there would be potential parameters which do not affect the target function, and which consequently cannot be determined in the fit. The requirement that roughly all distances for all combinations of atom types actually occur in the reference structures becomes especially problematic, if the atoms of one type form only a small minority, in which case small distances between such atoms might be completely absent in all reasonable reference structures. In such situations it might be unavoidable to use a much broader selection of reference structures with varying stoichiometry.

Reference structures are generated either from ab-initio molecular dynamics trajectories or from molecular dynamics with an ad-hoc potential. It is not advisable to restrict the selection of reference configuration to ground state structures only, as the pair distribution will in this case usually show large gaps, leading to problems. This is also the reason to include systems under external strains or at high molecular dynamics temperatures

in the set of reference configurations.

If a first potential has been generated with force matching, this potential may be used in molecular dynamics simulations to generate further snapshots, which in turn then are included in a further force matching run. This procedure will make the reference structures more realistic, i.e. the local environments more similar to the ones expected in reality.

2.3.3 Potential Models and Representations

The force matching method is fairly independent of the potential one wants to generate. It was first used in tabulated EAM potentials [28], but in principle it will work with any potential that is given by a finite set of parameters. In case of an EAM potential, that may be a list of sampling points together with an interpolation method (e.g. cubic splines). In other cases, the parameters might be those of an analytic representation of a function (e.g. [67]).

Below, I will discuss some points that should be kept in mind, when selecting a potential model to use in force matching.

Unsupported Parameters Any optimisation algorithm will only be able to optimise those parameters, whose values actually influence the target function. This is of course also true for force matching. Especially in the case of tabulated potential function it may happen that a sampling point cannot be substantiated by reference data. This emphasises the fact, that force matching potentials can only know about a system what can be found in the reference collection. If there is no information about how two atoms at a certain distance interact, then it is impossible to fit a parameter that describes this interaction.

With EAM potentials, it is not known a priori, which values will appear as the local density. Even more critical, these values may shift during an optimisation process. Here a dynamic adaption of the domain of the embedding function might solve the problem. Another possible solution is the introduction of additional constraints in the optimisation as described below.

If a parameter has no or only very little influence on the target function the value of the parameter can be chosen arbitrarily. Diverging parameter values are thus a clear sign of unsupported parameters. POWELL's

algorithm described above will fail if the target function is completely in-dependent of a parameter, as the equation system (2.71) cannot be solved in that case.

Overfitting As many reference values can be used in force matching (three force components per atom in the reference structures, easily several thousand in a force matching run), the method can also support a comparatively large number of parameters. But especially when using tabulated potentials, there is no further insight to be gained by increasing the sampling point density [77, 89]. In almost all cases, a certain potential model will not be able to represent the physics of a system perfectly. With a sufficiently large parameter set, though, it is possible to fit each reference value perfectly, but such a potential will fail in configurations not included in the reference set. A potential cannot be better than the limits of the potential model.

A strategy to avoid the problem of overfitting is splitting the reference database in two parts. One is actually used for fitting, the other part is used to test the results. If the root-mean-square (rms) deviation of the reference values is much higher in testing than in fitting, the potential is probably overfitted, i.e. there are too many parameters in the potential. MISHIN *et al.* [68] have suggested gradually increasing the sampling point density in an interpolated potential, until the rms deviation of the *testing* stage does not improve any further.

Gauge Degrees of Freedom Glue or EAM potentials have gauge degrees of freedom. By virtue of the transformations (2.38) and (2.40), the potential functions can be modified without changing the physics. In order to find unique solutions, these gauges have to be fixed, as suggested in Sec. 2.2.2.

There are several possibilities to do that. Firstly, additional constraints in the target function (2.50) can be used to "punish" deviation from a chosen gauge. The other possibility is using the gauge transformations periodically to re-set a potential to a chosen scale. Both methods have their advantages and disadvantages. Additional constraints add some computational overhead at each step, while periodic rescaling introduces some error in the optimisation process, if the gauge transformation cannot be performed exactly due to the parametrisation of the potential. Thus, there

is no clear preference for either method.

Finally it should be noted, that an imperfect adherence to a certain gauge generally does not influence the quality of a potential, so it may be possible to ignore the gauge in the final stages of a force matching run, and only scale the final potential.

Chapter 3

potfit – a Force Matching Programme

In this chapter, the structure of the *potfit* programme designed to solve the force matching problem is described. The author started developing this programme together with Franz Gähler in 2002. The programme is still actively improved, see Sec. 3.5 for further plans.

  potfit is licensed under the GNU public licence[1] version 2. The documentation is licensed under the GNU free documentation licence[2] version 1.2. Source code and documentation are available online from the *potfit* homepage at `http://www.itap.physik.uni-stuttgart.de/~imd/potfit`. A complete description of all run-time options and compile flags as well as specifications for input and output files can be found there. The program package *potfit* was announced in [12]. Technical information on the programme can be found in App. A.

3.1 potfit Operation

The basic *potfit* programme cycle is shown graphically as a flow chart in Fig. 3.1. After *potfit* is invoked from the command line, it first reads the name of the parameter file from the command line (and aborts when it is missing). Then all run-time parameters are read from this file. Next both the starting potential and a set of reference configurations are read from files specified in the parameter file.

  Depending on the value of the `opt` parameter, *potfit* either uses the minimising algorithms described below to optimise the starting potential, or advances directly to the output section using the starting potential as final result. In the output section, potential tables in various formats (e.g. for

---

[1]`http://www.gnu.org/licenses/gpl.html`
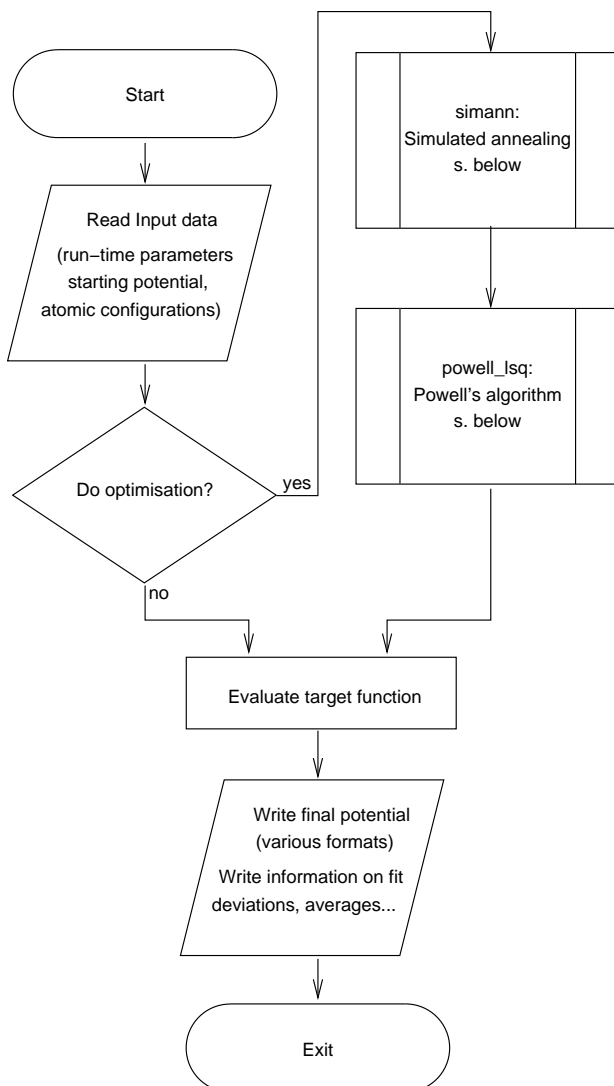[2]`http://www.gnu.org/licenses/fdl.html`

Figure 3.1: Flowchart of the *potfit* programme

use in IMD or plotting) are written to disk. Additionally, the target function is calculated a final time and information on the precision of the fit is written to standard output. By skipping the optimisation process, *potfit* can be used to test the quality and properties of an existing potential as well as create tables of this potential in different formats.

The programme consists of two largely independent parts. One of them calculates the differences resulting from a comparison of a test potential to the reference data, while the other optimises a set of parameters to minimise the sum of squares of these differences without regarding the meaning of those values. This separation simplifies the addition of force calculators for other potential models or different optimisation algorithms.

3.2 Optimisation Algorithms

3.2.1 Simulated Annealing

The Simulated Annealing algorithm used in *potfit* is that of CORANA *et al.* [19] (see also Sec. 2.3.1). A flowchart of the algorithm is shown in Fig. 3.2.

The algorithm is called from the *potfit* main programme with the potential parameter list ξ_i as argument. If the annealing temperature is set to zero, the algorithm is skipped. Otherwise, the algorithm starts by applying the basic Monte Carlo step to each parameter of the potential. If the parameter is a sampling point, then the basic step consists of adding a Gaussian of normally distributed width and height at the location of the sampling point. Using a Gaussian instead of just manipulating a single point prevents overswinging at the neighbouring sampling points. In any other case, a normally distributed random number is added to the value.

The basic step is then either accepted or rejected according to the Simulated Annealing rules depending on the change $\Delta Z = Z_{\text{old}} - Z_{\text{new}}$ of the target function Z.

$$\Delta Z < 0 : \quad \text{Change is accepted}$$
$$\Delta Z \geq 0 : \quad \text{Change is accepted with probability } P(\Delta Z) = e^{-\frac{\Delta Z}{T}}, \quad (3.1)$$
$$\text{otherwise rejected.}$$

This is done by comparing a uniformly distributed pseudo-random number in the range $[0; 1)$ with the exponential. If a new optimal value of Z is found,
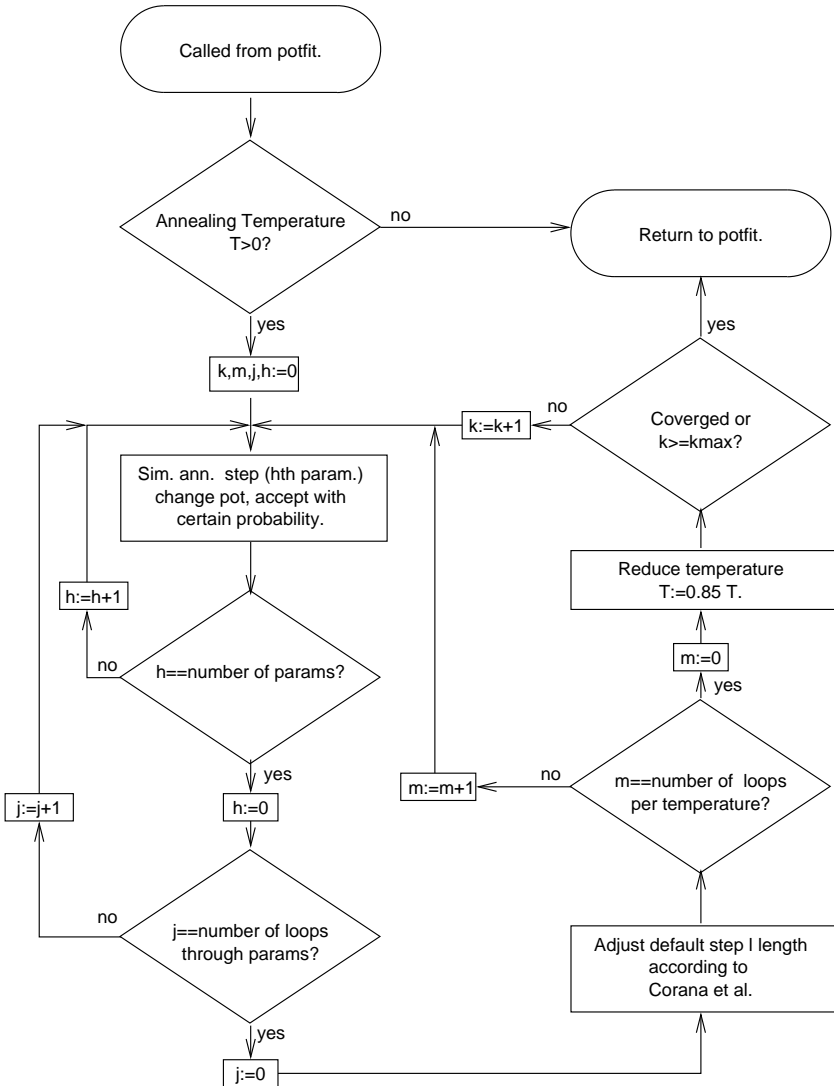
Figure 3.2: Flowchart of the Simulated Annealing subroutine

that value and the corresponding set of parameters are stored. As described in Sec. 2.3.1, this is performed for $N_s = 20$ times for each parameter and the number of successful tries is recorded. With that information, the average step length (i.e. the width of the normal distribution) is adjusted for each parameter individually. If the exit flag file (see App. A.1.2) exists at that time, the Simulated Annealing routine will finish its work immediately and return the optimal potential found so far. After $N_T = 3n$ step adjustments, where n is the number of parameters, the temperature is reduced by 15 %.

The algorithm is terminated when either the number of temperature reductions has exceeded the maximum number of 1000, or if the search is considered converged. This is the case, if the target function value has not changed for more than ϵ compared to the value at the last four temperature adjustments and is not further than ϵ from the best value obtained so far (cf. Sec. 2.3.1). Then, the optimal parameter set is returned to potfit. ϵ can be chosen relatively large – it is not necessary to use Simulated Annealing until final convergence is achieved. Once the basin of attraction of the global optimum has been reached, Powell's algorithm is much faster. Even an ϵ six orders of magnitude larger than the convergence limit of Powell's algorithm is usually enough to ensure that.

3.2.2 Powell's Conjugate Gradient Algorithm

The algorithm that *potfit* uses to find a local minimum is the one given by POWELL [84] (see also Sec. 2.3.1). Figure 3.3 shows a flowchart of the algorithm.

Firstly, the matrix $\gamma_i^{(k)}$ is initialised (2.70) and scaled (2.74). The ϵ_i in (2.70) are chosen as 10^{-4}, a value found to work well for potential functions. If the target function is independent of one of the parameters, the matrix $\boldsymbol{\gamma}$ will be singular. This happens, if a sampling point cannot be determined from the information in the reference data. For example, if all EAM embedding densities lie only in a small subset of the embedding functions, then the function values at points far outside that subset will not influence the target function. In these cases, as a last resort, *potfit* will rescale the potential to ensure at least an optimal coverage of the embedding function domain. If this also fails, the programme will abort with an error. Then, either the reference data has to be complemented or the potential needs to be modified, before potential optimisation can continue.
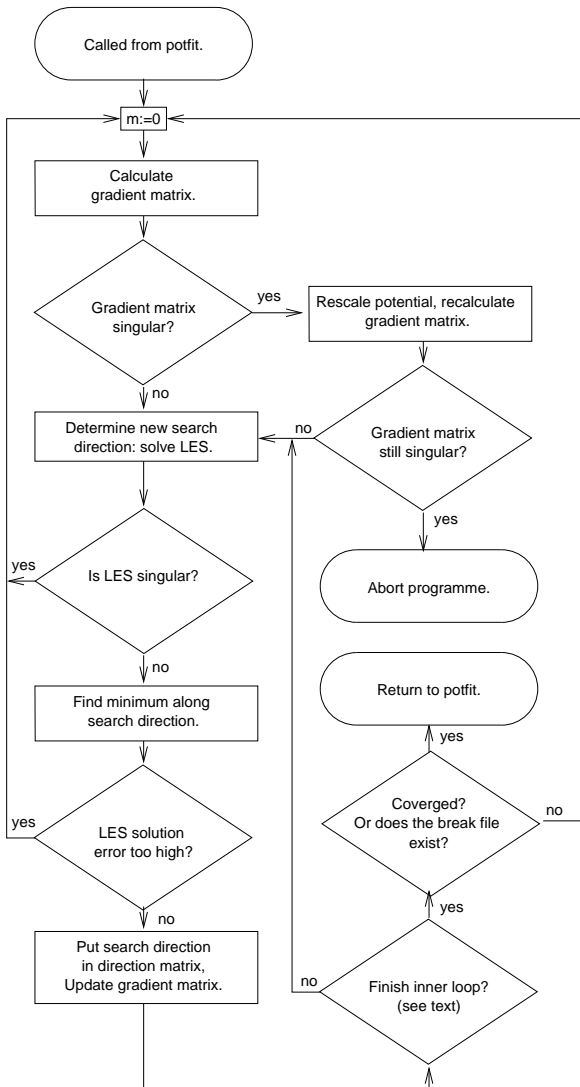
Figure 3.3: Flowchart of the least square minimisation subroutine according to Powell

In the next step, the linear equation system (2.71) is solved. The code uses the `dsysvx` driver routine from the LAPACK library [5], which must be installed separately, probably together with the BLAS library [25, 26, 61] LAPACK is based on. In the current implementation, *potfit* can use either the Intel Math Kernel Library [49] or the AMD Core Math Library [3]. With little adjustments to the source code any other implementation can be used alternatively. If the LES is singular at some time during minimisation, the algorithm is restarted with a complete recalculation of the matrix $\boldsymbol{\gamma}$.

The solution vector gives the direction of search for the minimum. A minimum is found by first bracketing it ($f(a) > f(m) < f(b)$ with $a < m < b$), and then localising it using BRENT's algorithm [10]. If the sum of forward and backward error estimate for the previous LES solution exceeds a threshold (here chosen as unity), the algorithm is restarted with the calculation of the matrix $\boldsymbol{\gamma}$. Otherwise, the search direction replaces one of the coordinate directions $\boldsymbol{d}(i)$ and the matrix $\boldsymbol{\gamma}$ and the linear equation system are updated accordingly. Here, the last two target function values and deviation vectors from BRENT's algorithm are reused to derive a numerical estimate for the gradient along that direction.

This procedure (solution of LES, minimisation in one dimension, update of LES) is repeated until either the algorithm converges (i.e. the improvement is less than 10^{-7}) or no further iterations are possible or meaningful. This is the case if the matrix $\boldsymbol{\gamma}$ becomes singular, the change of the target function value is very large ($> 10^4$, in which case the approximation of a spatially constant gradient matrix (2.69) is probably not valid any more) or if enough loops have been done. The latter condition is necessary, as the directions $\boldsymbol{d}(i)$ tend to become linearly dependent, so that a periodic restart of the algorithm is reasonable.

If a restart of POWELL's algorithm does not improve the target function by at least a tenth of the threshold of POWELL's algorithm, the programme assumes that a local minimum is obtained and returns that minimum to the main *potfit* programme. If the exit flag file (see App. A.1.2) exists, this minimisation routine will also finish up and return to the main programme.

3.3 Reference Data Comparison

At this time, reference data comparison is implemented for pair and EAM potentials. As *potfit* internally uses two potential tables, one that contains

the actual parameters and a lookup table used for force calculation (cf.
App. A.1.3), this routine will work with any type of pair and EAM input
potential (spline interpolated, analytic,...), provided there is a means of
deriving the lookup table from the input potential parameters.

Spline interpolation can be accelerated greatly, if a table containing the
second derivatives is precalculated before a spline interpolation. This table
needs to be re-done only if the potential has changed. As *potfit* should
not calculate the deviation from the reference values for the same potential
twice, the first step in the reference data comparison is initialising the table
containing the second derivatives.

All reference configurations can be treated absolutely independently,
therefore the next steps are performed for each configuration in turn. In a
first loop over all atoms in a configuration the data fields are initialised. In
the second loop, pair forces and pair energy contributions as well as EAM
densities and energy contributions are calculated. For EAM potentials, the
embedding force contributions are evaluated in a third loop.

In the following step, the weights u_k (cf. 2.3, Eq. (2.49)) are applied to
the contribution. The weights for energies and stresses can be specified in
the configuration file; suitable values are between 5 and 100 for the energies
and between 10 and 400 for the stresses (depending on the numeric value
of these quantities). By default, forces get a unit weight, but as it was
found useful to measure relative rather than absolute deviations from the
reference forces, except for very small reference value. Thus, the weighting
factor u_k for the forces becomes

$$u_k = \frac{1}{\boldsymbol{F}_k^2 + \epsilon}, \tag{3.2}$$

where $\boldsymbol{F}_k$ is the force *vector* of which F_k is a *component*, and ϵ is a small
positive quantity to prevent extremely large u_k for tiny forces.

After these steps have been performed for all configurations, additional
constraints (2.50) are evaluated and added to the target function. Finally,
the target function value is returned to the calling routine.

3.4 Parallelisation and Optimisation

The programme *potfit* spends almost all CPU time in calculating the ref-
erence data deviations for a given potential; using Simulated Annealing or

Powell's algorithm to find a new potential to be tested takes only a tiny fraction of that time. Therefore, the only promising lever for increasing the performance is reducing the time needed for force computations. This can be done either by reducing their number, or by making each target function evaluation faster.

Powell's algorithm leaves only little room for further reduction of the number of force calculations – it was designed with that goal in mind. One may adjust the precision for Brent's minimisation in one dimension. If the tolerance is too high, time is wasted in refining a minimum beyond need, whereas an insufficient precision may stop too far from the minimum, thus requiring more steps in total. Due to the quadratic convergence of Brent's algorithm, setting this parameter optimally will only save few target function evaluations, so the choice was made empirically.

It takes n function evaluations to set up the matrix $\boldsymbol{\gamma}$ (where n is the number of free potential parameters, easily a triple-digit number), so restarting Powell's algorithm is rather costly. The criteria described in section 3.2.2 above were chosen so that $\boldsymbol{\gamma}$ is recalculated only when necessary.

Reducing the number of force calculations in the Simulated Annealing algorithm is more difficult. Using the step adjustment proposed by CORANA [19] assures that not too many calculations are wasted (cf. Sec. 2.3.1). However, Simulated Annealing depends on a thorough search in parameter space at each temperature, so one cannot reduce the number of Monte Carlo trials at will without reducing the probability of finding the global minimum.

Generally, it is more effective to speed up the individual target function evaluations. Two properties of the force matching method can be exploited to achieve this goal. Firstly, the calculation of forces, stresses and energies in individual reference configurations do not depend on each other, so they can be distributed on several processes (parallelisation). Secondly, the reference configurations stay fixed, which allows the use of neighbour lists.

The standard Message Passing Interface (MPI [38]) is used to distribute the configurations on multiple processes. As only the reference data comparison can profit significantly from parallelisation, setup as well as all potential adjustments are performed by a master process only. The slave processes only get the atomic coordinates and reference data for "their" configurations and fundamental information on the potential, before skipping directly to the target function evaluation, where they wait for work. Before each target function call, the master process sends the changed potential

table to the other processes, which return the results afterwards. The master process may also signal the slave processes to update the complete potential (in contrast to just the table, e.g. if the tabulation points have changed) or to quit the programme completely. MPI parallelisation will significantly reduce the time needed for the calculation of forces, stresses and cohesive energies for a large reference data collection. If however the number of configurations per process drops below 10 to 15, the communication overhead and load balancing problems will become noticeable, thus limiting the speedup achieved by parallelisation. An OpenMP [20] shared memory parallelisation also exists, but produces inferior performance.

While neighbour lists can already accelerate ordinary MD calculations to some degree, they are perfect for Force Matching. Here, the configurations are absolutely static and pair distances do not change, so for each atom a list of neighbouring atoms within the interaction radius (largest of all cutoff radii r_c) can be created when the configurations are read in. This list not only contains distance and direction to the neighbour, but also pre-calculated information used for spline interpolation. Typically, when interpolating a function value with splines, one first needs to know where, and between which tabulation values, the desired point lies. If this information is known beforehand, the number of operations is dramatically reduced. Since spline interpolation is responsible for a significant share of computational effort, this measure speeds up the calculation noticeably. The neighbour table data only needs to be recalculated when the sampling points of the radially dependent functions change – which is not implemented at the moment.

3.5 Future Developments

The *potfit* force matching code is actively being developed. There are two major directions to explore: Firstly, potential specification is to become more flexible. Secondly, more potential types are to be supported. In this section, I will comment on these developments.

3.5.1 Flexibility in Potential Parametrisation

At the moment, *potfit* expects input potentials to be a list of spline interpolated sampling points. The parameters are the function values at sampling

points and – in certain cases – the gradients at the domain boundaries. With minor changes to the code, some of the sampling points can be kept fixed, e.g. to adjust only the interaction between certain types of atoms.

While spline polynomials allow for great flexibility in the specification of a potential, they do have the disadvantage that each parameter only influences the spline in a small region only. If there is not enough reference data for this region (e.g. a gap in the radial density distribution), the parameter might become unsupported (cf. Sec. 2.3.3). A potential representation, where each parameter influences the potential on a larger scale, might suffer less from this problem. A superposition of Gaussians, where width, position and height are the free parameters, might be such a representation, provided there is a lower limit to the width. Otherwise the Gaussian might degrade into a delta peak.

There are also EAM potential models with an analytic expression for the potential functions (e.g. [52]). The number of free parameters is comparatively small in such models. While the parameters are traditionally adjusted to reproduce correctly a number of experimental values, *potfit* could also be used to determine them.

potfit internally uses two tables for potentials, a parameter table and a calculation table (cf. App. A.1.3). If one changed the meaning of the potential parameters, one would only need a method to generate the calculation potential from these changed parameters (and of course the I/O facilities to identify and read this potential format from a file). The calculation table can sample the potential rather densely – memory is not an issue and a larger number of points affects the spline interpolation time only marginally.

3.5.2 Potential Models

There are other potential models going beyond pair and EAM potentials. Two of them are described in Sec. 2.2.2, and there are many others. Getting them to work with *potfit* is slightly more complex than just accommodating a changed representation. Now, the reference data comparison routine needs to be changed. Additionally, I/O infrastructure for this new potential model and the conversion code from parameter to calculation table mentioned above must be provided. The optimisation routines, however, are not potential dependent and can be reused without problem.

The first step to implement a different potential model is obtaining the

MD expressions for stresses, forces and energies in this model. This code needs to be adapted and optimised for force matching purposes (neighbour lists, spline lookup information). Preferably, the selection of potential model to use is done through preprocessor macros. This keeps the code clear and reduces the complexity of the resulting binary.

Chapter 4

Calculations and Results

This chapter starts with a detailed description of the process of potential generation with *potfit*. Potential testing and verification is also discussed. After that, reports on force matching in a number of example systems are given. Section 4.2 describes the generation of a potential for the Ni-rich decagonal Al–Co–Ni quasicrystal and its use in diffusion simulation. In Sec. 4.3, potentials for the icosahedral Ca–Cd quasicrystal and its approximant $CaCd_6$ are used to study the low-temperature order-disorder phase transition in $CaCd_6$. The chapter is concluded by studies of the dynamic properties in the Mg–Zn system with force-matched potentials (Sec. 4.4).

The programme *potfit* has also been used in other systems. Potentials have been generated for example for fracture simulations of the $NbCr_2$ Laves phase [91], or for diffusion in the Al–Co–Cu quasicrystal [45]. Those studies are however not part of this work; the interested reader may find more information in the references given.

4.1 Generation of Effective Potentials

As described in [11], the *potfit* programme is able to recover pair and EAM potentials perfectly. To check this, a *potfit* potential was used to calculate a series of MD snapshots. These classical snapshots were then given to *potfit* as reference data. The force matching programme recovered the original potential starting from an arbitrary potential. This shows that the algorithms work correctly.

4.1.1 General Procedure

Force matching can be used to develop potentials for a wide variety of materials and conditions. Although the detailed parameters may vary be-

tween different runs, the general procedure remains the same in all cases. The generation of a "new" potential can be broken into the following steps:

1. Select a suitable potential model and starting potential.

2. Select a range of model structures.

3. Generate MD snapshots of the model structures at various temperatures and pressures. If no potential for MD simulation is available, use an ad-hoc potential.

4. Calculate reference data with ab-initio methods.

5. Run *potfit*.

6. Use the new potential to make more realistic MD snapshots and calculate the reference data in those. Repeat if necessary.

7. Thoroughly test the resulting potential in MD simulation. Does it yield correct crystal structures, melting temperature, elastic constants, ... ?

In the following paragraphs I describe these steps in detail. A whole section (Sec. 4.1.2) is dedicated to the problem of testing a potential.

Potential Model and Starting Potential

For metals, EAM type potentials are the potential models of choice. As shown in [11], pair potentials cannot be successfully matched to reproduce cohesive energies and forces simultaneously. There are some pair potentials for Complex Metallic Alloys, like the AL-LEHYANI potentials for decagonal Al–Co–Ni derived from generalised pseudopotential theory [1], but those rely on an additional density dependent volume term that contributes to the total energy. If this term is neglected, elastic constants determined through the MD method are bound to become incorrect, if the simulation does not fail completely. Apart from that, pair potentials have some fundamental deficiencies as described in Sec. 2.2.2. As I will mainly discuss EAM potentials in this work, all further descriptions of the potential generation relate to this potential type.

A suitable starting potential might be a result of a previous *potfit* run, or a potential obtained from other sources. If one wants to start without

bias, however, it may be desirable to start with an absolutely arbitrary potential. While it is possible to choose the pair potentials to be zero, doing the same for transfer functions is problematic. If those functions are zero, then the embedding density for all atoms will also vanish, and a change in embedding energy for densities other than zero will not influence the target function. The same holds for the embedding energy: If this function is constant, the energy of the system will not depend on the transferred density and a change in the transfer function will go unnoticed. In both cases, parameters of the potential are unsupported (cf. Sec. 2.3.3), and optimisation will fail. Most non-constant embedding or transfer function are suitable as starting potential. In this work, the transfer functions of the starting potentials were chosen to decrease linearly to zero at the cutoff radius, while the embedding functions are proportional to the density. A gauge transformation was then applied to these potentials, so that they agree with the internal *potfit* convention.

A question that also needs to be addressed before starting potential development is the number and location of sampling points. As discussed in Sec. 2.3.3, overfitting should be avoided by continuously testing the quality of the fit in a separate set of reference configurations. This strategy suggested by MISHIN *et al.* [68] helps controlling the number of parameters. The potential range also has to be considered. Increasing the cutoff radius will also increase the computational effort in Molecular Dynamics simulations in the third power. On the other hand, the quality of the potential might suffer, if the cutoff is too short. Here, the optimal strategy is to start with a potential range as large as one is prepared to support. If the contributions of the potential functions at greater pair distances in a preliminary potential are small, then the user can reduce the cutoff, re-fit the potential and check the effects on a set of test reference configurations not used in the original potential generation.

The spline interpolation in *potfit* can handle both equidistant or arbitrarily spaced sampling points. From the position of potential optimisation, there is no clear preference for either method. While arbitrarily positioned sampling points allow for greater sampling point densities in regions where the potential function change rapidly, the potential generation may be biased by the selection of sampling points. However, there are some cases, where flexible sampling points are necessary. For the interatomic potentials between minority constituents, there may be larger intervals of pair distances that are not occurring in reference configurations. For these re-

gions, the number of sampling points can be reduced.

With the PDIST compile option, *potfit* offers help in positioning sampling points. For a given potential, the pair distances output file contains the information, how often pair distances occur in each sampling point interval (cf. Sec. A.1.2). The intervals can then be adjusted in a way that every one of them is represented adequately in the reference configurations.

Reference Structures

The following steps are crucial for generating a new potential. The transferability of the potential and the possible applications are controlled through the selection of reference structures. Also, deficiencies in this stage may hinder the optimisation process or make it impossible altogether. It should now be known what the new potential is going to be used for.

To generate reference structures, one first needs one or more model structures that are good representatives of the systems of interest. The alloy database[1] [106] offers models for a wide range of alloys. If such model structures are not available at first, other structures can be substituted temporarily. As described below, a preliminary potential can later be used to refine the reference structures in question. If a potential is going to be used over a wide range of compositions and structures, all these systems should be represented in the set of reference configurations (in some cases that may even include the elementary solids). On the other hand, for highly specialised potentials, the selection must be much narrower.

In most cases, the model structures alone will not be enough to generate a potential. The reason for this lies in the pair distribution. Especially if the composition range is very narrow, the pair distance distribution consists of a series of delta peaks with sometimes large gaps in between, and so the reference configurations will only contain force information for these distances. Only if the delta peaks are smeared out, the information contained in the reference data is increased. The most comfortable way to introduce some disorder into the model structures is Molecular Dynamics simulation at finite temperature. Luckily, the requirements on the potential used for this purpose are not too great. Any potential that more or less keeps the structures intact will suffice. As the force-matched potential is of course not yet available at this stage, an ad-hoc potential can be used.

---

[1] http://alloy.phys.cmu.edu

Another possibility to smear out the pair distribution function lies in straining the sample either before or after MD simulation. These structures will also help in determining the elastic constants of a material.

The exact combination of strained and heated structures is dictated by the purpose of the potential that is to be generated. A multifunctional potential will result from a balanced selection of ground state structures, heated structures (up to the melting temperature) and strained structures. Potentials used to refine ground state structures on the other hand require a higher share of ground state configurations and low-temperature MD simulation snapshots. In contrast, diffusion at temperatures just around the melting point should be studied with a potential that was matched to high-temperature configurations (here even some molten structures may be useful).

In addition to MD snapshots, *potfit* can also work with complete ab-initio Molecular Dynamics trajectories. Although this is much slower than classical MD, it does not require an effective potential at all, thus rendering the use of ad-hoc potentials unnecessary.

Finally, there may not be enough physical model structures in the desired composition range. In that case, the set of reference configurations can be complemented by "unphysical" structures. These may be redecorated structures from other alloy systems or structures with some atoms interchanged. These configurations assist in filling pair density distribution gaps.

Reference Data Calculation

While the reference data in principle can be calculated with any first-principles code, in this work VASP (cf. App. B.2) was used exclusively. The conversion utilities to generate VASP input from MD snapshots are included in the *potfit* package. VASP offers an easy way to determine the reference information, there are however a few points that should not be forgotten.

Firstly, the potentials are only as good as the reference information. *potfit* matches a potential to the reference information, not to the real world. If the potentials are to agree with reality, the reference information must be reasonable. It is absolutely possible to abuse any ab-initio code to a degree that the results are almost arbitrary. Consequently, the results of first-principles calculations must be sanity checked: Was convergence achieved

concerning k-point density and energy cutoff? What assumptions were made that could influence the result, like for example symmetry or spin polarisation? Were the appropriate pseudopotentials used? Only reference data that passes these checks will lead to meaningful potentials.

Secondly, all reference information should be calculated consistently. Even if for example cutoff energy convergence is achieved, the cohesive energy may shift if the cutoff energy changes. The same holds for the pseudopotentials. Thus all reference calculations must be made with the same set of pseudopotentials and cutoff energy, and the k-space density should be comparable.

The resulting reference data is split into two sets. One of them is actually used for force matching, while the other one serves to check the developed potential for overfitting (as described above).

Running potfit

After all preliminary work has been completed, *potfit* can be run for the first time. There are a number of parameters that are used to influence the optimisation, and usually, the first choice will not lead to the final potential. Intermediate potentials can either be rejected or used as a new starting potential. I will describe below, how these parameters can be tuned during the optimisation.

NORESCALE **compile option** This option is useful in later *potfit* runs, when an existing potential only needs to be fine tuned. As described in App. A.1.2, *potfit* binaries compiled with this option will not rescale a potential periodically to concur with the EAM gauge. The transformations during such a rescaling event cannot be performed perfectly with spline-interpolated potentials, so a rescaled potential may be worse than the original.

anneal_temp **parameter** With this parameter, the starting "temperature" of simulated annealing is controlled. If set to zero, annealing is skipped. As mentioned above, simulated annealing is a powerful method to find a global optimum, but it comes with a high computational cost. In most cases, Powell's conjugate gradient algorithm is enough to find a reasonable minimum, but if the optimisation gets stuck, then annealing can help in leaving the basin of attraction of that metastable minimum. Setting anneal_temp too high prolongs

the minimisation; if the value is too low, the global minimum might not lie in the accessible parameter space. The output of *potfit* helps in setting `anneal_temp` correctly. The fluctuations of the target function values at the starting temperature must be a significant fraction of the optimal value, otherwise only too small a slice of the parameter space is sampled.

`eng_weight` **and** `stress_weight` **parameters** Those two parameters control the relative weight of stresses and energies, respectively. Per reference configuration, there is only one energy value and six stress tensor components, but hundreds of force vector components that contribute to the target function. While the weight for the forces is such that the relative rather than the absolute deviations are measured (cf. Sec. 3.3, Eq. (3.2)), the target function weight for energies and stresses is set exclusively through these parameters. Reasonable values for `eng_weight` are between 5 and 100, and between 10 and 400 for `stress_weight` when the standard units described in Tab. B.1 are used.

Frequently, a chosen set of the aforementioned parameters will not yield a viable potential on the first try, and values that were useful in one case may fail in another. The optimisation can be restarted with slightly changed parameters using a previous result as the starting potential. In some cases, the potential develops undesired features (e.g. overswinging of splines, unsupported parameters). Then, the set of reference configurations needs to be changed. Alternatively, the location of sampling points can be adjusted. Finally, one ends up with a complete family tree of potentials, with parent potentials and their offspring. Few of them end up in the testing stage of force matching. As there are so many potentials involved, one must be able to identify them. This is necessary to know the background and the circumstances of the force matching run that led to the potential. Each potential is given a unique number. In most cases, this is the job number assigned by the queueing system. This number appears not only in all data files associated with the potential, but also in a database, where all relevant information (starting potential, annealing temperature, reference data used, . . .) is stored.

In some cases, strange features emerge in a potential during optimisation, like characteristic humps. To check if these features are "real" or just

artefacts, they can be removed manually from the potential – one of the advantages of plain text data files. If the features re-appear, they are probably justified by the reference data.

Iterative Potential Improvement

Especially if the MD snapshots used as reference structures were created by an ad-hoc potential, they only very approximately represent realistic configurations. However, the data will still suffice to generate a potential. This potential can then be used to calculate more realistic MD snapshots. After ab-initio evaluation, these new configurations may complement or replace the previous reference structures, and a new potential can be generated from this data. If necessary, this procedure can be iterated.

The intention is that the reference data contains more and more configurations that are representative of what might happen later in MD simulation. This information improves the final potential in two ways: Firstly, there are fewer distractions in the reference data set – atomic configurations that need not be described correctly, because they will not appear in the simulations that the potential is designed for. It was found that the optimisation works better, and the rms deviation decreases, if the share of realistic configurations is higher. More importantly, any force-matched potential will only work in situations it was trained for. These new configurations provide just that information.

The iterative potential improvement is vital for highly specialised potentials. There, detailed knowledge of forces in realistic atomic arrangements is essential. For potentials with a broader application range, this step is of less importance, but still useful.

4.1.2 Verification of Force-Matched Potentials

If one finally has obtained a candidate potential through force matching, it is still a long way before one knows, whether this potential can be used in production, i.e. to simulate and predict material behaviour. A potential may be the result of a force matching effort and still fail to perform as desired, for example when an inappropriate selection of reference data was used. To see whether a potential lives up to its promises, it needs to be thoroughly tested. In this section, I describe some of the tests that can be applied to a new potential. These tests include physical proper-

ties that are only indirectly included in the reference information, or even experimentally determined quantities.

Stability and Structure

The first and basic test a potential has to pass is the stability test: Is a given structure stable in MD simulation with that potential? A potential that fails this test has very obviously no future in Molecular Dynamics. The setup is rather simple: A given test structure that should be stable at zero Kelvin is relaxed with MD methods, i.e. the atomic positions and the unit cell is optimised. The final ground state should not be too far from the expectations. To check whether the test structure is only metastable at $T = 0\ K$, the structure is slightly heated before relaxation. Again, the system should not be able to find a minimum much below the experimental or ab-initio ground state. If there are large atom displacements, unit cell distortions or other undesired behaviour, the potential is to be rejected.

This test should be performed with all known structures in the designed application range of the potential. If there are competing structures, their energies can be calculated and compared. There is a problem however, if the ground state is unknown in all details, as it is frequently the case with complex alloys. Then it must sometimes suffice that the potential can stabilise a structure so that the unit cell volume stays reasonably constant.

The results of this test can be used to determine zero temperature lattice constants. This is a typical test quantity for the quality of the potential. It is not directly included in the reference configurations (and would be too costly to calculate during force matching), but all information needed to estimate it should be present in a suitable selection of reference configuration. It should be noted however, that the lattice constant determined from the potential will resemble the ab-initio lattice constant. If that constant is off due to incorrect first-principle calculations, no force-matched potential will be able to correct that error.

For simpler structures and potentials it is sometimes possible to calculate the lattice constants directly from the potential. For complex metallic alloys with their inherent disorder, this is usually not feasible. Then, MD cannot be avoided when determining the lattice constant. This also holds for the other testing criteria mentioned below. Although they may in principle be determined directly from the potentials in some simple cases, this is definitely impossible for CMAs.

Melting Point

The melting point T_m can be determined in various ways. The most basic test is slowly heating a structure with MD methods at constant pressure. The volume-temperature plot will show a discontinuity if the structure melts. It must be noted however, that this method systematically overestimates the melting point. Even a very slow temperature increase of 100 K over one million MD steps is, at a timestep of 10^{-14} s, equivalent to a heating rate of over 10^{11} K/s – which in the real world would be rather rapid heating. Under these circumstances it is unavoidable to overheat the structure a little bit before it melts. Additionally, there are no free surfaces, which hinders nucleation in the melting process [51, 91].

A more reliable estimate of T_m can be obtained from two-phase simulations. Here, the simulation box with periodic boundary conditions contains both liquid and solid phase of the substance. This construct is then simulated at various temperatures and the boundary between solid and liquid is traced. At temperatures below the melting point, the material solidifies, while at higher temperatures the solid part melts. This method to determine T_m is more difficult to set up, but yields superior results. Also, the presence of an interface avoids the overestimation of the melting temperature.

Elastic Constants

Elastic constants can easily be determined with Molecular Dynamics. Starting from Hooke's law, the energy E of a deformed solid can be described as

$$E = \frac{1}{2}\boldsymbol{\epsilon}^T \boldsymbol{C} \boldsymbol{\epsilon}, \tag{4.1}$$

where $\boldsymbol{\epsilon}$ is a strain tensor and $\boldsymbol{C}$ is the fourth order elastic tensor. Due to symmetry constraints, $\boldsymbol{C}$ can be written as a six-dimensional symmetric second-order tensor, with the abbreviations $xx = 1$, $yy = 2$, $zz = 3$, $yz = 4$, $zx = 5$, $xy = 6$. This elastic modulus matrix has at most 21 independent components. For most materials, the number is even lower. For isotropic materials, there are only two independent elastic constants. Decagonal quasicrystals have five independent components [16, 108], $c_{11} = c_{22}$, c_{33}, $c_{44} = c_{55}$, $c_{66} = \frac{1}{2}(c_{11} - c_{12})$, c_{12}, $c_{13} = c_{23}$, the others vanish. To determine those quantities, a suitable set of deformations needs to be set up. These deformations are then applied to a structure, and the energy

is plotted over the deformation. As the energy is a quadratic form of the deformation, parabolas can be fitted to these curves. From the curvature of the parabolas the elastic constants can be determined. This is described in detail in App. C.1.

As with the lattice constant, the information needed to calculate elastic constants of complex metallic alloys is indirectly present in the reference data. Still, the determination of elastic constants is a valid test of the potential.

Dynamical structure factor and phonon density of states

The dynamical structure factor and the phonon density of states can be determined from the MD trajectories of atoms. The results are compared with experimental data (e.g. from neutron scattering). This is an excellent test: Phonon spectra are sensitive to changes in the potential. They describe the dynamics of the atoms and should reproduce reasonably well the experimental information. They cannot, however, be included in the fit, as the determination requires a lengthy MD simulation.

In principle, the dynamical structure factor and other vibrational properties of a solid can be determined from its eigenfrequencies and eigenmodes. The system is relaxed to its ground state, from which the dynamical matrix is calculated by harmonic expansion of the potential. The matrix can then be diagonalised numerically. By sampling the Brioullin zone using Born-von-Karman boundary conditions, this method can work with such small systems, that they could even be handled by ab-initio MD. However, this method is not well suited for complex alloys. An ill-defined ground state with many shallow minima may lead to numerical problems like negative eigenvalues of the dynamical matrix. Additionally, the harmonic approximation may fail at higher temperatures in the presence of low-energy structural transformations. Both problems can occur in CMAs.

Inelastic neutron scattering is frequently used to study phonons experimentally. What is measured are certain correlation functions, which also can be determined from MD simulation. In those simulations, the experimental setup can be reproduced, including the temperature. This comes at a loss of Born-von-Karman boundary conditions, so that large systems have to be simulated over long times, thus excluding ab-initio methods.

There are one-particle and collective correlation functions. The former measure correlations of properties of a particle with its own history aver-

aged over the system. The vibrational density of states (DoS) $G(\omega)$ is for example the Fourier transform of the velocity auto-correlation $C_{vv}(t)$ [90]:

$$G(\omega) = \int\limits_{0}^{\infty} dt \, \cos(\omega t) C_{vv}(t), \qquad (4.2)$$

with

$$C_{vv}(t) = \frac{1}{N} \sum_{j=1}^{N} w_j \frac{1}{3} \langle \boldsymbol{v}_j(0) \cdot \boldsymbol{v}_j(t) \rangle, \qquad (4.3)$$

where $\boldsymbol{v}_j(t)$ is the velocity of particle j at time t and w_j is a weighting factor that depends on the coherent scattering length b_j^c. Angular brackets denote ensemble averaging.

The most interesting among the collective correlations is the dynamical structure factor consisting of a coherent and an incoherent part. While the incoherent part (which is only a one-particle correlation) generates a rather smooth background, the (collective) coherent part $S^c(\boldsymbol{q}, \omega)$ contains the relevant structural information. It is given by the Fourier transform of the coherent intermediate scattering function $\mathcal{F}^c(\boldsymbol{q}, t)$ [90]:

$$S^c(\boldsymbol{q}, \omega) = \frac{1}{2\pi} \int\limits_{-\infty}^{\infty} dt \, \exp(-i\omega t) \mathcal{F}^c(\boldsymbol{q}, t), \qquad (4.4)$$

with

$$\mathcal{F}^c(\boldsymbol{q}, t) = \frac{1}{N} \sum_{jk} b_j^c b_k^c \langle \exp(-i\boldsymbol{q} \cdot \boldsymbol{r}_j(0)) \exp(i\boldsymbol{q} \cdot \boldsymbol{r}_k(t)) \rangle, \qquad (4.5)$$

where $\boldsymbol{r}_l(t)$ is the position of particle l at time t.

Both intermediate scattering function and velocity auto-correlation function and their Fourier transforms dynamical structure factor and phonon DoS can be efficiently calculated with a MD data post-processor like the one included in the IMD package (cf. App. B.1). The results can be compared directly to experimental data.

Defect Energies

The simulation of defects, like for example vacancies or free surfaces, also provides some criteria for testing the quality of a potential. Possible quantities include surface energy, surface reconstruction or vacancy formation energy, all of which can be determined from ab-initio calculations or experiments.

As mentioned before, the quality and application range of a potential is directly determined by the selection of reference configurations. This is especially true for the simulation of defects. For example, with only bulk atoms in the reference structures, the behaviour of atoms with different coordination (e.g. surfaces, cracks, defects) will most certainly not be simulated correctly.

In this work, all potentials were applied to bulk systems only. However, *potfit* was used to generate potentials to simulate fracture by Rösch and coworkers [91]. These EAM potentials for the C15 Laves phase $NbCr_2$ could describe surface reconstruction and fracture behaviour much better than previous potentials.

Handling Testing Problems

In most cases, a newly generated potential will not immediately pass all tests proposed here. However, there are some strategies to improve a potential with certain deficiencies. A failure of the fundamental stability test indicates either an unfinished optimisation (i.e. the optimisation ended in a metastable state), or a too narrow selection of reference configurations. In the former case a restart of *potfit* with different weights for energies and stresses may help. In the latter case, the potential cannot handle very small deviations from the reference structures properly, and more or different reference configurations need to be included.

For the more complex tests mentioned above, the selection of reference configurations is also the key to a better potential. If a potential fails to describe a certain property correctly, then this happens mostly because the information was not included prominently enough in the reference data. If however a certain property persistently fails to be determined correctly from the force matched potential, this might also signify that the potential model is insufficient for the material.

4.1.3 Employing a Force-Matched Potential

When a potential performs satisfactorily at the testing stage, it is ready to
be used in MD simulation studies – of course only within its design limits
set by the selection of reference structures. If these studies prove success-
ful, there are probably some results one wants to publish, together with
the potentials. This is again the point to emphasise the capabilities and,
even more important, the limitations of a potential. Without specifying
this information, the potential might be used far beyond its design limits,
leading to inaccurate or simply wrong results, for which the blame is put
on the potentials.[2]

The time needed for generating a usable potential should not be under-
estimated. Force matching is not a black box that produces a potential
at the push of a button. It takes skill and experience to steer the poten-
tial generation process, and high quality potentials need many refinements.
Only a small share of that time is used for actually running *potfit*. It takes
much longer to create and improve the reference database and to verify a
set of potentials.

4.2 Effective Potentials for Decagonal Aluminium-Cobalt-Nickel

Aluminium can form complex metallic alloys together with one or more
transition metals. Over an extended composition range, there are thermo-
dynamically stable decagonal quasicrystals in the Al–Co–Ni system around
$Al_{70}Co_{15}Ni_{15}$ [88]. Especially interesting is the so-called basic Ni-rich (b-
Ni) phase with the composition around $Al_{70}Co_9Ni_{21}$. This phase shows
almost perfect quasicrystalline decagonal order with almost no diffuse scat-
tering in TEM images [87]. It is stable between 1100 and 1300 K. The
structure is periodic along the z axis with a period of $c = 4.08$ Å, without
period doubling present in other structural variants of d-Al–Co–Ni. There
is an effective pair potential [1] derived from Generalised Pseudopotential
Theory (GPT) [71]. GPT uses an expansion of the total energy in volume,
pair and many-body potentials. The effects of the many-body potentials

---

[2]Chances are that a published potential will be abused in spite of the disclaimer, but
then at least the reader was warned.

are incorporated through short-range modifications of the TM-TM pair interactions, and the volume term is neglected in simulations in a fixed unit cell.

These potentials were used to develop a tiling model for b-Ni Al–Co–Ni [65]. It was found that the system can be described by a tiling consisting of three tiles, a "hexagon", a "boat" and a "star" (HBS, cf. Fig. 2.1 (b)) [17] with virtually unique decoration. The atoms lie in two layers with 2.04 Å separation. The HBS tiles themselves are arranged to form a HBS supertiling on a length scale larger by a factor of τ^2, where $\tau = \frac{1}{2}\left(\sqrt{5} + 1\right)$ is the golden mean.

Those pair potentials were also used to study Al diffusion in that system [46], and reasonable values for the Al mobility were obtained. Unfortunately, the potentials also have some deficits. Due to the omission of the volume term in the multi-body expansion, the potential cannot describe the elastic behaviour correctly. Additionally, the potential was found to be too "hard" compared to ab-initio MD simulations: The spots of both Al and TM atoms are too sharp in atomic density maps[46].

Out of this motivation, an EAM potential for the basic Ni-rich Al–Co–Ni decagonal quasicrystal was to be designed. First efforts are documented in the author's diploma thesis [11], but they neglected stresses in the force matching progress. Those potentials needed an external pressure of 320 MPa to stabilise the system and failed to provide any estimation of the elastic constants due to structural relaxations during deformation. In this section, the development of improved EAM potentials for the b-Ni Al–Co–Ni quasicrystal is detailed.

4.2.1 Reference Structures

The Al–Co–Ni potentials are designed exclusively to model the b-Ni quasicrystal at high temperatures, especially diffusion processes and melting. This has direct consequences on the selection of reference structures: They have a very narrow composition range and only limited structural elements. Additionally, Al–Co–Ni is also a testing system for *potfit* development: For this system, GPT pair potentials already exist, and the question is, whether it is possible to generate potentials that perform better than the previously published ones.

The reference structures for the Al–Co–Ni quasicrystal come exclusively from the b-Ni tiling model described by Mihalkovič and coworkers [65].
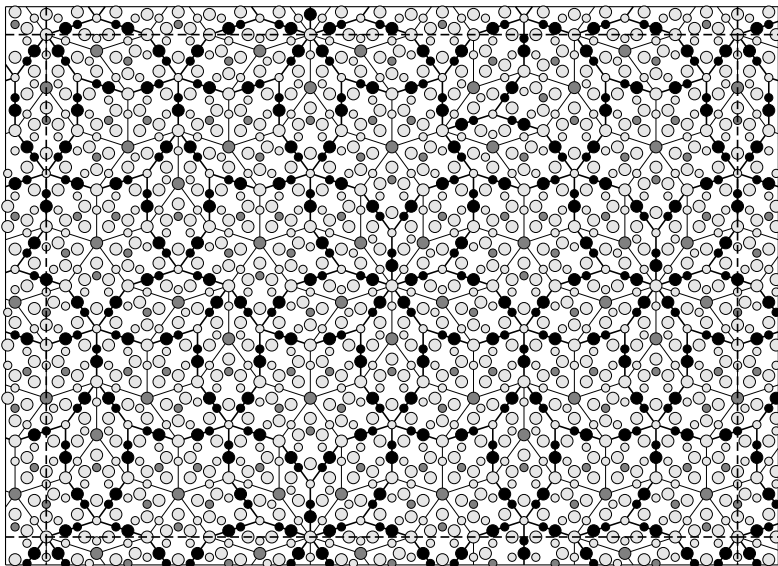
Figure 4.1: Rational approximant to the b-Ni d-Al–Co–Ni quasicrystal. Heavy lines mark the boundaries of HBS tiles in the τ^2-scaled supertiling. Light grey circles represent Aluminium, dark grey ones stand for Cobalt, and black ones for Nickel. The atoms lie in two planes signified by different radii. Decoration according to [65], from [11].

As basic building blocks, the τ^2-scaled supertiles were used. The model consists of three tiles, a hexagon (H) with the composition $Al_{17}Co_2Ni_6$, a boat (B) with composition $Al_{28}Co_4Ni_8$, and a star (S, $Al_{39}Co_6Ni_{10}$). A structure containing all three tiles is shown in Fig. 4.1.

potfit (as well as IMD) requires that unit cell diameters be larger than the cutoff radius of a potential. Thus, two of the basic tiles were stacked on top of each other along the periodic direction. This period doubling also allows a gradual increase of the number of Al atoms in certain sites. As shown in [45], most of the Al sites are large enough to accommodate more than one atom, at least for a short time. To account for this effect,

additional Al atoms were introduced in either or both copies of the basic unit cell. All basic structures that were used to generate the reference data are listed in Tab. 4.1.

No.	Type	# Al	# Co	# Ni	Comment
1	B1	56	8	16	1 Boat
2	B1+1	57	8	16	1 Boat + 1 add. Al
3	B1+2c	58	8	16	1 Boat + 2 add. Al
4	B1+2t	58	8	16	1 Boat + 2 add. Al
5	H1	34	4	12	1 Hexagon
6	H1+1	35	4	12	1 Hexagon + 1 add. A
7	H1+2	36	4	12	1 Hexagon + 2 add. Al
8	H2	68	8	24	2 Hexagons
9	H2+2	70	8	24	2 Hexagons + 2 add. Al
10	H2+4	72	8	24	2 Hexagons + 4 add. Al
11	H2S	146	20	44	2 Hexagons, 1 Star

Table 4.1: Reference structure prototypes for d-Al–Co–Ni effective potential generation. All structures are decorations of the HBS tiling [65].

From these structures the reference configurations were created in various ways. Only a small minority were taken directly from the optimal tiling decorations. Most configurations in a first potential generation attempt were MD snapshots taken with constant volume at high temperatures, partly far beyond the melting temperature. For these simulations the GPT pair potentials from [1] were used. As there are no Co-Co and Co-Ni nearest neighbours in the tiling decoration rules, additional artificial structures were generated by replacing half or all of the TM atoms with the other species. Some of the MD snapshots were compressed or expanded with scaling factors between 0.95 and 1.20. All these measures were necessary to broaden the peaks in the pair distribution functions: Due to the rather narrow composition range of the reference structures, there would have been wide gaps in the pair distributions leading to problems in MD simulation with the generated potential.

The set of reference structures obtained in this way were then used as input for VASP, and ab-initio forces, energies and stresses were calculated in the local density approximation (LDA) with PAW potentials. From 28 of these reference configurations, an EAM potential was generated, going

through a number of intermediate potentials. I will refer to this first production potential as potential 20003. The potential functions are plotted in Fig. 4.2.
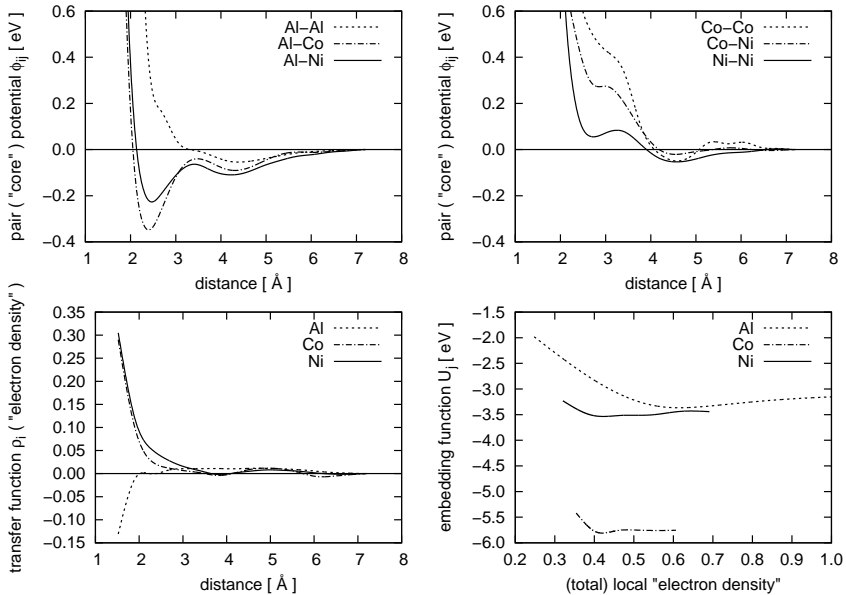
Figure 4.2: AlCoNi-20003: Effective potential for b-Ni d-Al–Co–Ni.

A second potential with the identifier 21714 was later generated using the similar reference structures, but this time using the generalised gradient approximation (GGA) to calculate the reference values. This potential is shown in Fig. 4.3. It can clearly be seen, that the range of the transfer functions is much shorter than in Fig. 4.2. This is a direct result of optimisation: Beyond 5 Å, the potential at some point of the force-matching process did not contribute very much to the total embedding density, so the sampling points in that region could be removed without reducing the quality of the fit.

Both potentials stabilise the b-Ni structure without external pressure (unlike the previous force-matched potentials mentioned in [11]). Tests and applications of these potentials are described below.

Figure 4.3: AlCoNi-21714: Effective potential for b-Ni *d*-Al–Co–Ni.

4.2.2 Test and Applications

Elastic Constants

Both potentials reproduce the experimental values reasonably well (see Tab. 4.2). However, the GGA-based potential 21714 is significantly softer. All those values are to be taken with some caution: The potentials w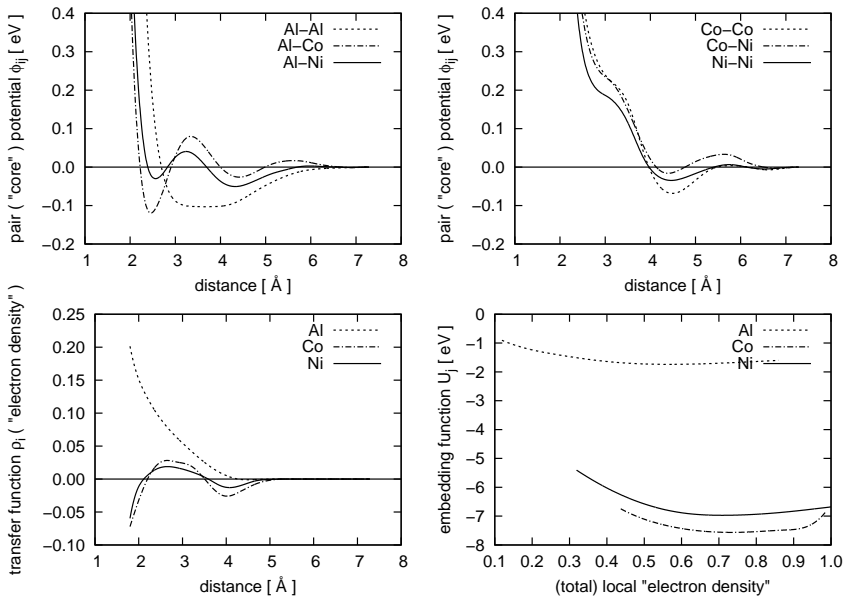ere optimised using mostly high-T reference structures taken from a model of a high-T structure. The experimental values [16] were determined at temperatures up to room temperature from the S1 superstructured quasicrystal.

[GPa]	c_{11}	c_{33}	c_{44}	c_{66} [a]	c_{12}	c_{13}
Experiment [16]	242	240	73	92	58	67
Potential 20003	230	231	55	70	91	91
Potential 21714	197	187	49	58	86	84

[a]In decagonal QC: $c_{66} = \frac{1}{2}(c_{11} - c_{12})$

Table 4.2: Elastic constants of decagonal Al–Co–Ni at 5 K (experiment) and at 0 K (MD).

During the deformation simulations, the quasicrystal did not show any tendency to undergo atomic reconstruction at deformations exceeding 1 %, unlike it was the case in simulations with the GPT potentials and the previously determined EAM potentials. Thus, it can be summarised that both potentials acceptably stabilise the b-Ni phase and provide reasonable estimates of the elastic constants.

Melting Process

The melting point of both potentials was determined in an MD simulation at zero pressure with a Nosé-Hoover thermostat. For the 21714 potential, a 5760-atom approximant of b-Ni Al–Co–Ni was heated to 1220 K. From this point, the simulation was continued at a slower heating rate up to a temperature of 1330 K. In Fig. 4.4, the volume per atom is plotted over the temperature. At 1300 K, the volume increases by about 1.5 %. With the 20003 potential, this jump was found at over 1500 K. In both cases, the decagonal structure dissolved completely at the jump.

The behaviour of the 21714 potential concurs with experiment [88], where an upper barrier of 1040 °C is given for the existence of the b-Ni phase. It

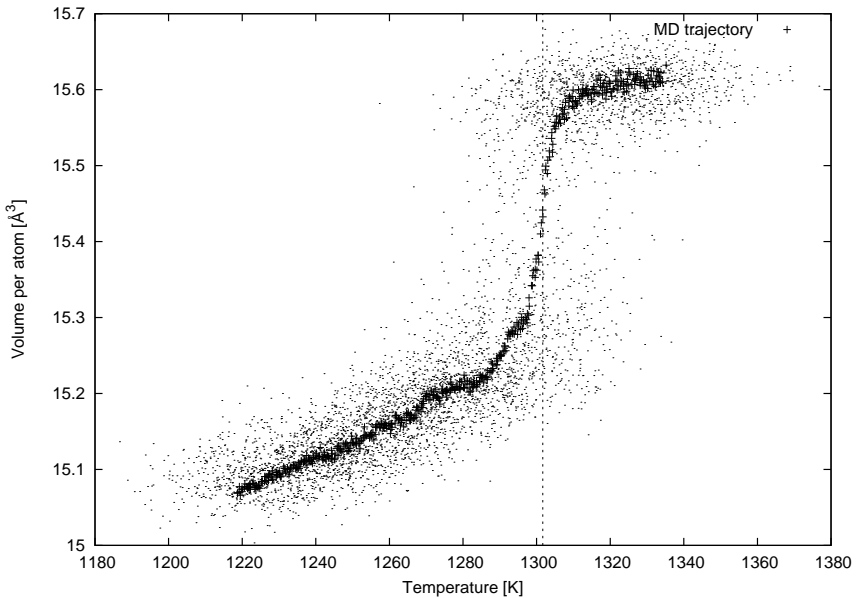**Figure 4.4:** MD simulation of temperature increase in b-Ni Al–Co–Ni quasicrystal with potential 21714. There is a distinct jump in the atomic volume just above 1300 K, corresponding to a melting transition. The exact location of this jump depends on the heating rate. The fine dots show temperature and atomic volume from each MD step, while the crosses mark a running average of 1000 MD steps.

must be considered however, that although slowly heated at 2×10^{-4} K per timestep, the heating rate still amounts to an incredible 2×10^{11} K/s. This method overestimates the melting temperature dependent on the heating rate, so the value determined in this work is quite good. The timescale of the atomistic processes in the phase transitions of the Al–Co–Ni system makes more detailed studies impossible.

It is quite remarkable, that the potential that produces superior elastic constants yields an inferior melting temperature and vice versa. This is a clear indicator that not all design goals of a potential may be realised simultaneously during potential optimisation.

Diffusion in Decagonal Al–Co–Ni

From the results above it was implied, that the potential 21714 performes better at temperatures near the melting temperature and is thus better suited to study diffusion processes in decagonal Al–Co–Ni. Those simulations are performed near the melting temperature. Especially the Al diffusion is inaccessible to experimental studies, as there are no suitable radiotracer elements available. In this section I summarise thesis work done by Stephen Hocker with potential 21714 [44, 45].

Qualitative Assessment   The b-Ni phase is by no means densely packed. There are many (especially Al) sites that can – at least for a short time – accommodate an additional Al atom. Also, Al atoms do not occupy a fixed location, but roam in a certain volume. This can be seen clearly in plots of the atom density distribution calculated from MD simulations. In these plots, the time-averaged density is projected onto a plane (in Fig. 4.5, the projection onto the quasiperiodic plane is shown). Darker colours represent a higher density. The rectangular box encloses an Al site. The volume occupied by that atom is greatly extended and communicates with those of neighbouring atoms in the xy-plane. Other Al sites like the ones between the two green Cobalt atoms are more smeared out along the periodic direction. Both features lead to fast diffusion channels and high Al mobility both in the decagonal plane and in the periodic direction.

In Fig. 4.5, the atomic density distributions resulting from GPT pair potentials and force-matched EAM potentials are compared to ab-initio MD simulations. It was found that while the TM spots from the pair potentials (cf. Fig. 4.5c) were too hard, the EAM potentials (a) reproduce

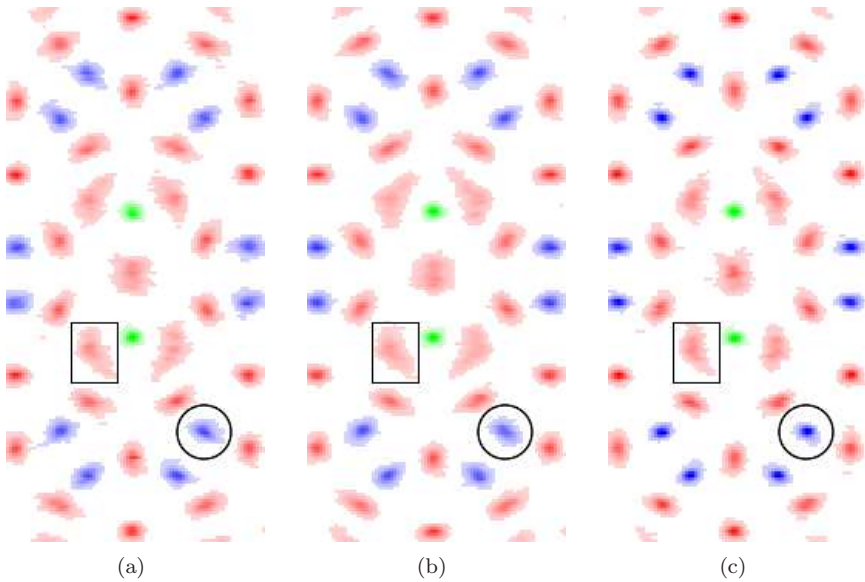(a)   (b)   (c)

Figure 4.5: Atom density distributions from MD simulations of a su-
pertile hexagon with force matched EAM potentials (a), ab-initio sim-
ulations (b) and GPT pair potentials (c) (Al: red, Ni: blue, Co: green,
simulations over 5 ps at 1200 K). EAM potentials provide a better de-
scription of Nickel (circles) and Aluminium (rectangles) dynamics [45].

the ab-initio spot size (b) much better, i.e. the the EAM potentials are softer than the GPT pair potentials.

During the course of a MD simulation with EAM potential, some transition metal atoms were found to jump to neighbouring sites. This was not the case in ab-initio or pair-potential simulations. It appears that this is the price to pay for softening the TM sites.

Quantitative Assessment Diffusion processes in Al–Co–Ni frequently involve several atoms moving simultaneously. For a few of these diffusion processes, the energy barriers were determined [45] and compared to results from ab-initio calculations. The barrier heights are higher than 2.5 eV for diffusion processes involving two Al and one Ni atom, and around 0.5 eV for three jumping Al atoms, and agree reasonably well with ab-initio results.

From the mean square displacements of atoms in MD simulations as a function of time, the diffusion constants for the species involved were determined. The temperature dependent diffusion constant D was fitted to an Arrhenius law of the form

$$D = D_0 \exp\left(-\frac{\Delta H + p\Delta V}{k_B T}\right), \qquad (4.6)$$

where ΔH is the activation enthalpy, ΔV the activation volume and D_0 the pre-exponential factor. In the Ni-rich phase, the activation enthalpies for movement in the decagonal plane and along the periodic direction were determined to be 0.70 eV and 0.58 eV, respectively for Al. This is significantly smaller than the value for vacancy diffusion in fcc Al (1.26 eV). However, it must be noted, that because of the short timescales in MD simulation, the vacancy concentration may not have been in equilibrium. So, only the migration enthalpy is measured, while the formation enthalpy is neglected [37].

4.3 Effective Potentials for CaCd$_6$

CaCd$_6$ can be understood as the cubic 1/1-approximant of the thermodynamically stable Ca–Cd icosahedral quasicrystal [39, 102]. Both quasicrystal and periodic CMA can be described as packings of essentially identical

clusters with some additional glue atoms in-between [66, 107]. In the cubic CaCd$_6$, these clusters are arranged on a bcc lattice.

The clusters each contain a total of 66 atoms in four shells: A Cd tetrahedron is believed to be the central shell, surrounded by a Cd dodecahedron, a Ca icosahedron and a Cd icosidodecahedron [36]. While the outer three shells are icosahedrally symmetric, this symmetry is broken by the innermost tetrahedron.

The cubic 1/1-approximant CaCd$_6$ (and the isostructural Cd$_6$Yb) show an order-disorder phase transition at 100 K (and 110 K respectively), which is attributed to a reordering or disordering of the orientations of the tetrahedral central shell. At the phase transition temperature, there is a peak in the heat capacity and a discontinuity of the electrical conductivity [99, 100].

From X-ray diffraction, Gómez and Lidin [36] concluded that the central shell is a distorted tetrahedron suffering from two types of disorder. The first is a 90° rotational disorder along the twofold axis of the tetrahedron, which leads to a cube with alternately occupied corners. The second type of disorder is a triple split of the tetrahedron corner atoms that arises when the threefold rotational axis does not coincide with the body diagonal of the cubic unit cell. These two types of disorder combined lead to 24 possible positions for four tetrahedral Cd atoms in each cluster's central shell (cf. Fig. 4.6). If one requires that the tetrahedral atoms occupy alternating corners, then there are 162 (2×3^4) possible combinations. Out of those, nine are unique, the others are rotations and mirror images of those.

Based on this information, Nozawa and Ishii used ab-initio methods to compare the energies of structures with different tetrahedron shapes and orientations [73, 74]. However, the computational demands of these methods make a similar treatment of larger supercells impossible.

The *potfit* programme was used to create an effective potential for Ca–Cd. Therewith, the precise structure and ordering of the innermost Cd$_4$ cluster shell could be studied in ways that are inaccessible to ab-initio methods.

4.3.1 Reference Structures and Potential Generation

The icosahedral quasicrystal and its periodic approximants (of which the 1/1-approximant is the CaCd$_6$ CMA) can be viewed as a decoration of the canonical cell tiling [107]. Thus, reference structures were generated from the smaller canonical cell approximants [66]. The hexagonal phase with
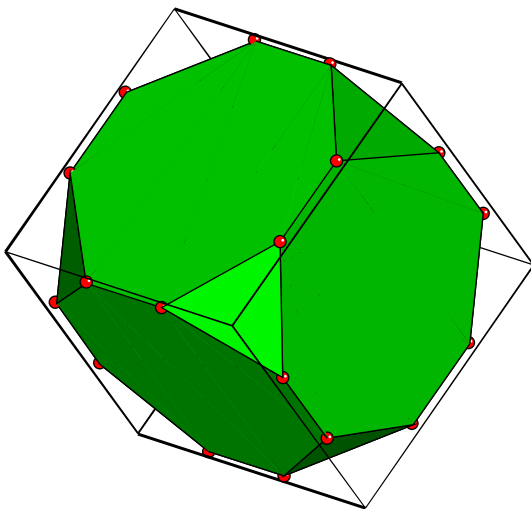
Figure 4.6: Potential locations of the Cd tetrahedral atoms according to GÓMEZ and LIDIN.

Pearson symbol hP68 was added to account for Ca–Cd pair distances that are not present in the canonical cell tiling approximants. All structures were taken from the alloy database [106]. These prototype structures were supplemented by snapshots at various temperatures between 200 K and 850 K generated by Molecular Dynamics simulations with an ad-hoc potential, as well as expanded and compressed variants thereof. A set of 19 reference structures was used to generate an intermediate potential. With this potential, 15 additional reference structures were calculated starting from the $CaCd_6$ structure determined from X-ray diffraction data [36]. All reference structure prototypes are listed in Tab. 4.3.

A glue type potential given by equidistant sampling points and cubic spline interpolation was matched against the reference data. The potential was designed to differentiate between competing ground state structures. Thus, the set of reference configurations includes a rather high share of ground state and low-temperature snapshots compared to the AlCoNi potential used for high-T diffusion (cf. Sec. 4.2). While the force matching process also needs to include some disorder (heat, deformation) to account

No.	Type	Pearson symbol	# Ca	# Cd	Comment
1	*i-CaCd	*A.cI2	24	144	CaCd$_6$, from CCT[b]
2	*i-CaCd	*BC	13	81	from CCT
3	*i-CaCd	*BC	14	79	from CCT
4	*i-CaCd	*BC	14	80	from CCT
5	*i-CaCd	*D	16	110	from CCT
6	*i-CaCd	*D	20	106	from CCT
7	*i-CaCd	*D	20	107	from CCT
8	Ag51Gd14	hP68	14	51	hexagonal
9	*i-CaCd	*alt	26	152	modified CCT
10	*i-CaCd	*alt2	26	152	modified CCT
11	CaCd$_6$	cI208	24	144	CaCd$_6$ [36]

[b]canonical cell tiling

Table 4.3: Reference structure prototypes for CaCd$_6$ effective potential generation. Unless marked otherwise, structures were taken from the alloy database [106] at `http://alloy.phys.cmu.edu`. Structure 11 was only used in the second stage of potential generation.

for interatomic pair distances not present in the ground state, the final rating of different candidate potentials determined unter different circumstances (additional weights, starting potentials, dummy constraints) only compares performance in describing ground state structures. The final potential with the designation CaCd-23170 has a rms error in the energy *differences* of under 1.3 meV per atom. The energies are determined with a rms deviation of 1.7 meV, with the effective potential slightly tending to underestimate the cohesion determined with VASP. Is has to be remarked that the precision of the fit almost reaches the precision of the ab-initio calculation. The potential CaCd-23170 is shown in Fig. 4.7.

The potential stabilises approximants of the icosahedral CaCd quasicrystal including the complex metallic alloy CaCd$_6$.

4.3.2 Applications

A preliminary potential was successfully used by MIHALKOVIČ and WIDOM [66] in structure optimisation. Without an effective potential, candidate
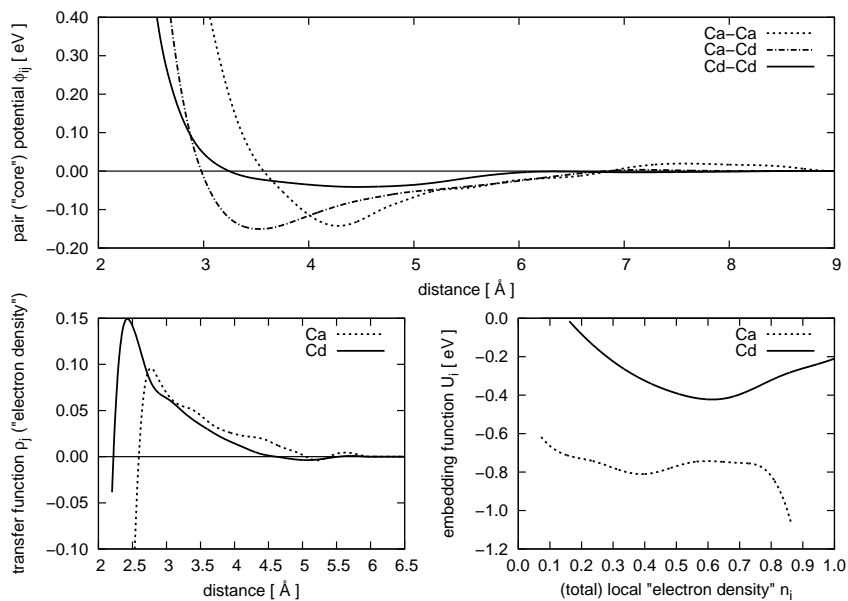
Figure 4.7: CaCd-23170: Effective potential for CaCd$_6$
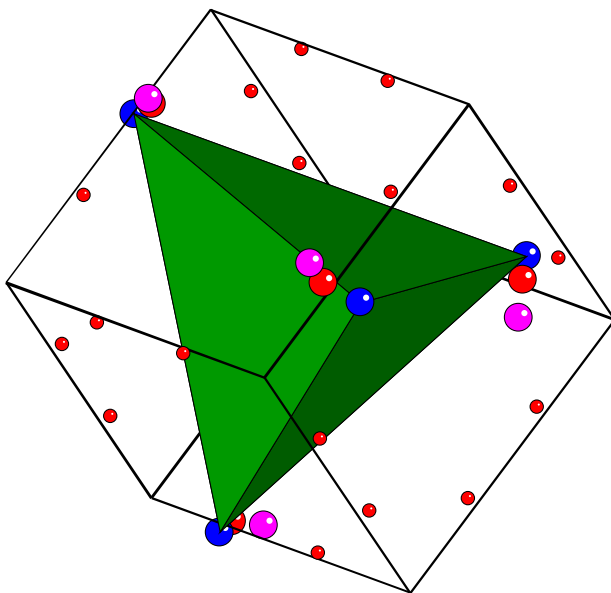
Figure 4.8: Distortion of the inner Cd tetrahedron. Red spheres are the original Gómez-Lidin positions (cf. Fig. 4.6), and blue spheres mark the refined positions determined by MD simulation. Pink spheres are atomic locations belonging to other orientations of the optimal tetrahedron. The cube is drawn as guide to the eye [13].

structures would have to be relaxed with ab-initio MD – an extremely time-consuming process. A reasonable effective potential facilitates structure optimisation in two ways. Firstly, candidate structures can be pre-relaxed with classic MD (which is orders of magnitudes faster) in order to save some ab-initio MD steps. Secondly, many variations of a candidate structure can be studied simultaneously, and the best selected for further ab-initio study. This allows handling of a larger number of candidates.

The CaCd-23170 potential was used intensively to optimise the atomic arrangement in the central Cd$_4$ cluster shell. To that effect, all possible combinations of orientation of the tetrahedra in a cubic cell with two clusters were generated and relaxed. The resulting relaxed structures had six different energies in total, differing maximally by 0.17 meV/atom. The

relaxed tetrahedra were all identical (up to symmetry), the energy difference coming from the different relative orientations of the two tetrahedra [13]. This ideal tetrahedron is not equal to the Gómez-Lidin one, however. Each atom relaxes in a specific way (two atoms by 0.29 Å, the other two by 0.17 Å) to new tetrahedron corners, without further symmetry breaking. The ideal tetrahedron appears in 12 different orientations. If the Gómez-Lidin positions were used, that number would be the same, although the total number of possible corner positions has doubled. The distortion is shown in Fig. 4.8.

In a second step, finite temperature MD simulations were performed with a larger sample, consisting of $5 \times 5 \times 5$ cubic unit cells (250 clusters). These simulations show that, starting from an ordered low-temperature state, the tetrahedron orientations begin to change at around 100 K, and even a few non-ideal tetrahedra show up. Their share increases even further, if the system is heated to higher temperature. Atomic density plots of the tetrahedral atoms are shown in Fig. 4.9. It was not possible, however, to detect any clear sign of the expected phase transition, like a peak in the heat capacity or a jump in the potential energy. Most probably, the number of clusters in the sample is too small and the accessible time scale too short in order to obtain sufficient statistics.

To study the order-disorder phase transition, the relevant degrees of freedom must be isolated. This is described in detail in the following section.
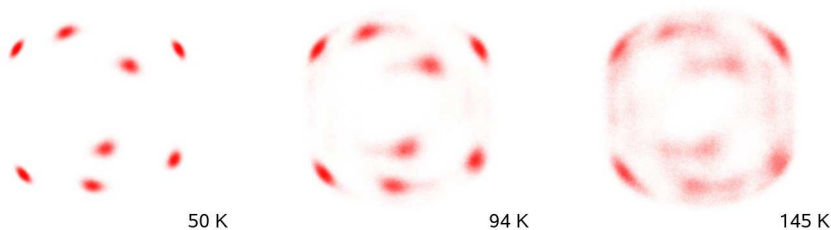

50 K   94 K   145 K

Figure 4.9: Atomic density plots of the tetrahedral atoms in 250 clusters. At low temperature, the tetrahedra at the origin and at the body centre are oriented differently, so eight distinct spots can be seen. With increasing temperature, further orientations appear. Beyond 120 K, non-ideal tetrahedra become more numerous.

4.3.3 Effective Cluster Bond Hamiltonian

At temperatures below and just above the experimentally determined phase transition only one Cd$_4$ tetrahedron can be found in MD simulations. The energy differences result from different orientations of this tetrahedron only. It must be noted, that the atoms of neighbouring tetrahedra do not interact directly in MD simulations – the range of the potential is shorter than the tetrahedral spacing. However, the tetrahedron distorts the surrounding shells in a unique fashion, which then interact directly. The only degrees of freedom are the orientations of the central tetrahedra.

In such a system, an effective cluster bond Hamiltonian can be introduced. An energy contribution E_α is assigned to each bond between clusters. E_α shall only depend on the relative orientations of the tetrahedra at both ends and the bond type. Neighbouring clusters can be in contact along two-fold or three-fold directions. A detailed geometric analysis of the bonds shows that there are 26 different 2-fold bonds and 16 types of 3-fold bonds. The bonds are oriented and are shown in figures 4.10 and 4.11 for bonds along twofold and threefold axes, respectively.

In order to determine the energies E_α, 9394 supercell configurations with up to 64 clusters containing randomly oriented ideal tetrahedra were generated and relaxed to their ground state, using the EAM potentials. For each of the relaxed configurations, the total energy and the bond frequencies were analysed. As the initial structures consisted of clusters with undeformed outer shells, with only the inner tetrahedra replaced, the relaxation is performed in two steps. In a first step, the tetrahedron atoms (already in almost ideal position) were held fixed, so that the deformation of the surrounding shells could develop. Only in a second step, a final relaxation with all atoms mobile was performed. The energies E_α were then determined in a least-square fit. Both the bond frequencies and the energies were considered in relation to a randomly chosen reference structure. Unlike the highly non-linear problem of force matching, determining the bond energies is a linear least squares problem, where the optimal values can be found by solving the normal equations (2.56), a system of linear equations.

However, not all of the 42 parameters E_α can be determined independently. For example, each cluster has six 2-fold and eight 3-fold neighbours. Thus, the total number of 2-fold and 3-fold bonds is fixed, and if the frequency of all but one of each class of bonds is known, the frequency of the

Figure 4.10: Arrangement of the tetrahedra in the bonds along twofold axes. The tetrahedra are shown in the direction of the bond. The rear tetrahedron is displaced, so that the view is unobstructed.
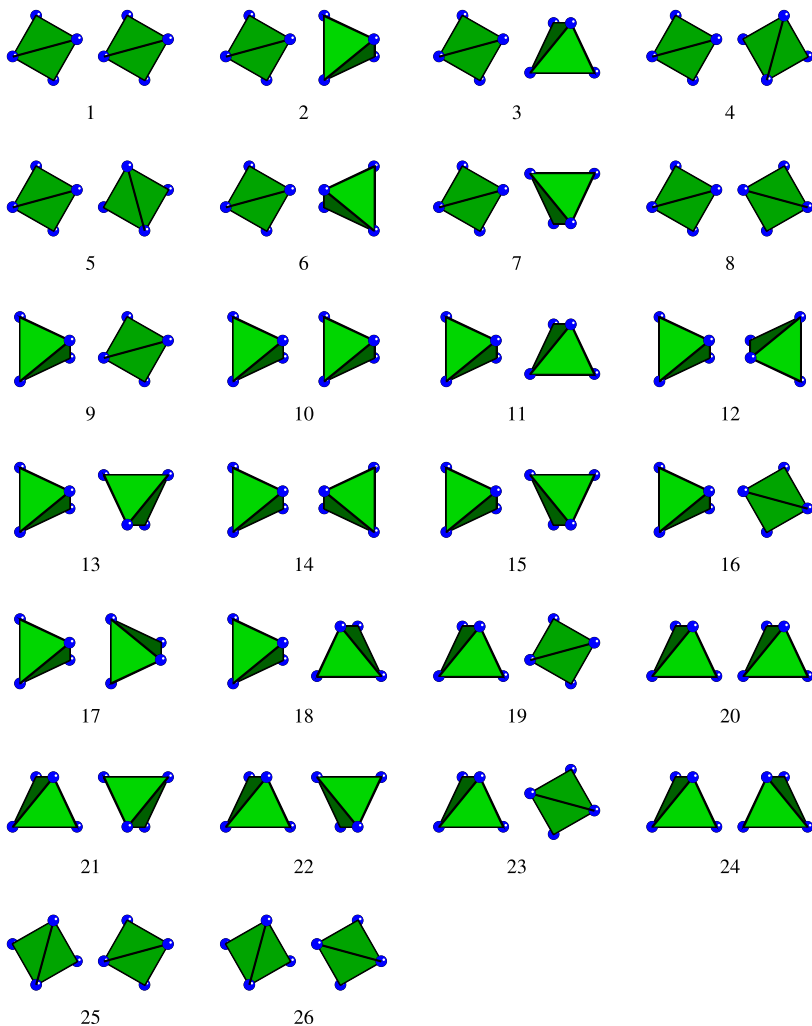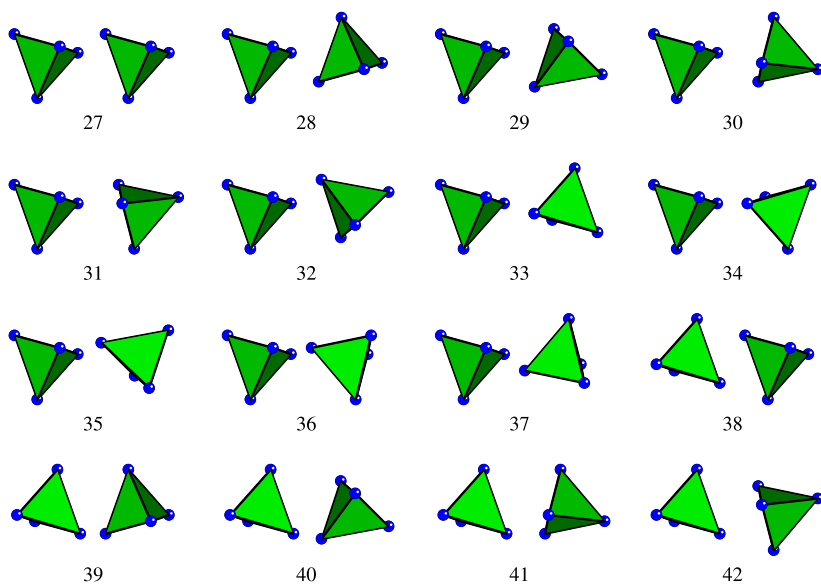
Figure 4.11: Arrangement of the tetrahedra in the bonds along threefold axes. The tetrahedra are shown in the direction of the bond. The rear tetrahedron is displaced, so that the view is unobstructed.

final two is known as well. This means that two of the E_α (one two-fold and one three) can be set to be zero. There are other, more complicated relations between the bond frequencies. They can be found by studying the bond frequency matrix (corresponding to matrix $\mathbf{C}$ in the error equation (2.55)). If all bond numbers were independent, that matrix would have to have rank 42. To find the dependent bond frequencies (and thus also the E_α that can be set to zero), the kernel of the matrix $\mathbf{C}$ was examined. For finite periodic systems, the kernel has at least rank 6, and there are consequently at most 36 remaining independent parameters. Of the six constraints, four are applying to 2-fold bonds, and two to 3-fold bonds.

Two of the constraints are related to the fixed number of two-fold and three-fold bonds mentioned above. The third results from the fact that six of the optimal tetrahedra are inverted images of the other six, while the tetrahedra in each subset are linked by ordinary rotations. Along the threefold axes, there are five bonds with a "standard" cluster at the beginning and an "inverted" cluster at the other end, and five bonds the other way around (the other bonds link clusters from the same subset). In a periodic structure, the number of bonds from either class must of course be the same, thus creating another dependent parameter. There is no simple geometric explanation for the other three constraints.

In supercells with less than 64 clusters (the supercell with the dimensions $2\sqrt{2} \times 2\sqrt{2} \times 4$ in dimensions of the simple cubic unit cell), there are additional constraints and consequently fewer free parameters due to the limited system size. For example, in the simple cubic cell, there are only five parameters remaining. The numbers of independent coefficients E_α in the smallest tetragonal and cubic supercells are given in Tab. 4.4 for 2-fold and 3-fold bonds respectively.

The coefficients determined from least squares optimisation yield energies resulting in a RMS deviation of about 1.7 meV per cluster, which is 3% of the width of the spectrum [13]. The coefficients of a sample Hamiltonian are given in Tab. 4.5. The Hamiltonian appears to be governed by a few very large contributions. However, there is no easy interpretation for this fact, as the values of the E_α depend on the choice of constrained coefficients which can be set to arbitrary values.

As in force matching, the properties of a Hamiltonian depend on the selection of structures that were used in optimising its coefficients, albeit not as drastically. While randomly oriented clusters will yield a set of coefficients that will work for all temperatures, more specialised sets can

Supercell	# Clusters	# 2-fold bonds	# 3-fold bonds
$1 \times 1 \times 1$	2	0	5
$\sqrt{2} \times \sqrt{2} \times 2$	8	15	14
$2 \times 2 \times 2$	16	15	14
$2\sqrt{2} \times 2\sqrt{2} \times 4$	64	22	14

Table 4.4: Number of independent parameters for bonds along 2-fold and 3-fold axes in selected tetragonal and cubic CaCd$_6$ supercells. Supercells larger than $2\sqrt{2} \times 2\sqrt{2} \times 4$ do not offer more independent parameters.

#	Energy	#	Energy	#	Energy	#	Energy
1	-7.674	14	-9.558	23	4.663	34	**-17.581**
5	0.619	15	0.975	24	11.265	35	**-15.054**
6	1.132	16	0.724	25	5.792	36	-8.843
7	0.878	17	**21.572**	26	6.417	37	8.425
8	-5.260	18	11.090	28	1.793	38	0.533
10	**22.660**	19	4.085	29	3.274	39	2.218
11	1.101	20	5.477	30	-2.350	40	3.368
12	-9.133	21	9.101	31	-4.571	41	7.724
13	10.236	22	3.030	32	-4.548	42	6.965

Table 4.5: Parameters E_α from a cluster bond Hamiltonian. Missing coefficients are arbitrarily chosen to be zero due to constraints in the bond frequencies. Coefficients with large absolute values are highlighted in red and green respectively. Coefficients Nos. 1–26 belong to 2-fold bonds, Nos. 27–42 to 3-fold bonds. All energies are given in meV/cluster bond.
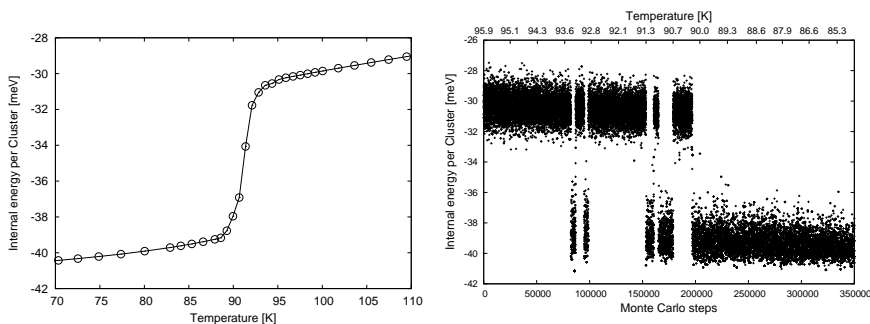
Figure 4.12: Internal energy of the effective cluster Hamiltonian in a $4 \times 4 \times 4$ supercell. The left panel shows a distinct jump is at about 91 K [13]. The right panel shows a sample MC trajectory of that phase transition. For both figures, the same MC temperature schedule was used, but for the left figure, the number of steps at each temperature is twenty times larger.

be generated for low-energy configurations or configurations near a phase transition.

The cluster Hamiltonian so derived can now be used in extensive Monte Carlo simulations. These simulations only involve a very limited set of the degrees of freedom of the system, and extracting relevant data is thus much less demanding than in MD simulations with the full atomic degrees of freedom. With a sample of $4 \times 4 \times 4$ unit cells containing 128 clusters, it was possible to determine the internal energy as a function of temperature [13], which shows a distinct jump at about 91 K (Fig. 4.12), not far from the experimental transition temperature of 100 K [100]. This energy jump ΔE corresponds to an entropy jump $\Delta E/k_B T_0$ of roughly 1 k_B per cluster, which is about twice the amount estimated in [99].

The sample Monte Carlo trajectory shown in the right panel of Fig. 4.12 gives some insight into the energetics of the phase transition. There appear to be two distinct sets of states, one centred around -30 meV/cluster, the other around -39.5 meV/cluster, with few accessed states in-between. With decreasing temperature, the system starts to jump between both states, spending more and more MC steps in the lower state, until the MC energy does not allow any more jumps back to the higher state. In MC

schedules with too few steps per annealing temperature, the internal energy fluctuates strongly in the transition range between 90 K and 94 K. Only if the system remains at a each temperature for a sufficient number of MC steps, the average internal energy converges, and a smooth curve for the temperature dependence can be obtained (cf. left panel of Fig. 4.12).

In principle, it should also be possible to determine the order in the low-temperature state by simulated annealing. For smaller supercells of up to ten clusters, all possible orientational configurations can be evaluated with the cluster bond Hamiltonian within reasonable time. The optimal tetrahedron orientations for the $\sqrt{2} \times \sqrt{2} \times 1$ supercell are shown in Fig. 4.13. Stacked twice in z direction, this is also the optimal configuration for the doubled $\sqrt{2} \times \sqrt{2} \times 2$ supercell, so the larger periodicity in that direction does not lead to any improvement.

(a) Front view

(b) Top view
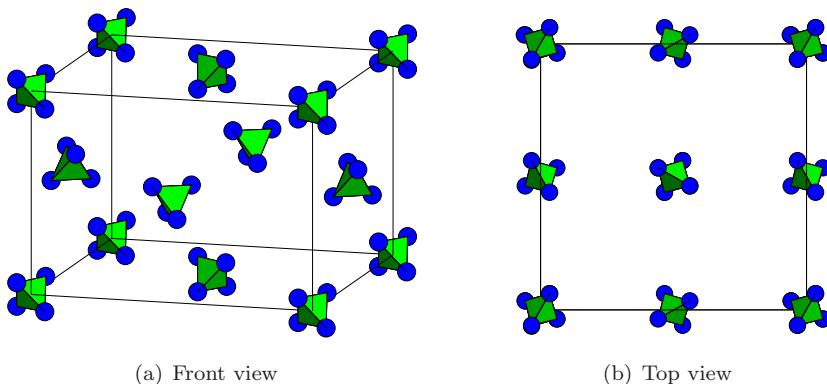
Figure 4.13: Optimal Cd$_4$ tetrahedron orientation in $\sqrt{2} \times \sqrt{2} \times 1$ supercell of CaCd$_6$

From electron and X-ray diffraction experiments, TAMURA *et al.* [101] deduced, that the periodicity of the ground state is indeed $\sqrt{2} \times \sqrt{2} \times 1$. Their favourite candidate greatly resembles the ground state in Fig. 4.13. There are some differences related to the fact that they use the undistorted Gómez-Lidin tetrahedra.

Simulated annealing Monte Carlo runs in larger supercells did not yield any result superior to the structure in Fig. 4.13. This of course does not
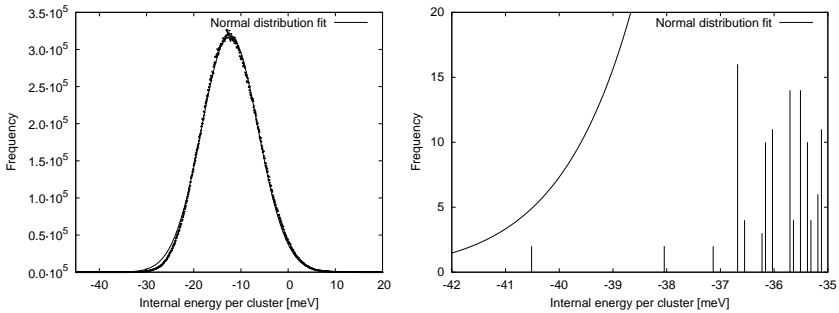
Figure 4.14: Distribution of internal energies in $\sqrt{2} \times \sqrt{2} \times 2$ supercell. The right plot is an enlargement for the optimal structures.

mean that this is already the optimal structure. The problem of MC simulations near temperature zero might be related to the low density of very good structures. A histogram of the energies of all $\sqrt{2} \times \sqrt{2} \times 2$ supercells is shown in Fig. 4.14. There is the optimal structure around -40.5 meV/cluster, one around -38 meV and one further just below -37 meV. All structures appear in two orientations, and several clusters need to change their orientations to get from one to the other. Similarly, changing the orientation of a single cluster in the optimal structure costs almost 4 meV per cluster. All this might obstruct the path to an improved structure in larger supercells.

Through a drastic reduction of the degrees of freedom, the effective cluster bond Hamiltonian offers insight into the structure of $CaCd_6$ in a way that classical Molecular Dynamics cannot provide. However, there is a price to pay for progress: Information on the dynamics of cluster reorientation is lost along the way.

4.4 Effective Potentials for Magnesium-Zinc

Magnesium is a technologically important metal. Especially its alloys are widely used due to their low density and favourable mechanical properties. Unfortunately, its use is limited by its poor corrosion and creep resistance at high temperature. Intermetallic particles on the scale from nanometres to micrometers that form during processing can improve the stability and

resistance of magnesium alloys [48]. In magnesium-zinc alloys, the hexagonal C14 Friauf-Laves phase $MgZn_2$ [34, 60] forms in rod-like or disc-like precipitates during annealing. While the Laves phases are rather brittle at low or ambient temperatures, due to their low density, comparatively high melting point and temperature strength, they are promising materials both on their own and as microscopic particles in other alloys.

Among the complex metallic alloys, the C14 Laves phase is one of the simpler with 12 atoms in the unit cell. There are also much more complex phases in the magnesium-zinc alloy system up to both decagonal and icosahedral quasicrystals [43] in the Mg-(Al,Zn) Frank-Kasper [32, 33] alloy phases. There are also d- and i-quasicrystals in the Mg-Zn-RE systems [93, 103], but they belong to a different class of structures and are not covered in this work.

Both the C14 Laves phase $MgZn_2$, the Mg-(Al,Zn) quasicrystal and the periodic Frank-Kasper phases can be understood as decorations of tiles of the three-dimensional Penrose tiling. In this tiling, there are prolate and oblate rhombohedra and a rhombic dodecahedron, a redecoration of two oblate and two prolate rhombohedra [43]. In those structures, the smaller atoms (Al, Zn) have mostly ideal icosahedral coordination shells, while the larger atoms (Mg) have a coordination number between 13 and 16. In the more complicated structures, Bergman icosahedral clusters [8] can be found.

In this work, effective potentials were generated for the binary Mg–Zn system. Aluminium and zinc atoms are interchangeable in the complex phases to a large extent, so all small atoms were taken to be Zn. This greatly reduces both the number of EAM potential functions and parameters.

4.4.1 Reference Structures and Potential Generation

To generate a potential for the Zn-rich side of the MgZn phase diagram, structures from several classes were selected. The first class are quasicrystal approximants for both icosahedral and decagonal quasicrystals. The icosahedral approximants are decorations of a canonical cell tiling [107], while the decagonal approximants are created from decagonal variants of the Mg_4Zn_7 structure. Those structures are predicted to be metastable only [106]. The second class are stable phases, ranging in Mg content from elemental zinc to Mg_4Zn_7. The $Al_6Mg_{11}Zn_{11}$ (with aluminium sub-

stituted) is a representative of the Frank-Kasper alloys with icosahedrally coordinated atoms. To broaden the spectrum of pair distances in these structures, a ficticious hexagonal phase with 65 atoms in the unit cell was also used. This structure was taken from the CaCd system, the atoms were exchanged and the unit cell was rescaled to accommodate the size difference. All reference structure prototypes can be found in Tab. 4.6. The actual reference configurations were (beyond the ground state configurations mentioned in that table) MD snapshots at various temperatures up to 850 K at fixed volume as well as strained samples generated from the prototype structures.

No.	Type	Pearson symbol	# Mg	# Zn	Comment
1	*i-MgZn	*BC.hR3	34	56	from CCT[c]
2	*i-MgZn	*D	42	80	from CCT
3	*d-MgZn	*H2S	22	34	from HBS tiling
4	*d-MgZn	*RT11	14	80	decagonal
5	$Al_6Mg_{11}Zn_{11}$	cI160	32	48	unstable
6	Mg_2Zn_{11}	cP39	6	33	stable
7	$MgZn_2$	hP12	4	8	stable
8	$Ag_{51}Gd_{14}$	hP68	14	51	artificial,
					rescaled CaCd
9	Mg	hP2	0	2	stable
10	Mg_4Zn_7	mC110	20	34	stable

[c]canonical cell tiling

Table 4.6: Reference structure prototypes for MgZn effective potential generation. All structures were taken from the alloy database [106] at `http://alloy.phys.cmu.edu`.

The reference data (forces, energies and stresses) were determined with VASP using Projector Augmented Waves (PAW) and the Generalised Gradient Approximation (GGA) for the exchange-correlation potential. All calculations were performed using the "Accurate" setting of VASP.

As for Ca–Cd, a glue type potential given by equidistant sampling points and cubic spline interpolation was matched against the reference data. For the first run, an ad-hoc Lennard-Jones potential was used to calculate the MD snapshots. These snapshots were replaced in a second run by

configurations from MD simulations with the intermediate potential.
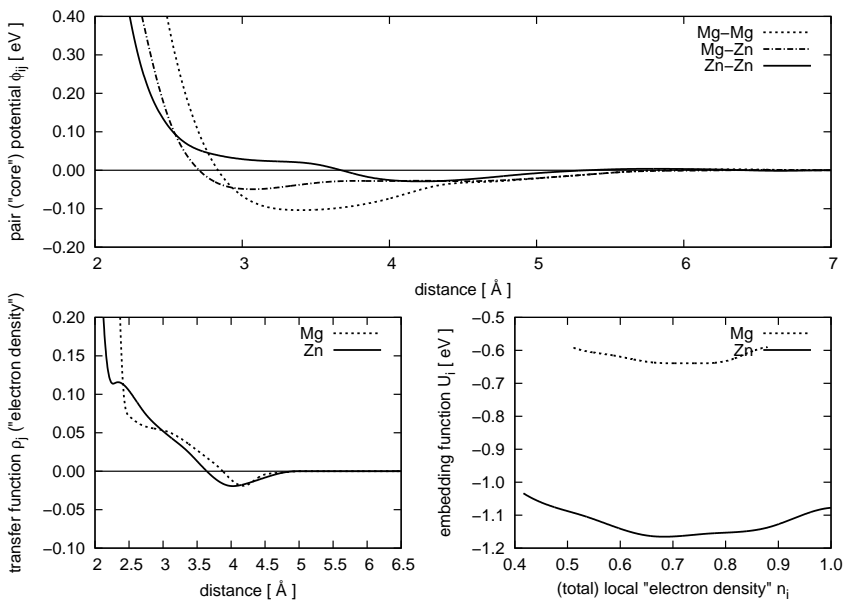
Figure 4.15: MgZn-21719: Effective potential for the Mg–Zn system

In this way, the potential MgZn-21719 shown in Fig. 4.15 was obtained. It successfully stabilises various Mg–Zn structures and reproduces both energy differences and absolute energies with a RMS error of around 5 meV. This potential was used by MIHALKOVIČ to pre-relax structure candidates for the alloy database [106].

An effort to generate a potential specialised on the $MgZn_2$ Laves phase was unsuccessful; it was not possible to improve the potential MgZn-21719 significantly. During that optimisation it was found that the $MgZn_2$ structure given in the alloy database [106] was not relaxed completely. Apparently, $MgZn_2$ shows a soft elastic mode in along the c-axis of the hexagonal unit cell. VASP calculations showed that a structure with lattice constant a shortened by 1.2 % to 5.177 Å and lattice constant c elongated by 1.2 % to 8.480 Å is energetically favourable by 2.8 meV/atom or about 2 % compared to the values in the alloy database. The improved values also agree

better with the experimental data of $a = 5.15$ Å and $c = 8.48$ Å [34].

As a consequence, all reference structures based on the $MgZn_2$ prototype show considerable stress along the c axis. If there are many such structures in the selection, the resulting bias may hinder the generation of an accurate specialised potential. To generate an improved potential, one would first need to relax the $MgZn_2$ structure to its true ground state. Then this structure could be used as prototype for the generation of new reference data through straining and MD simulation. In this way, the potential would learn how to treat that soft vibrational mode along the c axis.

4.4.2 Vibrational Properties of MgZn$_2$

The potential MgZn-21719 (s. Fig. 4.15) was used to study the dynamical properties of the $MgZn_2$ Laves phase. An orthorhombic $32 \times 32 \times 16$ supercell of $MgZn_2$ was simulated at a temperature of 300 K. From MD trajectories in these simulations, the vibrational density of states was determined according to Eq. (4.2). It is shown in Fig. 4.16, where the results from MD simulation are compared to values determined from the potential in harmonic approximation and to experimental data from neutron scattering experiments [95].

While the potential can at least qualitatively reproduce the peaks at 18 and 26 meV (4.1357 meV = 1 THz), the peak at around 10 meV is missing completely. The lowest peak is associated with the dynamics of the heavier of two nuclei, Zn. So the potential has obviously deficiencies in the descriptions of zinc dynamics. This may also be related to the soft (i.e. low-energy) elastic mode described in the previous section.

From the MD simulation, the coherent part of the dynamical structure factor S^c was determined as described in Eq. (4.4). A sample result is shown in Fig. 4.17, where $S^c(\boldsymbol{q}, \omega)$ is plotted for $\boldsymbol{q} = (q_x, 0, 0)$. In the figure, several optic and acoustic branches of the phonon dispersion relation can be identified.

SHIBATA and coworkers have measured phonon dispersion relations for several trajectories in reciprocal space [95]. Their results are shown as black points and curves in Figs. 4.18 and 4.19. The trajectory directions are given in the form $(h + a\xi, k + b\xi, l + c\xi)$, which means that one starts at the Bragg peak (h, k, l) and then moves in the (a, b, c) direction.

Superimposed on the experimental data is the coherent part of the dynamical structure factor from MD simulation. The q scale was left un-

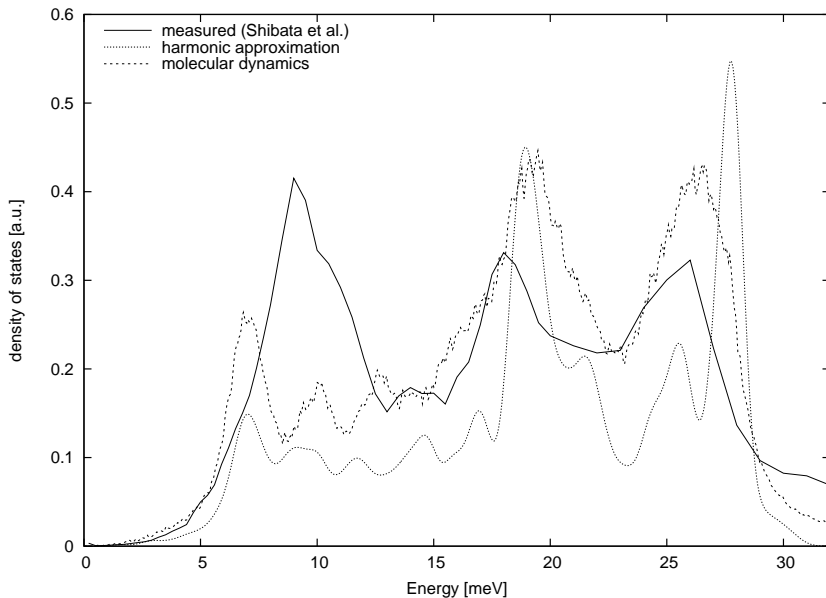**Figure 4.16:** Vibrational density of states of MgZn$_2$. Both the DoS from harmonic approximation and molecular dynamics were calculated with the potential MgZn-21719. The peak in the experimental DoS at around 10 meV is missing in the calculated results. Experimental data from [95].
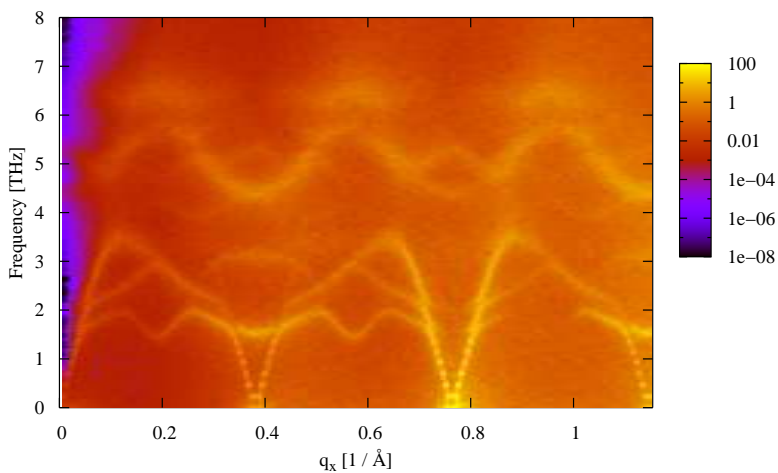
Figure 4.17: Dynamical structure factor of $MgZn_2$ (longitudinal phonon dispersion, determined from MD trajectories)

changed, but the energy scale was adjusted to agree with the experimental result. The scaling factors lie between 1.10 and 1.29 and are given in Tab. 4.7. It is reasonable to adjust only the frequency axis: While the q scale is given by the dimensions of the unit cell, which agree in simulation and experiment, the energy scale is related to the velocity of sound for the given direction and polarisation. The velocity of sound in turn depends on the elastic constants for this deformation, which need not necessarily be correct for a given potential.

Figure	Direction	Scaling factor
4.18(a)	$(-2 + \xi, 4, 0)$	1.29
4.18(b)	$(3 + \xi, -2\xi, 0)$	1.10
4.19(a)	$(\xi, \xi, 6)$	1.11
4.19(b)	$(2, 2, \xi)$	1.21

Table 4.7: Scaling factors for dynamical structure factor from MD simulation

MD simulations can predict the shape of the acoustic phonon branch at least up to the Brillouin zone boundary. The optic bands are not reproduced as well, although there is good agreement for some bands, e.g. the 'opt1' band marked by empty circles in Fig. 4.18(a) and for the 'opt5' band (black squares) in Fig. 4.18(b). It also must be noted, that on some of the experimental values the error bars are rather large.

Especially in the hexagonal plane (Fig. 4.18) the correlation is more than just qualitative. Here, simulation may even suggest q values to be examined in experiment. The structure factor out of the hexagonal plane might be adversely influenced by the soft mode mentioned in the previous section.

In summary, the potentials derived for the Mg–Zn system show some promising results in the description of atomic dynamic processes in the MgZn$_2$ Laves Phase. Force-matched potentials can be used to study these processes in detail. However, the quality of the potential still leaves room for further improvement.
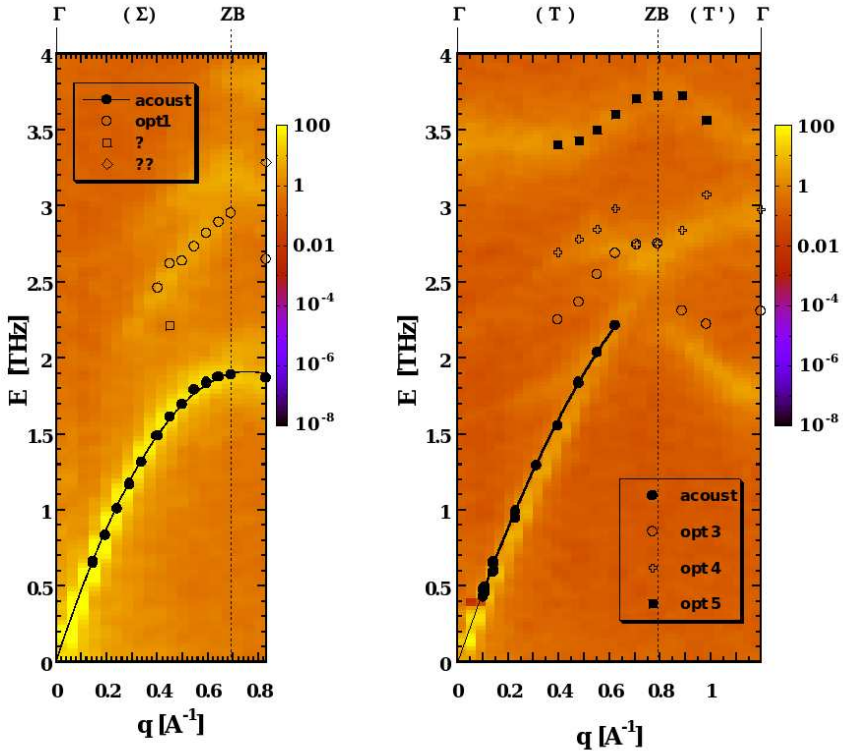
(a) Direction $(-2 + \xi, 4, 0)$ (b) Direction $(3 + \xi, -2\xi, 0)$

Figure 4.18: Dynamical structure factor in the hexagonal plane in experiment [95] and simulation. See text for details.
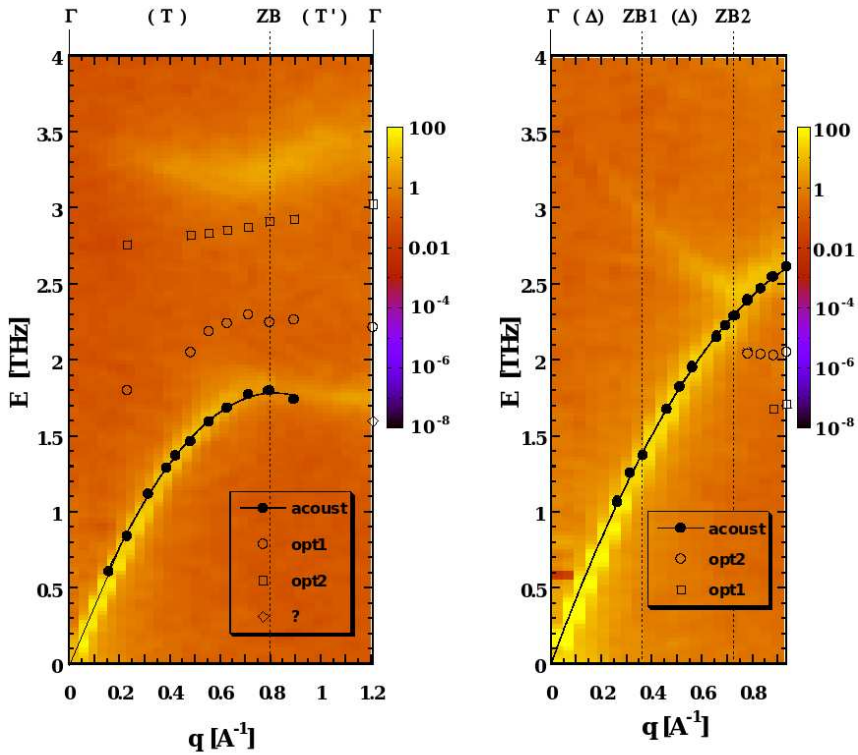
(a) Direction $(\xi, \xi, 6)$ (b) Direction $(2, 2, \xi)$

Figure 4.19: Dynamical structure factor orthogonal to the hexagonal plane in experiment [95] and simulation. See text for details.

Chapter 5

Conclusion

The programme *potfit* was developed as an implementation of the force matching method. It was used to generate Embedded Atom Method (EAM) potentials for a number of Complex Metallic Alloys (CMAs).

potfit – a force matching programme

In this work, *potfit* is established as a flexible tool to generate potentials. The programme consists of two parts: One part calculates for a given potential the forces, stresses and energies of a set of configurations and compares it to reference data. The other part uses only the vector of differences between calculated and reference values to optimise the parameters that specify the potential. The design thus allows easy integration of different effective potential models with only minor adaptions to the programme structure, even though *potfit* is at the moment limited to generating spline-interpolated EAM and pair potentials.

There are two optimisation algorithms implemented in *potfit*. One of them is a variant of Simulated Annealing, which tries to sample the potential parameter space at decreasing values of the target function to find a global optimum. This needs an enormous number of calculations of the target function and takes thus a long time to converge. The other algorithm is conjugate-gradient like and descends into the nearest local minimum with a minimal number of target function calls. The evaluation of the target function, i.e. the comparison between reference data and data from the candidate potential, is by far the most time-consuming part of the potential optimisation, which is why *potfit* can most effectively be improved by either reducing the number of function calls or the time it takes to perform a single call. Both issues have been addressed in the design of the programme.

However, it has been found that among the steps of potential generation, it is not the actual optimisation with *potfit* that takes up most of the time. While selection of suitable reference structures and the calculation of reference data with an ab-initio code can also be laborious, most effort usually goes into the testing stage of potential generation. There, a potential is checked for usability and reliability. The results from testing are used to improve the potential by delicately tweaking the set of reference data and the weights given to the different parts of the target function.

Potentials for Complex Metallic Alloys

In the framework of this thesis, potentials were developed for three systems. The first is the basic-Ni Al–Co–Ni decagonal quasicrystal and its approximants. The potentials developed were used to study high-temperature processes like diffusion near the melting temperature and the melting transition. Thus, the reference data contained a large fraction of high temperature structures, some of which were molecular dynamics snapshots at temperatures far beyond the melting temperature. While one of the two potentials generated yields reasonable values for the elastic constants, the other is better in describing atomic mobility and melting at high temperatures. It can thus be concluded, that in some cases it is not possible to reproduce competing quantities equally well. The latter potential allows the study of diffusion processes in decagonal Al–Co–Ni. It was found that while diffusion barrier heights compare well to those determined from ab-initio simulations, the activation enthalpies for Al are rather low. This however might be related to the simulation technique – it ignores the vacancy formation enthalpy.

A potential for the $CaCd_6$ icosahedral quasicrystal approximant was developed. It was used to study the ground state configuration with special attention to shape and orientation of the innermost tetrahedral cluster shell of the multi-shelled $CaCd_6$ structure. Here, the possible positions of Cd atoms in that shell were refined by MD simulations. A low-temperature effective cluster bond Hamiltonian was developed, with which the ground state and the order-disorder phase transition was studied. The temperature of that phase transition could be reproduced reasonably well.

Finally, the dynamic properties of the $MgZn_2$ Laves phase were examined. The dynamic structure factor from molecular dynamics simula-

tions and phonon dispersion relations from neutron scattering show definite agreement, albeit with a considerable error on the energy scale. That error might be related to a biased selection of reference configurations.

In summary, the *potfit* programme can help greatly in improving the quality of effective potentials for molecular dynamics simulations. Potentials generated with *potfit* were used successfully for metals under a variety of conditions from near the ground state up to the melting temperature. Beyond this work, fracture of a complex metallic alloy was studied in MD simulation with a *potfit*-generated potential. This shows, that force-matched potentials are not limited to application in the bulk.

All those potentials share that they were specifically designed for a purpose, and they would fail if used (or rather abused) in any other way. This is due to the limitations of force-matched potentials. For once, they can only describe those situations correctly for which they were trained. This is why it helps to include snapshots from MD trajectories with intermediate potentials in the selection of reference configurations. Secondly, they naturally can not go beyond the limits of the potential model used. If a material can not be described satisfactorily with EAM potentials, then not even force-matching will be able to procure such a potential.

Outlook

The programme *potfit* introduced in this thesis shows an enormous potential for improving the quality of molecular dynamics simulations. It already has been used to generate potential for several systems, not only by the author, but also by other members of the Institute for Theoretical and Applied Physics at the University of Stuttgart. There have been several download requests from all over the world.

Work on the *potfit* package is far from finished; there are continuous efforts to advance the programme, which is a key component of project B1 of the Collaborative Research Centre 716[1] concerned with the MD simulation of large systems with long-range interactions. Within the framework of that project, *potfit* is going to be extended to generate long-range potentials for ionic solids and metal-oxide interfaces.

There are other potential models that could also with ease be included in *potfit*: The ADP and MEAM potentials mentioned in Sec. 2.2.2 are

---

[1] http://www.sfb716.uni-stuttgart.de/

candidates to be implemented in future releases of the programme. For the already existing EAM and pair potentials, potential representations other than spline interpolated values at sampling points are to be included. For example, a superposition of fat Gaussians might have some advantages, as changing the value of one parameter affects the potential function in a larger domain, thus countering the problem of unsupported parameters (cf. Sec. 2.3.3).

Finally, the already existing potentials for complex metallic alloys are to be improved further. Currently, the optimisation of the potential for $MgZn_2$ for the study of dynamic properties is subject of a doctoral thesis offered at the ITAP.

In this thesis, I show that *potfit* is an effective tool in generating physically justified effective potentials even for complex metallic alloys. But even with *potfit*, this is still an involved task. It needs skill, experience and time to arrive at a usable effective potential. However, realistic potentials are a requirement for large-scale molecular dynamics simulations, a key technique in studying complex metallic alloys and quasicrystals. The potentials generated so far offer new insights into statics and dynamics of those systems.

Appendix A

potfit Technical Information

A.1 General Information

potfit is implemented in ANSI C. On startup, it reads most options from a parameter file, the name of which is given on the command line. The options include the names of further input and output files, what task to perform, or which weight to assign to forces or energies. However, some fundamental choices must be made when compiling the programme, including which potential model to use, whether to allow automatic rescaling in EAM potentials and which additional output files to generate. This is a compromise between convenience and computation speed – the programme binary is smaller and does not contain unnecessary code segments. All compile time options can be activated by passing them to the make command, so no changes to the source files are required.

A.1.1 System Requirements

The programme is distributed as source code. To build a binary executable, a working C compiler with standard I/O, math and string libraries is needed. There is a make file included in the distribution that facilitates compilation and includes optimisation flags for a number of systems. The system type is passed to the make file in an environment variable.

To solve the linear equation system in Powell's algorithm (2.71), *potfit* makes use of routines from the LAPACK library [5], which must be installed separately, including the BLAS library [61] on which LAPACK is based.

Memory requirements for force matching are rather moderate, most modern desktop computers or workstations are more than amply equipped. A typical *potfit* run uses less than 100MB of memory. Similarly, hard disk space should not be an issue, as all required files, including all output, do

not exceed a few megabytes. Performance limiting factors are bare processor speed and memory latency and bandwidth. Any system that is able to perform the ab-initio calculations needed as reference information will most certainly be able to run *potfit*.

For parallel execution, *potfit* relies on the standard Message Passing Interface (MPI [38]). Here, network latency is a greater issue than network bandwidth. More details on the parallelisation of *potfit* can be found in Sec. 3.4.

A.1.2 Input and Output Files

As the volume of data involved in force matching is rather small, all input and output files of *potfit* are plain text. This allows for great flexibility in the treatment of those files, from hand editing to scripting.

Potential Files Tabulated potential functions can be specified with equidistant or with arbitrary tabulation points. All *potfit* potential files consist of a header specifying the type of potential and the number of potential functions to follow. This number of course has to be consistent with the number of atom species and the potential model used. For equidistant tabulation points, the header is followed by one line for each potential function, where the boundaries of the domain and the number of sampling points is given, followed by a lists of function values and the gradient at the domain boundaries. In the case of free tabulation points, only their number for each function is given at the beginning, followed by lists of argument-value pairs and again the gradients of the potential functions at the domain boundaries. In both cases, the gradients can also be used as optimisation parameters. Sample potential files are available for download from the *potfit* homepage.

During the run of a minimisation, the best current potential is written to a temporary storage regularly. In case of an uncontrolled programme abort (power outage, programme fault) the effort is not lost completely, and the optimisation can be restarted from the temporary file.

potfit can also create potential files for use in IMD [96], the classical MD code developed at ITAP (see also App. B.1). These files cannot be used directly as starting potentials for force matching, however. Instead, an input filter is included in the distribution. While a large number of sampling points is no problem at all for MD codes, in force matching each

sampling point is one free parameter that must be adjusted. Also, IMD uses a different interpolation scheme and expects radial functions to be equidistant in the square of the distance. Thus, IMD potentials are generated by densely sampling the potential functions (usually 10^4 sampling points per function). These potentials are also extrapolated to smaller pair distances. This should only be seen as a backup for stray atoms. In an ideal case, such small distances should either not occur or be covered by the reference configurations.

Finally, *potfit* also creates potential tables suitable for plotting, both by sampling the potentials smoothly (around 1000 points) and by printing the tabulated points in abscissa-ordinate pairs.

Reference Configurations   Reference configuration files (also called force files) contain the number of atoms in the reference structure, the box vectors, the cohesive energy and the stresses on the unit cell, followed by a list of atoms, with atom species, position and reference force for each atom. Force files can simply be concatenated. The header of the force files may also contain information whether to use forces on atoms and stresses on the unit cell of this configuration in the optimisation. This feature can be used to increase the weight of cohesive energies in the reference data set.

potfit was designed to cooperate closely with the ab-initio code VASP [57, 58]. Therefore, an import filter to convert VASP output to force files is included in the *potfit* package. Also, IMD has a mode to create snapshots in force file format for testing purposes.

Exit Flag File   The programme regularly checks for the existence of a flag file specified in the parameter file. Should this file exist, the minimisation is finished prematurely, but cleanly (i.e. all output files are written).

Pair Distances File   If *potfit* is compiled with the PDIST option, an additional pair distance output file is written. This file contains the information how often each sampling point interval of the radially dependent functions is hit by the reference configurations. For EAM potentials the same data is given for the embedding function and the final embedding density. This file is useful to check whether a set of reference configurations provides adequate information on each sampling point. If for atoms of types A and B pair distances in a certain interval are not occurring within the reference

data, then potential sampling points in that interval can be chosen almost arbitrarily without significantly influencing the target function. The pair distance file will show such gaps and the user can take the appropriate measures: either complement the reference configurations or rearrange the sampling points.

A.1.3 Potential Representation

Internally, *potfit* potentials are represented by two tables. The first one contains the actual potential parameters as read from the input file ("parameter table"), the other is a lookup table for the force calculation ("calculation table"). For spline tabulated pair or EAM potentials, the two tables are identical. However, in the case of a more complex potential definition (e.g. potentials given by analytic functions) it is computationally unfavourable to use these parameters directly. Instead, a spline interpolated potential table is calculated from the potential definition.

Neither the optimisation routine nor the reference data comparison routine need to know about the meaning of the potential parameters. So, the optimisation part of *potfit* only sees a parameter vector ξ_i and a deviation vector f_j. The parameter vector only contains those parameters that actually can be changed. Usually, it is desirable to keep some potential parameters fixed. For example, potentials should go smoothly to zero at the cutoff radius. This is achieved by setting the final sampling point of the curve and the gradient at that point to zero and excluding them from the parameter vector ξ_i.

A typical potential improvement step thus starts by recalculating the lookup table (if necessary). Then the forces, energies and stresses are calculated and compared to the reference values. The deviations are returned to the minimisation routine which then corrects the adjustable parameters accordingly.

EAM potentials have additional degrees of freedom (cf. Sec. 2.2.2), that must be controlled during optimisation (Sec. 2.3.3). In the current implementation, this is done by periodically rescaling the embedding functions and pair potentials. By using the NORESCALE compiling option, this behaviour can be suppressed. Conventionally, EAM potentials are scaled such that the gradient of the embedding function vanishes at the average density. This convention is used for exporting potentials for plotting and MD simulation. As the average density might change during optimisation,

potfit internally uses a slightly different gauge: It requires that the gradient vanish at the centre of the domain of the respective embedding function. The units of the density n_i in (2.40) can be chosen arbitrarily. Here, the densities computed for the reference configurations shall be contained in the interval $(-1; 1]$, but not in any significantly smaller interval.

A.2 Utilities

Included in the *potfit* package is a number of utilities to help in force matching. These utilities assist the user in providing the necessary input needed for force matching (reference data, starting potential) and using final potential in MD simulation. Some of these functionalities were implemented in the main programme (*potfit* can create potentials for plotting and simulation on its own), but in other cases these tasks are left to external programmes. The advantage of this approach is a leaner force matching code and greater flexibility: Other programmes can be used as data sources without making any changes to the source code of the main programme, the user just needs to write a conversion filter in a language of his choice. The utilities that come with *potfit* are outlined below.

A.2.1 Configuration Conversion Utilities

vasp2force   *potfit* was designed to work with the ab-initio package VASP (cf. Sec. B.2). However it is not possible to take VASP output directly as input for force matching. The information has to be selected and compiled from various locations in two VASP files. The shell script `vasp2force.sh` does just that when executed in a VASP directory and prints the force information to standard output. If the VASP calculation spans several ab-initio MD time steps, `vasp2force.sh` will generate a reference configuration from each ionic time step.

force2poscar   Sometimes it is necessary to recalculate a reference configuration with different VASP parameters. In these cases, `force2poscar` can generate a `POSCAR`[1] file from a reference data file. `force2poscar` is a ANSI C programme.

---

[1]VASP reads atomic positions from this file

IMD (cf. App. B.1) also contains a set of filters that may be of use in force matching. Firstly, there is the option to create reference configurations from classical MD runs. These can be used in testing the force matching programme: The classical interaction potential should be recovered perfectly. Secondly, one may setup VASP calculations directly from MD snapshots.

A.2.2 Potential Conversion Utility: pottrans

While *potfit* can write potentials in various formats needed for plotting or MD simulation with IMD (cf. B.1), there is also an external programme called *pottrans* to convert an IMD potential to *potfit* input format.

The conversion programme reads a parameter file that contains information on input and output potential. The *potfit* potential created is a tabulated potential with equidistant sampling points, the number of which is also read from the input file.

pottrans can be used to create a starting potential for potential optimisation. Due to the nature of cubic splines, the *potfit* potential is by no means an exact representation of the originating potential, and the user is well advised to check the created potential for undesired features, like oscillations caused by spline interpolation. It also should be kept in mind that radially dependent IMD potentials can be given for arbitrarily small pair distances r, while the reference configurations only yield information down to the minimal pair distances. Sampling points at much smaller r cannot properly be determined, so that manual adjustment of either the input or the output potential may be necessary.

Appendix B

Other Programmes Used

B.1 ITAP Molecular Dynamics (IMD)

The ITAP Molecular Dynamics (IMD) programme was developed – as implied by its name – at the Institute for Theoretical and Applied Physics (ITAP) of the University of Stuttgart. This work was funded by the German Research Council (DFG) within the Collaborative Research Centre (SFB) 382 [96]. IMD is still actively being developed at ITAP within the framework of SFB 716. The institute also maintains the IMD homepage,[1] where a detailed manual can be found.

IMD supports a large number of potential types and integrators and it is efficiently parallelised. Beyond pair and EAM potentials used in this work, IMD also supports the ADP and MEAM potentials, covalent interactions like Tersoff, Stillinger-Weber and Keating potentials, Ewald summation for ionic solids (albeit not parallelised) and even Gay-Berne interactions for uniaxial molecules. Some of those potentials are given in analytic form, but most are read as tabulated values from flat files.

Simulations can be performed in a number of thermodynamical ensembles. In the microcanonical NVE ensemble, volume is fixed and the energy is constant. By coupling to a heat bath with the Nosé-Hoover thermostat [72], the temperature can be controlled. The thermostat temperature may vary over time and even over space. Similarly, the simulation can be coupled to a barostat to allow volume adjustments, either isotropically or axially.

Additionally, there are a number of relaxation ensembles that can be used to search for ground state structures. Those relaxators work by removing kinetic energy from a system in a way that the atoms still reach their final

---

[1] http://www.itap.physik.uni-stuttgart.de/~imd

positions as fast as possible. These integrators are complemented with some special purpose integrators like fracture simulation.

IMD is parallelised using the Message Passing Interface (MPI) and allows simulating large samples with many millions of atoms. The sample is decomposed into a number of domains that are then distributed among the processes. The details of this method are given in [96]. IMD is known to work on a wide range of systems, from desktop workstations over large clusters up to modern supercomputers, with excellent scaling with the number of processors.

The typical execution time is in the order of 5–10 microseconds per atom and timestep on modern computers. The length of a timestep has to be chosen with the characteristic oscillation frequencies in a solid in mind; typical timesteps are in the order of femtoseconds.

IMD is not bound to a particular set of units; a convenient set of units is the one described in App. B.3 below, which was also used exclusively in this work.

There is a lower limit on the sample size: The dimensions of the simulation box must exceed the range of the potentials, for otherwise an atom would interact with a periodic copy of itself. However, one can put several copies of a unit cell in the simulation box. IMD then can link all copies of an atom and forbid relative motion between those copies, thus effectively reducing the minimal cell size required.

The programme *potfit* closely cooperates with IMD. On the one hand, IMD can produce snapshots that can directly be used as reference configurations for debugging and testing purposes, e.g. to recover a known potential. More importantly, *potfit* can write out the force-matched potentials in IMD format. Those can then be directly used for MD simulation. Additionally, there is also a tool that converts IMD potentials to *potfit* potentials.

IMD is still actively being developed. Current projects include the simulation of laser ablation. For this purpose, the temperature of the electron gas is introduced as a continuous quantity given on a grid, and energy is transferred between the ionic and the electronic system. Another task is the parallelisation of long-range (ionic) interactions, which at the moment only work in serial calculations, effectively limiting the maximal system size. Finally, IMD is continuously adapted to work on the most current computer systems like for example the Blue Gene supercomputers.

B.2 Vienna Ab-Initio Simulation Package (VASP)

The Vienna Ab-Initio Simulation Package (VASP) is a first-principles code developed by KRESSE *et al.* [55–58]. It is now maintained by the Institute for Computational Material Science at the University of Vienna.[2]

VASP is based on density-functional theory. It can work both with LDA [54] and GGA [81] (cf. Sec. 2.2.1), and it uses a plane wave basis set. Core electrons can be treated with either ultrasoft pseudopotentials [105] or the PAW method [59]. Like any other first-principles code that is based on plane waves, VASP has some parts that scale with the third power of the number of atoms. However, the share is so small, that VASP can reasonably be used in systems with up to 4000 valence electrons.

Included with VASP comes a large pseudopotential and PAW database containing almost every element. Their use allows for a drastic reduction of the basis: Typically 50–100 plane waves per atom in the unit cell suffice.

VASP can also do molecular dynamics in the Born-Oppenheimer approximation. For MD simulations, the electronic ground state is calculated for each ionic step, the forces on the atoms are calculated and the atoms are moved according to Newton's equations of motion. In subsequent steps, the information on the electronic wave functions from the previous steps is extrapolated, so only the first MD step takes the full time, while later steps are considerably faster. Typical execution times are in the order of hours for a reference configuration with 100 atoms in the unit cell in the precision required for *potfit*.

There are utilities included in the *potfit* package that can convert VASP output (configurations, forces, energies and stresses) to reference data for *potfit*.

B.3 Units

IMD and *potfit* do not require any particular set of units, they can work with any system. The units are implicitly defined in the reference configurations for *potfit* and in the potentials and initial configuration files of IMD by the distances, forces, stresses, masses and energies given there. Table B.1

---

[2]http://cms.mpi.univie.ac.at/vasp/

specifies a possible set of units. All calculations in the framework of this thesis were done using those units. One advantage of these units is that all quantities are not too many orders of magnitude away from one. Typical cohesive energies are 1–5 eV, atomic distances are around 2–3 Å, and so on.

Quantity	Unit	SI Value
Distance	Å	10^{-10} m
Energy	eV	$\approx 1.602 \times 10^{-19}$ J
Force	eV/Å	$\approx 1.602 \times 10^{-9}$ N
Stress	eV/Å^3	$\approx 1.602 \times 10^{11}$ Pa
Mass	u	$\approx 1.661 \times 10^{-27}$ kg
Time	Å$\sqrt{\frac{u}{eV}}$	$\approx 1.018 \times 10^{-14}$ s

Table B.1: Possible set of units used in this work and their SI equivalents. In *potfit*, mass and time do not appear directly in the reference configurations, however in MD simulations with the force-matched potentials the choice of mass determines the unit of time and vice versa.

VASP output uses the same units for distances, energies and forces, but the stress on the unit cell is given in kBar. The `vasp2force` utility mentioned in Sec. A.2.1 above converts kBar to eV/Å^3 by dividing by 1602.

Appendix C

Auxiliary Calculations

C.1 Determination of Elastic Constants

The elastic constants can be determined by examining the cohesive energy during a homogeneous deformation of a sample. Recapitulating from Sec. 4.1.2, Hooke's law can be written as follows:

$$E = \frac{1}{2}\boldsymbol{\epsilon}^T \boldsymbol{C} \boldsymbol{\epsilon}, \tag{C.1}$$

where E is the energy density of a deformed solid, $\boldsymbol{\epsilon}$ is a second order strain tensor and $\boldsymbol{C}$ is the fourth order elastic tensor. If one exploits symmetry constraints, the elastic tensor can be written as a six-dimensional symmetric second-order tensor with 21 components using the abbreviations $xx = 1$, $yy = 2$, $zz = 3$, $yz = 4$, $zx = 5$, $xy = 6$. The strain is then a six-dimensional vector. Dependent on the symmetry of the material, the number of independent components may be as low as two for an isotropic solid.

If a system is deformed with a deformation vector $\boldsymbol{\epsilon}_\alpha$, the energy shows a quadratic dependence on the magnitude of the strain. In MD simulation, a relaxed sample is homogeneously deformed by a minute amount every few steps. Both the simulation box and the atomic positions are changed accordingly. Simultaneously, the structure is continously relaxed with a MD relaxator.

Then, the energy per volume is plotted over the strain and a second-order polynomial of the form $f(x) = a \cdot x^2 + b \cdot x + c$ is fitted to the curve. The value of a determined from the fit is recorded as $a(\boldsymbol{\epsilon}_\alpha)$. This value is related to the elastic tensor components c_{ij} by the relation $a(\boldsymbol{\epsilon}_\alpha) = E(\boldsymbol{\epsilon}_\alpha) = \frac{1}{2}\boldsymbol{\epsilon}_\alpha^T \boldsymbol{C} \boldsymbol{\epsilon}_\alpha$. For a set of m distinct deformations, this leads to a linear equation system

for the n independent tensor components c_k among the 21 components c_{ij}:

$$
\begin{array}{ccccccccc}
a_1 & = & b_{11}c_1 & + & b_{12}c_2 & + & \ldots & + & b_{1n}c_n \\
a_2 & = & b_{21}c_1 & + & b_{22}c_2 & + & \ldots & + & b_{2n}c_n \\
\vdots & & \vdots & & \vdots & & \ddots & & \vdots \\
a_m & = & b_{m1}c_1 & + & b_{m2}c_2 & + & \ldots & + & b_{mn}c_n
\end{array}
\tag{C.2}
$$

or written in matrix notation:

$$
\boldsymbol{a} = \boldsymbol{B}\boldsymbol{c},
\tag{C.3}
$$

where $\boldsymbol{c}$ is the vector consisting of the up to 21 independent components of the elastic tensor, which can be determined by solving the linear equations system. The elastic constants can only be calculated, if the matrix $\boldsymbol{B}$ has full rank n. There is a unique and exact solution, if $m = n$. If $m > n$, the system is over-determined. In this case, one can use the method of least squares described in Sec. 2.3.1 to find those values for the c_i that minimise the Euclidian norm of the residue vector $\boldsymbol{r}$ with $\boldsymbol{r} = \boldsymbol{B}\boldsymbol{c} - \boldsymbol{a}$ (cf. Eq. (2.54) ff.).

In the case of a decagonal quasicrystal, the elastic tensor has five independent components. The non-zero elements are $c_{11} = c_{22}$, c_{33}, $c_{44} = c_{55}$, $c_{66} = \frac{1}{2}(c_{11} - c_{12})$, c_{12}, $c_{13} = c_{23}$. A set of deformations that lead to a matrix $\boldsymbol{B}$ with full rank is for example the first five of the following deformations:

$$
\begin{array}{rclccccccc}
\epsilon_1 & = & (& 1 & 1 & 1 & 0 & 0 & 0 &), \\
\epsilon_2 & = & (& 1 & 0 & 0 & 0 & 0 & 0 &), \\
\epsilon_3 & = & (& 0 & 0 & 0 & 1 & 0 & 0 &), \\
\epsilon_4 & = & (& 1 & 1 & -2 & 0 & 0 & 0 &), \\
\epsilon_5 & = & (& 0 & 0 & 0 & 0 & 0 & 1 &), \\
\epsilon_6 & = & (& 1 & -1 & 0 & 0 & 0 & 0 &), \\
\epsilon_7 & = & (& 0 & 0 & 1 & 0 & 0 & 0 &).
\end{array}
\tag{C.4}
$$

By adding the latter two one can broaden the basis of the elastic constants, thus reducing the statistical error.

Bibliography

[1] Al-Lehyani, I., Widom, M., Wang, Y., Moghadam, N., Stocks, G. M., and Moriarty, J. A.: Transition-metal interactions in aluminum-rich intermetallics. *Phys. Rev. B*, **64**, 075109, 2001.

[2] Allen, M. P. and Tildesley, D. J.: *Computer Simulation of Liquids*. Oxford Science Publications (Clarendon Pr., Oxford, 1987).

[3] AMD Core Math Library. `http://www.amd.com/acml`.

[4] Andersen, O. K.: Linear methods in band theory. *Phys. Rev. B*, **12** (8), 3060–3083, 1975.

[5] Anderson, E., Bai, Z., Bischof, C., Blackford, S., Demmel, J., Dongarra, J., Du Croz, J., Greenbaum, A., Hammarling, S., McKenney, A., and Sorensen, D.: *LAPACK Users's Guide, Third Edition* (Society for Industrial and Applied Mathematics, 1999). ISBN 0–89871–447–8.

[6] Ashcroft, N. W. and Mermin, N. D.: *Solid State Physics* (HRW International Editions, 1976).

[7] Baskes, M. I.: Application of the Embedded-Atom Method to Covalent Materials: A Semiempirical Potential for Silicon. *Phys. Rev. Lett.*, **59** (23), 2666–2669, 1987.

[8] Bergman, G., Waugh, J. L. T., and Pauling, L.: The crystal structure of the metallic phase $Mg_{32}(Al,Zn)_{49}$. *Acta Crystallogr.*, **10**, 254–259, 1957.

[9] Blöchl, P. E.: Projector augmented-wave method. *Phys. Rev. B*, **50** (24), 17953–17979, 1994.

[10] Brent, R. P.: *Algorithms for minimization without derivatives*. Prentice-Hall series in automatic computation (Prentice-Hall, Englewood Cliffs, NJ, 1973). ISBN 0–13–022335–2.

[11] Brommer, P.: *Entwicklung und Test von Wechselwirkungspotenzialen in Quasikristallen.* Master's thesis, Universität Stuttgart, 2003.

[12] Brommer, P. and Gähler, F.: Potfit: effective potentials from abinitio data. *Modelling Simul. Mater. Sci. Eng.*, **15** (3), 295–304, 2007. http://www.itap.physik.uni-stuttgart.de/~imd/potfit/.

[13] Brommer, P., Gähler, F., and Mihalkovič, M.: Ordering and correlation of cluster orientations in $CaCd_6$. *Phil. Mag.*, **87** (18–21), 2671–2677, 2007.

[14] Car, R. and Parinello, M.: Unified approach for molecular dynamics and density–functional theory. *Phys. Rev. Lett.*, **55** (21), 2471–2474, 1985.

[15] Cheney, W. and Kincaid, D.: *Numerical mathematics and computing* (Pacific Grove, Bonn, 1999). ISBN 0–534–35184–0.

[16] Chernikov, M. A., Ott, H. R., Bianchi, A., Migliori, A., and Darling, T. W.: Elastic moduli of a single quasicrystal of decagonal Al-Ni-Co: Evidence for transverse elastic isotropy. *Phys. Rev. Lett.*, **80** (2), 321–324, 1998.

[17] Cockayne, E. and Widom, M.: Ternary model of an Al-Cu-Co decagonal quasicrystal. *Phys. Rev. Lett.*, **81**, 598, 1998.

[18] Cohen, M. L. and Heine, V.: The Fitting of Pseudopotentials to Experimental Data and Their Subsequent Application. *Solid-State Phys.*, **24**, 37, 1970.

[19] Corana, A., Marchesi, M., Martini, C., and Ridella, S.: Minimizing Multimodal Functions of Continuous Variables with the "Simulated Annealing" Algorithm. *ACM Trans. Math. Soft.*, **13** (3), 262–280, 1987.

[20] Dagum, L. and Menon, R.: OpenMP: An industry standard API for shared-memory programming. *Comp. Sc. Eng.*, **5** (1), 46–55, 1998.

[21] Davidson, E. R.: The Iterative Calculation of a Few of the Lowest Eigenvalues and Corresponding Eigenvectors of Large Real-Symmetric Matrices. *J. Comput. Phys.*, **17**, 87–94, 1975.

[22] Daw, M. S. and Baskes, M. I.: Semiempirical, Quantum Mechanical Calculation of Hydrogen Embrittlement in Metals. *Phys. Rev. Lett.*, **50** (17), 1285–1288, 1983.

[23] Daw, M. S., Foiles, S. M., and Baskes, M. I.: The embedded-atom method: a review of theory and applications. *Mater. Sci. Rep.*, **9** (7–8), 251–310, 1993.

[24] Dilger, C.: *Versetzungsbewegungen in dreidimensionalen Quasikristallen.* Master's thesis, Universität Stuttgart, 1995.

[25] Dongarra, J., Croz, J. D., Hammarling, S., and Hanson, R.: An extended set of fortran basic linear algebra subprograms. *ACM Trans. Math. Soft.*, **14** (1), 1–32, 1988.

[26] Dongarra, J. J., Croz, J. D., Hammarling, S., and Duff, I. S.: A set of level 3 basic linear algebra subprograms. *ACM Trans. Math. Soft.*, **16** (1), 1–17, 1990.

[27] Engel, M. and Trebin, H.-R.: A unified projection formalism for the Al-Pd-Mn quasicrystal Ξ-approximants and their metadislocations. *Phil. Mag.*, **85** (20), 2227–2247, 2005.

[28] Ercolessi, F. and Adams, J. B.: Interatomic Potentials from First-Principles Calculations: the Force-Matching Method. *Europhys. Lett.*, **26** (8), 583–588, 1994.

[29] Ercolessi, F., Parrinello, M., and Tosatti, E.: Simulation of gold in the glue model. *Phil. Mag. A*, **58** (1), 213–226, 1988.

[30] Feynman, R. P.: Forces in Molecules. *Phys. Rev.*, **56** (4), 340–343, 1939.

[31] Finnis, M. W. and Sinclair, J. E.: A simple empirical n-body potential for transition metals. *Phil. Mag. A*, **50** (1), 45–55, 1984.

[32] Frank, F. C. and Kasper, J. S.: Complex alloy structures regarded as sphere packings. I. Definitions and basic principles. *Acta Crystallogr.*, **11**, 184–190, 1958.

[33] Frank, F. C. and Kasper, J. S.: Complex alloy structures regarded as sphere packings. II. Analysis and classification of representative structures. *Acta Crystallogr.*, **12**, 483–499, 1959.

[34] Friauf, J. B.: The crystal structure of Magnesium Di-Zincide. *Phys. Rev.*, **29** (1), 34–40, 1927.

[35] Gähler, F. and Benkert, K.: Atomistic simulations on scalar and vector computers. In *High Performance Computing on Vector Systems*, (editors M. Resch, T. Bönisch, K. Benkert, T. Furui, Y. Seo, and W. Bez), page 173 (Springer, 2006). ISBN 3–540–29124–5.

[36] Gómez, C. P. and Lidin, S.: Comparative structural study of the disordered MCd_6 quasicrystal approximants. *Phys. Rev. B*, **68**, 024203, 2003.

[37] Grabowski, S., Kadau, K., and Entel, P.: Atomistic modeling of diffusion in aluminum. *Phase Trans.*, **75**, 265, 2002.

[38] Gropp, W., Lusk, E., and Skjellum, A.: *Using MPI - 2nd Edition* (The MIT Press, 1999). ISBN 0–262–57132–3.

[39] Guo, J. Q., Abe, E., and Tsai, A. P.: Stable icosahedral quasicrystals in binary Cd-Ca and Cd-Yb systems. *Phys. Rev. B*, **62**, R14605, 2000.

[40] Hamann, D. R., Schlüter, M., and Chiang, C.: Norm-Conserving Pseudopotentials. *Phys. Rev. Lett.*, **43** (20), 1494–1497, 1979.

[41] Heine, V. and Hafner, J.: Volume and Pair Forces in Solids and Liquids. In *Many-Atom Interactions in Solids*, (editors R. M. Nieminen, M. J. Puska, and M. J. Manninen), pages 12–33 (Springer-Verlag, 1990).

[42] Henley, C. L.: Cell geometry for cluster-based quasicrystal models. *Phys. Rev. B*, **43** (1), 993–1020, 1991.

[43] Henley, C. L. and Elser, V.: Quasicrystal structure of $(Al,Zn)_{49}Mg_{32}$. *Phil. Mag. B*, **53** (3), L59 L66, 1986.

[44] Hocker, S.: *Molekulardynamiksimulationen von Diffusion in dekagonalen Quasikristallen mit optimierten Wechselwirkungspotenzialen.* Ph.D. thesis, University of Stuttgart, 2007.

[45] Hocker, S., Gähler, F., and Brommer, P.: Molecular dynamics simulation of aluminium diffusion in decagonal quasicrystals. *Phil. Mag.*, **86** (6–8), 1051–1057, 2006.

[46] Hocker, S. and Gähler, F.: Aluminium diffusion in decagonal quasicrystals. *Phys. Rev. Lett.*, **93** (7), 075901, 2004.

[47] Hohenberg, P. and Kohn, W.: Inhomogeneous Electron Gas. *Phys. Rev.*, **136** (3 B), B864 B871, 1964.

[48] Hort, N., Huang, Y., and Kainer, K. U.: Intermetallics in Magnesium Alloys. *Adv. Eng. Mat.*, **8** (4), 235–240, 2006.

[49] Intel math kernel library.
http://www.intel.com/software/products/mkl/.

[50] Janot, C.: *Quasicrystals: A Primer* (Clarendon Press, Oxford, 1994).

[51] Jin, Z. H., Gumbsch, P., Lu, K., and Ma, E.: Melting Mechanisms at the Limit of Superheating. *Phys. Rev. Lett.*, **87** (5), 055703, 2001.

[52] Johnson, R. A.: Alloy models with the embedded-atom method. *Phys. Rev. B*, **39** (17), 12554–12559, 1989.

[53] Kirkpatrick, S., Gelatt, C. D., and Vecci, M. P.: Optimization by simulated annealing. *Science*, **220** (4598), 671–680, 1983.

[54] Kohn, W. and Sham, L. J.: Self-Consistent Equations Including Exchange and Correlation Effects. *Phys. Rev.*, **140** (4A), A1133 A1138, 1965.

[55] Kresse, G.: *Ab initio Molekulardynamik für flüssige Metalle.* Ph.D. thesis, Technische Universität Wien, 1993.

[56] Kresse, G. and Furthmüller, J.: Efficiency of ab-initio total energy calculations for metals and semiconductors using a plane-wave basis set. *Comp. Mat. Sci.*, **6** (1), 15–50, 1996.

[57] Kresse, G. and Furthmüller, J.: Efficient iterative schemes for *ab initio* total-energy calculations using a plane wave basis set. *Phys. Rev. B*, **54** (16), 11169–11186, 1996.

[58] Kresse, G. and Hafner, J.: *Ab initio* molecular dynamics for liquid metals. *Phys. Rev. B*, **47** (1), 558–561, 1993.

[59] Kresse, G. and Joubert, D.: From ultrasoft pseudopotentials to the projector augmented-wave method. *Phys. Rev. B*, **59** (3), 1758–1775, 1999.

[60] Laves, F. and Witte, H.: Die Kristallstruktur des MgNi$_2$ und seine Beziehungen zu den Typen MgCu$_2$ und MgZn$_2$. *Metallwirtsch.*, **14** (33), 645–649, 1935.

[61] Lawson, C. L., Hanson, R. J., Kincaid, D. R., and Krogh, F. T.: Basic Linear Algebra Subprograms for FORTRAN usage. *ACM Trans. Math. Soft.*, **5** (3), 308–323, 1979.

[62] Levine, D. and Steinhardt, P. J.: Quasicrystals: a new class of ordered structures. *Phys. Rev. Lett.*, **53** (26), 2477–2480, 1984.

[63] Mackay, A. L.: A dense non-crystallographic packing of equal spheres. *Acta Crystallogr.*, **15** (9), 916–918, 1962.

[64] Metropolis, N., Rosenbluth, A., Rosenbluth, M., Teller, A., and Teller, E.: Equation of State Calculations by Fast Computing Machines. *J. Chem. Phys.*, **21**, 1087–1092, 1953.

[65] Mihalkovič, M., Al-Lehyani, I., Cockayne, E., Henley, C. L., Moghadam, N., Moriarty, J. A., Wang, Y., and Widom, M.: Total-energy-based prediction of a quasicrystal structure. *Phys. Rev. B*, **65**, 104205, 2002.

[66] Mihalkovič, M. and Widom, M.: Canonical cell model of Cadmium-based icosahedral alloys. *Phil. Mag.*, **86** (3–5), 519, 2006.

[67] Mishin, Y.: Atomistic modeling of the γ and γ'-phases of the Ni-Al system. *Acta Mater.*, **52** (6), 1451–1467, 2004.

[68] Mishin, Y., Farkas, D., Mehl, M. J., and Papaconstantopoulos, D. A.: Interatomic potentials for monoatomic metals from experimental data and *ab initio* calculations. *Phys. Rev. B*, **59** (5), 3393–3407, 1999.

[69] Mishin, Y., Mehl, M. J., and Papaconstantopoulos, D. A.: Phase stability in the Fe-Ni system: Investigation by first-principles calculations and atomistic simulations. *Acta Mater.*, **53** (15), 4029–4041, 2005.

[70] Monkhorst, H. J. and Pack, J. D.: Special points for Brillouin-zone integrations. *Phys. Rev. B*, **13** (12), 5188–5192, 1976.

[71] Moriarty, J. A. and Widom, M.: First-principles interatomic potentials for transition-metal aluminides: Theory and trends across the 3d series. *Phys. Rev. B*, **56** (13), 7905–7917, 1997.

[72] Nosé, S.: A Molecular Dynamics Method for Simulations in the Canonical Ensemble. *Mol. Phys.*, **52** (2), 255–268, 1984.

[73] Nozawa, K. and Ishii, Y.: First-Principles Calculations for Structures of Cubic Approximant Cd_6Ca. *preprint*, 2005.

[74] Nozawa, K. and Ishii, Y.: First-principles studies on orientational ordering of atomic clusters in Cd_6Ca. *Phil. Mag.*, **86**, 615–620, 2006.

[75] Pauling, L.: The crystal structure of magnesium stannide. *J. Am. Chem. Soc.*, **45**, 2777–2780, 1923.

[76] Pauling, L.: The stochastic method and the structure of proteins. *American Scientist*, **43**, 285–297, 1955.

[77] Payne, M. C., Robertson, I. J., Thomson, D., and Heine, V.: Ab-initio databases for fitting and testing interatomic potentials. *Phil. Mag. B*, **73** (1), 191–199, 1996.

[78] Payne, M. C., Teter, M. P., Allen, D. C., Arias, T. A., and Joannopoulos, J. D.: Iterative minimization techniques for *ab initio* total-energy calculations: molecular dynamics and conjugate gradients. *Rev. Mod. Phys.*, **64** (4), 1045–1097, 1992.

[79] Penrose, R.: The Rôle of Aesthetics in Pure and Applied Mathematical Research. *Bull. Inst. Math. and its Appl.*, **10**, 266–271, 1974.

[80] Perdew, J. P.: Unified theory of exchange and correlation beyond the local density approximation. In *Electronic structure of solids '91*, (editors P. Ziesche and H. Eschrig), volume 17, pages 11–20 (Akademie Verlag, 1991). ISBN 3–05–501504–5.

[81] Perdew, J. P., Burke, K., and Ernzerhof, M.: Generalized Gradient Approximation Made Simple. *Phys. Rev. Lett.*, **77** (18), 3865–3868, 1996.

[82] Perdew, J. P. and Zunger, A.: Self-interaction correction to density-functional approximations for many-electron systems. *Phys. Rev. B*, **23** (10), 5048–5079, 1981.

[83] Phillips, J. C.: Energy-Band Interpolation Scheme Based on a Pseudopotential. *Phys. Rev.*, **112** (3), 685–695, 1958.

[84] Powell, M. J. D.: A method for minimizing a sum of squares of non-linear functions without calculating derivatives. *Comp. J.*, **7** (4), 303–307, 1965.

[85] Press, W. H., Teukolsky, S. A., Vetterling, W. T., and Flannery, B. P.: *Numerical Recipes in C: The Art of Scientific Computing* (Academic Press, Cambridge, 1992), 2 edition.

[86] Pulay, P.: Convergence acceleration of iterative sequences – the case of scf iteration. *Chem. Phys. Lett.*, **73** (2), 393–398, 1980.

[87] Ritsch, S., Beeli, C., Nissen, H. U., Gödecke, T., Scheffer, M., and Lück, R.: Highly perfect decagonal Al-Co-Ni quasicrystals. *Phil. Mag. Lett.*, **74** (2), 99–106, 1996.

[88] Ritsch, S., Beeli, C., Nissen, H.-U., Gödecke, T., Scheffer, M., and Lück, R.: The existence regions of structural modifications in decagonal Al-Co-Ni. *Phil. Mag. Lett.*, **78** (2), 67–75, 1998.

[89] Robertson, I. J., Heine, V., and Payne, M. C.: Cohesion in Aluminum Systems: A First-Principles Assessment of "Glue" Schemes. *Phys. Rev. Lett.*, **70** (13), 1944–1947, 1993.

[90] Róg, T., Murzyn, K., Hinsen, K., and Kneller, G. R.: nMoldyn: A program package for a neutron scattering oriented analysis of molecular dynamics simulations. *J. Comput. Chem.*, **24**, 657–667, 2003. `http://dirac.cnrs-orleans.fr/nMOLDYN/index.html`.

[91] Rösch, F., Trebin, H.-R., and Gumbsch, P.: Interatomic potentials and the simulation of fracture: C15 $NbCr_2$. *Int. J. Fracture*, **139** (3–4), 517–526, 2006.

[92] Samson, S.: The crystal structure of the phase β Mg$_2$Al$_3$. *Acta Crystallogr.*, **19**, 401–413, 1965.

[93] Sato, T. J., Abe, E., and Tsai, A. P.: Decagonal quasicrystals in the Zn–Mg–R alloys (R = rare-earth and Y). *Mater. Sci. Eng. A*, **304–306**, 867–870, 2001.

[94] Shechtman, D., Blech, I., Gratias, D., and Cahn, J. W.: Metallic phase with long-range orientational order and no translational symmetry. *Phys. Rev. Lett.*, **53** (20), 1951–1953, 1984.

[95] Shibata, K., Francoual, S., and de Boissieu, M.: Experimental study of the dynamics in MgZn$_2$, 2006. Phonon dispersion relations in MgZn$_2$, *unpublished*.

[96] Stadler, J., Mikulla, R., and Trebin, H.-R.: IMD: a software package for molecular dynamics studies on parallel computers. *Int. J. Mod. Phys. C*, **8** (5), 1131–1140, 1997.
http://www.itap.physik.uni-stuttgart.de/~imd/.

[97] Stott, M. J. and Zaremba, E.: Quasiatoms: An approach to atoms in nonuniform electronic systems. *Phys. Rev. B*, **22** (4), 1564–1583, 1980.

[98] Tamura, N.: The concept of crystalline approximants for decagonal and icosahedral quasicrystals. *Phil. Mag. A*, **76** (2), 337–356, 1997.

[99] Tamura, R., Edagawa, K., Aoki, C., Takeuchi, S., and Suzuki, K.: Low-temperature structural phase transition in a Cd$_6$Y 1/1 approximant. *Phys. Rev. B*, **68**, 174105, 2003.

[100] Tamura, R., Edagawa, K., Murao, Y., Takeuchi, S., Suzuki, K., Ichihara, M., Isobe, M., and Ueda, Y.: Order-disorder transition in cubic Cd$_6$Yb and Cd$_6$Ca. *J. Non-Cryst. Solids*, **334&335**, 173–176, 2004.

[101] Tamura, R., Edagawa, K., Shibata, K., Nishimoto, K., Takeuchi, S., Saitoh, K., Isobe, M., and Ueda, Y.: Group theoretical treatment of the low-temperature phase transition of the Cd$_6$Ca 1/1-cubic approximant. *Phys. Rev. B*, **72**, 174211, 2005.

[102] Tsai, A. P., Guo, J. Q., Abe, E., Takakura, H., and Sato, T. J.: A stable binary quasicrystal. *Nature*, **408**, 537–538, 2000.

[103] Tsai, A. P., Niikura, A., Inoue, A., Masumoto, T., Nishita, Y., Tsuda, K., and Tanaka, M.: Highly ordered structure of icosahedral quasicrystals in Zn–Mg–RE (RE≡rare earth metals) systems. *Phil. Mag. Lett.*, **70**, 169–175, 1994.

[104] Urban, K. and Feuerbacher, M.: Structurally complex alloy phases. *J. Non-Cryst. Solids*, **334 & 335**, 143–150, 2004.

[105] Vanderbilt, D.: Soft self-consistent pseudopotentials in a generalized eigenvalue formalism. *Phys. Rev. B*, **41** (11), 7892–7895, 1990.

[106] Widom, M. and Mihalkovič, M.: Alloy database. `http://alloy.phys.cmu.edu`.

[107] Widom, M. and Mihalkovič, M.: Order-disorder transition in the Cd-Ca cubic approximant. *Mat. Res. Soc. Symp. Proc.*, **805**, LL1.10.1 LL1.10.6, 2004.

[108] Yang, W., Hu, C., Ding, D., and Wang, R.: Differences in elastic behavior between pentagonal and decagonal quasicrystals. *Phys. Rev. B*, **51** (6), 3906–3909, 1995.

List of Publications

[1] Brommer, P.: *Entwicklung und Test von Wechselwirkungspotenzialen in Quasikristallen.* Master's thesis, Universität Stuttgart, 2003.

[2] Brommer, P., Gähler, F., and Trebin, H.-R.: *Force Matching – Grundlagen und erste Ergebnisse.* Technical report, 2004.

[3] Brommer, P. and Gähler, F.: Effective potentials for quasicrystals from ab-initio data. *Phil. Mag.*, **86** (6–8), 753–758, 2006.

[4] Hocker, S., Gähler, F., and Brommer, P.: Molecular dynamics simulation of aluminium diffusion in decagonal quasicrystals. *Phil. Mag.*, **86** (6–8), 1051–1057, 2006.

[5] Brommer, P. and Gähler, F.: Potfit: effective potentials from ab-initio data. *Modelling Simul. Mater. Sci. Eng.*, **15** (3), 295–304, 2007.

[6] Brommer, P., Gähler, F., and Mihalkovič, M.: Ordering and correlation of cluster orientations in $CaCd_6$. *Phil. Mag.*, **87** (18–21), 2671–2677, 2007.

Danksagung

Diese Arbeit wäre nicht ohne die Unterstützung zahlreicher Personen zustande gekommen. Aus der Masse möchte ich einige besonders hervorheben.

Mein erster und besonderer Dank gilt dem Hauptberichter und Institutsleiter Prof. Dr. Hans-Rainer Trebin. Er stellte mir im Anschluss an meine Diplomarbeit direkt eine Assistentenstelle zur Verfügung. Während der vergangenen Jahre war er stets an meinem Fortschritt interessiert und ließ mir alle wissenschaftlichen Freiheiten. Die großzügige Unterstützung durch sein Institut erlaubte mir auch den Besuch wichtiger Tagungen und Fortbildungen im In- und Ausland.

Prof. Dr. Ulrich Weiß gebührt Dank für die Übernahme des Mitberichts und die damit verbundene Mühe.

Dr. Franz Gähler war wie schon bei meiner Diplomarbeit ein fachkundiger Betreuer und geduldiger Zuhörer. Seine Kenntnisse der Simulation komplexer Materialien waren von unschätzbarem Wert und haben sehr zum Gelingen dieser Arbeit beigetragen.

Dr. Marek Mihalkovič danke ich für die Zusammenarbeit und die wichtigen Diskussionen zum Verständnis der Struktur von $CaCd_6$.

Michael Engels Programm `injavis` verdanke ich die meisten der 3D-Zeichnungen in dieser Arbeit.

Danken möchte ich auch allen Benutzern von *potfit*, insbesondere Stephen Hocker und Frohmut Rösch, für ihre sehr geschätzten Rückmeldungen über Fehler, neue Funktionen und andere Force-Matching-Angelegenheiten.

Steffen Sonntag hat mich lange als Büronachbar ertragen. Er war für mich in vielen Fragen erster Ansprechpartner. Allen Mitgliedern der Arbeitsgruppe Trebin danke ich sowohl für die inspirierenden Gespräche und Kommentare als auch für die unterhaltsamen Aktivitäten außerhalb der Arbeitszeit.

Den Sekretärinnen Frau Mergenthaler, Frau Blümlein, Frau Jakob und Frau Heldele und allen anderen Mitarbeitern des Instituts danke ich für die freundliche Unterstützung in administrativen Angelegenheiten und die angenehme Arbeitsatmosphäre.

Meine treuen Freunde und Studienkollegen Stephan Walter und Christoph Schlegel standen mir jederzeit als Gesprächspartner in allen Dingen zur Verfügung. Sie möchte ich hier nicht unerwähnt lassen.

Ohne Gegengewicht kann man die Balance nicht halten. Aus diesem Grund danke ich hier auch den Teilnehmern der Mittwochsrunde, den Skatbrüdern und -schwestern, dem Weekend-Kneipen-Team, den Inselhoppern und den Baseball-Kameraden.

Schließlich möchte ich meiner Familie danken. Sie hat mich in meiner Arbeit immer bestärkt. Insbesondere meine Mutter Erneliese Brommer und meine Tante Anna-Elisabeth Brommer haben den Fortschritt meiner Arbeit mit Interesse verfolgt. Besonders herausheben möchte ich auch meine Großmutter Elisabeth Brommer, die meine Bildung sowohl mit persönlichem Einsatz als auch finanziell großzügig förderte. Ihr ist diese Arbeit gewidmet.

Hiermit erkläre ich, dass ich die vorliegende Arbeit selbständig und nur mit den angegebenen Hilfsmitteln angefertigt habe und dass alle Stellen, die im Wortlaut oder dem Sinne nach anderen Werken entnommen sind, durch Angabe der Quellen als Entlehnung kenntlich gemacht worden sind.

Stuttgart, im September 2007   *Peter Brommer*